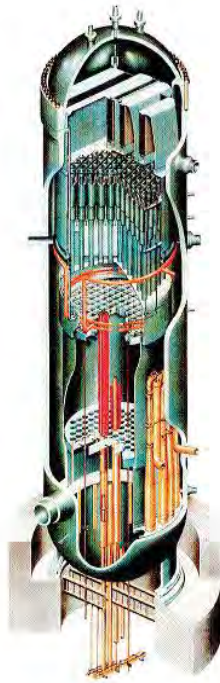


BWVRVIP-59NP-A: BWR Vessel and Internals Project

Evaluation of Crack Growth in BWR Nickel Base Austenitic Alloys in RPV Internals



WARNING:
Please read the Export Control Agreement on the back cover.



NON-PROPRIETARY INFORMATION

NOTICE: This report contains the non-proprietary information that is included in the proprietary version of this report. The proprietary version of this report contains proprietary information that is the intellectual property of BWVRVIP utility members and EPRI. Accordingly, the proprietary report is available only under license from EPRI and may not be reproduced or disclosed, wholly or in part, by any Licensee to any other person or organization.

BWRVIP-59NP-A: BWR Vessel and Internals Project

Evaluation of Crack Growth in BWR Nickel
Base Austenitic Alloys in RPV Internals

1014874NP

Final Report, May 2007

EPRI Project Manager
R. Pathania

DISCLAIMER OF WARRANTIES AND LIMITATION OF LIABILITIES

THIS DOCUMENT WAS PREPARED BY THE ORGANIZATION(S) NAMED BELOW AS AN ACCOUNT OF WORK SPONSORED OR COSPONSORED BY THE BWR VESSEL AND INTERNALS PROJECT (BWRVIP) AND ELECTRIC POWER RESEARCH INSTITUTE, INC. (EPRI). NEITHER BWRVIP, EPRI, ANY MEMBER OF EPRI, ANY COSPONSOR, THE ORGANIZATION(S) BELOW, NOR ANY PERSON ACTING ON BEHALF OF ANY OF THEM:

(A) MAKES ANY WARRANTY OR REPRESENTATION WHATSOEVER, EXPRESS OR IMPLIED, (I) WITH RESPECT TO THE USE OF ANY INFORMATION, APPARATUS, METHOD, PROCESS, OR SIMILAR ITEM DISCLOSED IN THIS DOCUMENT, INCLUDING MERCHANTABILITY AND FITNESS FOR A PARTICULAR PURPOSE, OR (II) THAT SUCH USE DOES NOT INFRINGE ON OR INTERFERE WITH PRIVATELY OWNED RIGHTS, INCLUDING ANY PARTY'S INTELLECTUAL PROPERTY, OR (III) THAT THIS DOCUMENT IS SUITABLE TO ANY PARTICULAR USER'S CIRCUMSTANCE; OR

(B) ASSUMES RESPONSIBILITY FOR ANY DAMAGES OR OTHER LIABILITY WHATSOEVER (INCLUDING ANY CONSEQUENTIAL DAMAGES, EVEN IF BWRVIP, EPRI OR ANY EPRI REPRESENTATIVE HAS BEEN ADVISED OF THE POSSIBILITY OF SUCH DAMAGES) RESULTING FROM YOUR SELECTION OR USE OF THIS DOCUMENT OR ANY INFORMATION, APPARATUS, METHOD, PROCESS, OR SIMILAR ITEM DISCLOSED IN THIS DOCUMENT.

ORGANIZATION(S) THAT PREPARED THIS DOCUMENT

Structural Integrity Associates, Inc.

Dominion Engineering, Inc.

NON-PROPRIETARY INFORMATION

NOTICE: This report contains the non-propriety information that is included in the proprietary version of this report. The proprietary version of this report contains proprietary information that is the intellectual property of BWRVIP utility members and EPRI. Accordingly, the proprietary report is available only under license from EPRI and may not be reproduced or disclosed, wholly or in part, by any Licensee to any other person or organization.

NOTE

For further information about EPRI, call the EPRI Customer Assistance Center at 800.313.3774 or e-mail askepri@epri.com.

Electric Power Research Institute and EPRI are registered service marks of the Electric Power Research Institute, Inc.

Copyright © 2007 Electric Power Research Institute, Inc. All rights reserved.

CITATIONS

This report was prepared by

Structural Integrity Associates, Inc.
3315 Almaden Expressway
San Jose, CA

Principal Investigator
N. Cofie

Dominion Engineering, Inc.
11730 Plaza America Drive, Suite 310
Reston, VA 20190-4748

Principal Investigator
D. Gross

This report describes research sponsored by the Electric Power Research Institute (EPRI) and its BWRVIP participating members.

The report is a corporate document that should be cited in the literature in the following manner:

BWRVIP-59NP-A: BWR Vessel and Internals Project, Evaluation of Crack Growth in BWR Nickel Base Austenitic Alloys in RPV Internals. EPRI, Palo Alto, CA: 2007. 1014874NP.

This report is based on the following previously published report:

BWR Vessel and Internals Project, Evaluation of Crack Growth in BWR Nickel Base Austenitic Alloys in RPV Internals (BWRVIP-59), EPRI, Palo Alto, CA: 1998. TR-108710, authored by Structural Integrity Associates (N. Cofie, A. Giannuzzi, and D. Delwiche); Dominion Engineering (A. Turner, J. Broussard, and E. Hunt); Berkeley Research and Engineering (W. Cheng); EPRI Repair and Replacement Center (A. Peterson); and, GE Nuclear Energy (R. Horn).

REPORT SUMMARY

The Boiling Water Reactor Vessel and Internals Project (BWRVIP), formed in June 1994, is an association of utilities focused exclusively on BWR vessel and internals issues. This BWRVIP report provides a methodology for assessing crack growth in BWR nickel base alloy shroud support structures and in other nickel base alloy components. A previous version of this report was published as BWRVIP-59 (TR-108710). This report (BWRVIP-59-A) incorporates changes proposed by the BWRVIP in response to U.S. Nuclear Regulatory Commission (NRC) Requests for Additional Information, recommendations in NRC Safety Evaluations (SE) and other necessary revisions identified since the previous publication of the report. All changes are marked with margin bars. In accordance with a NRC request, the Safety Evaluations are included here as appendices and the report number includes an "A" indicating the version of the report accepted by the NRC staff.

Background

Events in 1993 and 1994 involving the core shroud confirmed that intergranular stress corrosion cracking (IGSCC) is a significant issue for austenitic materials used in BWR internals. Following the initial evidence of IGSCC, U.S. BWR utilities formed the BWRVIP in June 1994, to address integrity issues arising from service related degradation of key BWR internals components.

Among the key BWR internals components are the core shroud support structure which includes the shroud support plate, the access hole covers, the shroud support legs and/or gussets and the vessel attachment brackets. These components are fabricated from nickel base wrought materials and weld metal. Although limited cracking has been observed to date in these materials in BWR internals, difficulty in inspection of many of these internals components requires that the crack growth rates of these materials for the key shroud support locations be determined. Without this information, premature shroud support reinspection may be required, imposing an unnecessary economic hardship on utilities.

Objective

To formalize the methodology for determination of through-thickness IGSCC growth rates in nickel base alloys based upon empirical field and laboratory test data and field in-service inspection information.

Approach

The approach used was to determine through-thickness residual stress and stress intensity distributions for core support structure welds representative of the BWR fleet. Both experimental and analytical techniques were used to determine the residual stress distributions with reasonable agreement obtained. These residual stresses were used in a fracture mechanics analysis to determine weld-specific through-wall stress intensity distributions for welds H8, H9, H10, H11, and H12. Crack growth distribution curves obtained from field and laboratory data and the stress intensity factor distributions were used to perform crack growth evaluations for the individual welds.

Results

Crack growth rate disposition curves were developed for normal water chemistry (NWC) and hydrogen water chemistry (HWC) environments using Alloy 182 field and laboratory crack growth data. The NWC curve was developed based on the EPRI Action Level 1 condition.

Content Deleted - EPRI Proprietary Information

EPRI Perspective

The correlations developed in this study can be used to conservatively predict the through-thickness IGSCC growth of nickel base materials in the BWR environment in core support structure components. The residual stress distributions developed for a BWR-5, 6 design are believed to be generic to other BWR designs and can be used to disposition IGSCC in those welds. Application of this methodology provides assurance that BWRs with IGSCC in their nickel base welds can continue to operate safely while reducing utility costs by establishing reasonable inspection or reinspection intervals for these welds.

Keywords

Boiling Water Reactor
Core Shroud Support
Crack Growth Rate
Residual Stress
Stress Corrosion Cracking
Nickel Base Alloys

EXECUTIVE SUMMARY

The purpose of this report is to provide a methodology for assessment of crack growth in BWR nickel base austenitic alloy shroud support structure materials and welds, including attachments to the reactor pressure vessel made from these alloys. This work is applicable to components of Alloy 82, 182, and 600 types of nickel base austenitic materials. This methodology has been developed specifically for crack growth in the through-thickness direction. Residual and applied stresses and stress intensity factors have been developed for crack propagation in this orientation.

The steps involved in the development of the methodology include determination of residual stresses, stress intensity factors and crack growth rates based on an extensive database. The methodology involves development of crack growth disposition curves which can account for the variability of important intergranular stress corrosion cracking (IGSCC) parameters in providing a conservative, yet realistic assessment of the crack growth rate (CGR) in BWR nickel base austenitic alloys.

In Section 2 of this report, various core support structure configurations that are encountered in the BWR industry are discussed. The materials used in the design of the various configurations are presented. Most of the components are fabricated using Alloy 600 with welding performed using Alloy 82 and/or Alloy 182. The residual stress calculations done for this report used the specific geometry for a BWR-6 RPV fabricated by CBI Nuclear Company (CBIN). This geometry was chosen for the analyses because samples from an unused vessel were available for experimental stress analysis. The CBIN support structure design includes a number of weld configurations that are distinctly different from the geometries previously evaluated for BWR shrouds (Reference: BWRVIP-14). These geometries include welds at the ends of support legs that are long slender beams (H10, H11, and H12), a weld between the annular shroud support plate and the OD of the shroud support cylinder (H8), and a weld between the shroud support plate and the ID of the cylindrical pressure vessel (H9). These welds are present with minor differences in component dimensions in vessels fabricated by CBIN for all BWR models. Vessels fabricated by Babcock and Wilcox (B&W) use a similar leg design for the shroud support, though with thinner material for the legs. The results of the analyses in this report are considered to be representative of the stress and stress intensity distributions for corresponding weld geometries in all CBIN and B&W fabricated vessels when scaled to the correct component thicknesses (i.e., dimensions for distributions are normalized by the component thickness). Vessels fabricated by Combustion Engineering (CE) used an annular shroud support plate reinforced by gusset plates shroud support design. This design includes an H9 weld similar to the one analyzed for this report. Weld H8 for the CE shroud support design is between the end of the shroud support cylinder and the top surface of the shroud support plate. This configuration is similar to shroud welds H3, and H6a. Thus, the results of shroud weld evaluations (Reference: BWRVIP-14) can be used to evaluate the H8 weld in the CE design shroud support.

Also in Section 2, the performance of the core support structural materials and welds relative to IGSCC is discussed. In general, the performance of Alloys 600, 82 and 182 have been relatively good in the absence of a crevice condition or weld defects. This is borne out by field experience which has shown that these components have not exhibited significant cracking when compared to austenitic stainless steel components. However, under creviced condition, these alloys can become highly susceptible to IGSCC. These materials have a very long crack initiation phase which contributes to their relatively good performance.

In order to calculate the fracture mechanics stress intensity factor, the stresses in the core shroud support structure must be known. The operating stresses of the shroud support structure are relatively low and can be determined readily from the stress reports. A major portion of Section 3 of this report deals with weld residual stresses developed during the fabrication of the shroud and the shroud support structure. Both experimental measurements and analytical techniques were used to determine surface and through-wall residual stress distributions for the welds of the support structure. In the initial analysis, a welding sequence, which was based on information available at that time was used. Because of the hardware and software limitations at that time, the analysis consisted of separate models of the individual welds. The results of the individual models were subsequently combined using superposition principles to get the final state of stress for all the welds. Subsequent to this initial analysis, an alternate welding sequence was identified which was used by Chicago Bridge and Iron (CBI) in a number of vessels including River Bend. At this time, computational capabilities have improved to the point where it is practical to develop one integrated model containing all the welds for the analysis. Hence all the initial analyses were redone using this integrated model and in addition, the alternate welding sequence was also analyzed. The residual stresses resulting from both of these welding sequences were determined and used in the crack growth evaluation of the shroud support structure welds.

In Section 4 of this report, established fracture mechanics models were used to determine the through-wall stress intensity factor (K) distributions for the through-wall stress profiles. Individual stress distributions determined for each weld of the core support structure were used to develop the through-wall K distribution for each weld. For welds H8 and H9, the K distributions were determined for various finite length flaws. For the leg welds, H10, H11 and H12, the K distribution was derived assuming the flaw extends over the entire width of the leg.

In Section 5 of this report, an extensive database consisting of nickel base austenitic alloy crack growth rates is described. These data came from General Electric Nuclear Energy (GENE) and BWRVIP data generated through the peer review process and include both experimental data points and in-plant crack arrest verification system (CAVS) data. Most of the data in the database have adequate definition of environmental conditions and other important crack growth parameters thus permitting a more realistic generic crack growth model to be developed. The database has been used to derive crack growth disposition curves which account for environmental conditions such as conductivity of the water and the electrochemical potential (ECP). The crack growth relationships have two regimes. For K less than $25 \text{ ksi-in}^{1/2}$, the crack growth is K dependent. For K greater than $25 \text{ ksi-in}^{1/2}$, the crack growth is K independent.

In Section 6, evaluations using the crack growth dispositions curves and the derived through-wall stress intensity factor distributions were performed to determine the crack growth for all the welds under various water chemistry conditions. Crack growth for Welds H8 and H9 initially starts in the K independent regime, but as the crack grows deeper, the crack growth becomes K dependent.

**Content Deleted -
EPRI Proprietary Information**

It is noted that the crack growth behavior of Alloy 82 and Alloy 600 in the BWR environment is expected to be far better than that of Alloy 182 as demonstrated by field experience. Hence, the crack growth evaluation methodology presented in this report is conservative in application to Alloys 82 and 600. The BWRVIP proposes that the methodology presented in this report be used to evaluate crack growth in core support structure welds and other Alloy 82, 182 and 600 welded internal components. Application of the methodology presented in this report provides assurance that BWRs with cracks in the core support structure can continue to operate safely while reducing utility costs by supporting reasonable intervals for reinspection and avoiding the costs of unnecessary or premature repairs.

ACKNOWLEDGMENTS

The members of the BWRVIP Crack Growth Working Group, listed below, are gratefully acknowledged for their efforts which led to the successful completion of the original version of this document.

Dana Covill	GPU Nuclear
Jai Brihmadeseam	Entergy Operations
George Inch	Niagara Mohawk Power Corp.
Tony Giannuzzi	Structural Integrity Associates
Ron Horn	GE Nuclear Energy
Dave Morgan	Pennsylvania Power and Light
Larry Nelson	EPRI
Raj Pathania (Project Manager)	EPRI
John Wilson	Illinois Power
Steve Leshnoff	General Public Utilities
Ed Hartwig	Tennessee Valley Authority
John Grimm	First Energy Corp
Bob Carter	EPRI

RECORD OF REVISIONS

Revision Number	Revisions
BWRVIP-59	Original Report (TR-108710).
BWRVIP-59-A	<p>The report as originally published (TR-108710) was revised to incorporate changes proposed by the BWRVIP in responses to NRC Requests for Additional Information, recommendations in the NRC Safety Evaluations (SE), and other necessary revisions identified since the last issuance of the report. All changes, except corrections to typographical errors, are marked with margin bars. In accordance with a NRC request, the SEs are included here as appendices and the report number includes an “A” indicating the version of the report accepted by the NRC staff. Non-essential format changes were made to comply with the current EPRI publication guidelines.</p> <p>Appendices F and G added: NRC Safety Evaluations.</p> <p>Details of the revision can be found in Appendix H.</p>

CONTENTS

1 INTRODUCTION	1-1
1.1 Background	1-1
1.2 Susceptibility of Nickel Based Components in the BWR Environment.....	1-2
1.3 BWR Plant Operating Experience	1-3
1.3.1 Surface Crack Growth Rates of Nickel Base Alloys	1-4
1.4 Objectives and Approach	1-4
1.5 Implementation Requirements	1-5
2 BWR SHROUD SUPPORT WELD CONFIGURATIONS	2-1
2.1 Conical Shroud Support Plate (BWR-2)	2-3
2.2 Thick Shroud Support Plate (Hatch Unit 2)	2-3
2.3 Shroud Support Plate With Legs	2-5
2.4 Shroud Support Plate With Gussets.....	2-8
2.5 Shroud Support Structure Used in this Study and Applicability to Other Shroud Support Structures	2-9
2.6 Weld Sequence During Fabrication of Shroud Support Structure.....	2-14
3 OPERATING AND RESIDUAL STRESSES	3-1
3.1 Operational Stresses.....	3-1
3.2 Weld Residual Stresses	3-1
3.2.1 Through-Thickness Residual Stress Measurements at River Bend Nuclear Station	3-2
3.2.2 Analytical Determination of Residual Stresses	3-8
3.2.2.1 Initial Analyses With Discrete Weld Models.....	3-8
3.2.2.2 Updated Analyses With Integrated Model.....	3-10
3.2.2.3 Summary of Analytical Results	3-12
3.2.3 Comparison of Initial and Updated Analytically Predicted Residual Stresses With Experimental Measured Data	3-13
3.2.4 Critical Sections Selected for Further Analyses	3-23

4 FRACTURE MECHANICS CONSIDERATIONS	4-1
4.1 Stress Intensity Factor for Welds H8 and H9	4-1
4.2 Stress Intensity Factor Determination for Welds H10, H11 and H12	4-5
5 CRACK GROWTH DISPOSITION CURVES	5-1
5.1 Review of Alloy 182 Disposition Efforts	5-1
5.2 Rates Determined from Field Cracking Events	5-2
5.3 Review of Recent Data	5-2
5.4 Modeling Assessments	5-3
5.5 Disposition Crack Growth Rate Approach	5-3
5.6 Specific Curves	5-3
5.6.1 Normal Water Chemistry Below EPRI Guidelines Action Level 1	5-3
5.6.2 Normal Water Chemistry With Conductivity at or Below 0.15 μ S/cm	5-5
5.6.3 Hydrogen Water Chemistry Within EPRI Guidelines	5-5
5.6.4 Crack Growth Rates for Assessing Crack Lengthening	5-5
5.7 Effect of Fluence on Crack Growth	5-5
6 CRACK GROWTH EVALUATION	6-1
7 SUMMARY AND CONCLUSION	7-1
8 REFERENCES	8-1
A NICKEL BASE CRACK GROWTH DISPOSITION CURVES.....	A-1
A.1 Background.....	A-3
A.2 Report Outline.....	A-4
A.3 Review of Previous Efforts to Evaluate Alloy 182 Cracking in Operating BWRS	A-5
A.3.1 Review of Alloy 182 Disposition Efforts.....	A-7
A.3.2 Historical Disposition Crack Growth Discussion	A-7
A.3.2.1 Limerick 1: First Disposition Effort: 1989	A-7
A.3.2.2 Hatch Access Hole Cover Disposition	A-9
A.3.2.3 Limerick 1: Follow-Up Disposition Effort: 1990.....	A-13
A.4 Discussions With the U.S. NRC on Alloy 182 Crack Growth Rates.....	A-14
A.4.1 IGSCC Technology Update Meeting for NRC: June 9, 1987	A-14
A.4.2 IGSCC Technology Update Meeting for the NRC: March 22, 1989.....	A-15
A.5 Rates Determined from Field Cracking Events.....	A-15

A.6 Review of Recent Data	A-22
A.6.1 Recent CAV Data	A-22
A.6.2 Recent Crack Growth Rate Data	A-22
A.6.3 Recent GENE Crack Growth Rates Efforts	A-28
A.7 Modeling Assessments	A-31
A.8 Proposed Interim Disposition Curves	A-34
A.8.1 Review of Basis for Approach	A-34
A.8.2 Specific Curves	A-35
A.8.2.1 Normal Water Chemistry Below EPRI Guidelines Action Level 1	A-35
A.8.2.2 Normal Water Chemistry With Conductivity Below 0.15 $\mu\text{S}/\text{cm}$	A-40
A.8.2.3 Hydrogen Water Chemistry Within EPRI Guidelines	A-40
A.8.3 Comparison With PLEDGE and the SKI Disposition Curves	A-40
A.8.4 Applicability to Alloy 600	A-48
A.9 Conclusions and Recommendations	A-48
A.10 References	A-49

B THROUGH-THICKNESS RESIDUAL STRESS MEASUREMENT AT RIVER BEND NUCLEAR STATION..... B-1

B.1 Introduction	B-1
B.1.1 Theoretical Background	B-2
B.1.2 Experimental Procedures	B-4
B.2 Measurement of Residual Stresses through the Thickness of Welds	B-4
B.2.1 Residual Stress Distribution Measured for Weld H8	B-4
B.2.2 Residual Stress Distribution Measured for Weld H10	B-7
B.2.3 Residual Stress Distribution Measured in Shroud Support Plate for Weld H9	B-9
B.2.4 Residual Stress Distribution Measured in Vessel Wall for Weld H9	B-11
B.2.5 Residual Stress Distribution Measured for the Shroud Support Leg Weld (H12)	B-13
B.3 Measurement of Residual Stresses Near the Surface of Weld H9	B-15
B.4 Conclusion	B-18
B.5 References	B-19

C CRACK GROWTH EVALUATION RESULTS C-1

**D ANALYTICAL PREDICTION OF RESIDUAL STRESSES IN BWR SHROUD
SUPPORT STRUCTURE WELDS D-1**

D.1 Weld Joints Analyzed	D-1
D.2 Analysis Approach	D-5
D.2.1 Factors which Affect Weld Residual Stresses	D-5
D.2.2 Key Modeling Assumptions.....	D-5
D.2.3 Material Properties	D-7
D.2.4 References.....	D-8
D.2.5 Finite Element Mesh Characteristics	D-9
D.2.6 Fabrication Sequence	D-14
D.2.7 Modeling of Welding Process	D-14
D.2.8 Modeling of Post Weld Heat Treatment	D-16
D.3 Analysis Results	D-17
D.3.1 Residual Stresses Without Post Weld Heat Treatment	D-17
D.3.2 Effects of Stress Relief Post Weld Heat Treatment	D-26
D.4 Comparison of Calculated and Measured Residual Stresses	D-48
D.5 Use of FEA Results in Predicting Crack Stress Intensities.....	D-54
D.5.1 FEA Work Supporting H8 and H9 Weld Crack Predictive Models	D-54
D.5.2 FEA Work Supporting H10 and H12 Weld Crack Predictive Models	D-57
D.6 References	D-57

**E ANALYTICAL PREDICTION OF RESIDUAL STRESSES IN BWR SHROUD
SUPPORT STRUCTURE WELDS (INTEGRATED MODEL RESULTS) E-1**

E.1 Weld Joints and Sequences Analyzed.....	E-2
E.2 Analysis Approach	E-6
E.2.1 Fabrication Sequence	E-6
E.2.2 Treatment of H10 and H11/H12 Welds	E-7
E.3 Post-Processing Section Line Locations.....	E-7
E.4 Analysis Results.....	E-12
E.4.1 Residual Stresses Without Post Weld Heat Treatment.....	E-12
E.5 Section Line Data for Use in Crack Growth Calculations.....	E-28
E.6 Comparison to Previous Work	E-47
E.7 References.....	E-48

<i>F</i> INITIAL NRC SAFETY EVALUATION	F-1
<i>G</i> FINAL NRC SAFETY EVALUATION	G-1
<i>H</i> RECORD OF REVISIONS	H-1

LIST OF FIGURES

Figure 2-1 Typical Arrangement of Core Shroud and Support Structure (BWR-6)	2-2
Figure 2-2 BWR-2 Shroud Support Configuration	2-3
Figure 2-3 Hatch Unit 2 Shroud Support Configuration	2-4
Figure 2-4 Shroud Support Plate With Legs (CBIN BWR-4, 5, 6 Design).....	2-6
Figure 2-5 Shroud Support Plate With Legs (B&W BWR-3, 4 Design).....	2-7
Figure 2-6 Shroud Support Plate With Gussets Configuration (CE BWR-3, 4, and 5 Design).....	2-8
Figure 2-7 Geometry and Dimensions of the Core Support Structure at River Bend	2-10
Figure 2-8 Photomacrograph of Weld H8 at River Bend	2-11
Figure 2-9 Photomacrograph of Weld H9 at River Bend	2-12
Figure 2-10 Photomacrograph of Weld H10 at River Bend	2-13
Figure 2-11 Photomacrograph of Weld H12 at River Bend	2-14
Figure 3-1 Through-Thickness Measured Residual Stress Distribution (σ_x) for Weld H8	3-4
Figure 3-2 Through-Thickness Measured Residual Stress Distribution (σ_x) for Weld H9	3-5
Figure 3-3 Through-Thickness Measured Residual Stress Distribution (σ_x) for Weld H10	3-6
Figure 3-4 Through-Thickness Measured Residual Stress Distribution (σ_x) for Weld H12	3-7
Figure 3-5 Weld Section Line Definitions in Updated Analyses With Integrated Model.....	3-11
Figure 3-6 Comparison of Results from Initial and Updated Models (Initial Analysis) With Measured Residual Stress for Weld H-8.....	3-15
Figure 3-7 Comparison of Analytical Results from Initial and Updated Models With Measured Residual Stress for Weld H-9.....	3-16
Figure 3-8 Comparison of Analytical Results from Initial and Updated Models With Measured Residual Stress for Weld H10	3-17
Figure 3-9 Comparison of Analytical Results from Initial and Updated Models With Measured Residual Stress for Weld H12	3-18
Figure 3-10 Strain Gage and Cut Locations During Measurement at Grand Gulf	3-19
Figure 3-11 Deflection (Towards Vessel Wall) of Support Leg After Cutting	3-20
Figure 3-12 Change in Axial Strain in the Support Legs at Grand Gulf After Cutting	3-21
Figure 3-13 Change in Transverse Strains in the Support Legs at Grand Gulf After Cutting.....	3-22
Figure 3-14 Critical Residual Stress Distribution for Weld H8 from Updated Analyses (Run E, Section 3).....	3-25

Figure 3-15 Critical Residual Stress Distribution for Weld H9 from Updated Analyses (Run E, Section 4).....	3-26
Figure 3-16 Critical Residual Stress Distribution for Weld H10 from Updated Analyses (Run C, Section 5).....	3-27
Figure 3-17 Critical Residual Stress Distribution for Weld H11 from Updated Analyses (Run G, Section 3)	3-28
Figure 3-18 Critical Residual Stress Distribution for Weld H12 from Updated Analyses (Run B, Section 4).....	3-29
Figure 4-1 K_I Distribution for Weld H8 in As-Welded Condition	4-3
Figure 4-2 K_I Distribution for Weld H9 in As-Welded Condition	4-4
Figure 4-3 An Edge-Cracked Beam With Non-Uniform Thickness and Fixed Ends	4-6
Figure 4-4 Normalized K_I Computed for Weld H10	4-7
Figure 4-5 Normalized K_I for Weld H11.....	4-8
Figure 4-6 Normalized K_I for Weld H12.....	4-9
Figure 5-1 Proposed Disposition Curve for NWC at or Below Action Level 1.....	5-4
Figure 5-2 Proposed NWC Disposition Curve CAVS Data and Old GENE Lab Data.....	5-6
Figure 5-3 NWC Disposition Curve vs. Screened BWRVIP Alloy 182 Data	5-7
Figure 5-4 Comparison of NWC Curve With Field Inspection Field Data	5-8
Figure 5-5 Proposed High Purity NWC Disposition Curve	5-9
Figure 5-6 Comparison of High Purity NWC Disposition Curve With Screened Lab and CAV Data	5-10
Figure 5-7 HWC Disposition Curve Compared With CAVS and Lab Data Under HWC Conditions	5-11
Figure A-1 Alloy 182 Crack Growth Rate Dependency [A-15–A-18].....	A-8
Figure A-2 Alloy 182 Crack Growth Rate Dependency With Conductivity	A-9
Figure A-3 Crack Growth Rates for Alloy 182 (<0.5 $\mu\text{S}/\text{cm}$) [A-19–A-28]	A-10
Figure A-4 SCC Crack Growth Rates for Alloy 182 (<0.5 $\mu\text{S}/\text{cm}$ and >0.5 $\mu\text{S}/\text{cm}$: [A-19–A- 26])	A-11
Figure A-5 SCC Crack Growth Rates for Nickel Base Alloys as a Function of Conductivity [A-29]	A-12
Figure A-6 SCC Crack Growth Rates for Alloy 600	A-13
Figure A-7 CAVS Alloy 182 Data: Limerick 1.....	A-18
Figure A-8 CAVS Data from Various Plants [A-19–A-25]	A-19
Figure A-9 Comparison of the Predicted and Observed Rates vs. Stress Intensity for Data on Alloy 182 [A-19–A-25].....	A-19
Figure A-10 Field Inspection Crack Growth Rate Data (as a Function of Time when Inspection was Performed)	A-20
Figure A-11 Inspection Field Data: Axial and Circumferential Nozzle Cracking	A-21
Figure A-12 GENE Lab and CAV Data vs. K Level	A-23
Figure A-13 CAVS Data Along With GENE Disposition Band	A-24
Figure A-14 Alloy 600 CAVS Data (All ECP Conditions)	A-25

Figure A-15 Full BWRVIP Alloy 182 Data Base.....	A-26
Figure A-16 BWRVIP Alloy 182 Data Screened by GE	A-27
Figure A-17 CAVS Data Under HWC Conditions	A-29
Figure A-18 Alloy 600 CAVS Data (ECP < -230mV, she).....	A-30
Figure A-19 Crack Growth Rates for Alloy 182 Compared With PLEDGE Predictions.....	A-32
Figure A-20 PLEDGE Calculations vs. Proposed NWC Disposition Curve	A-33
Figure A-21 Proposed Disposition Curve for NWC at or Below Action Level 1	A-36
Figure A-22 Proposed NWC Disposition Curve vs. GENE CAV and Lab Data	A-37
Figure A-23 NWC Disposition Curve vs. Screened BWRVIP Alloy 182 Data	A-38
Figure A-24 Comparison of NWC Curve With Field Inspection Field Data	A-39
Figure A-25 Proposed High Purity NWC Disposition Curve	A-41
Figure A-26 Proposed NWC Disposition Curved With CAVS Data and Old GENE Curves ...	A-42
Figure A-27 Comparison of High Purity NWC Disposition Curve With Screened Lab and CAV Data	A-43
Figure A-28 Proposed HWC Disposition Curve	A-44
Figure A-29 HWC Disposition Curve Compared With CAVS and Lab Data Under HWC Conditions	A-45
Figure A-30 PLEDGE Calculations vs. Proposed Curves.....	A-46
Figure A-31 Proposed Disposition Curves vs. SKI Curves	A-47
Figure B-1 Illustration of Linear Superposition for Determining Strains Due to Introducing a Crack into Body With Residual Stresses.....	B-2
Figure B-2 Residual Stress Distribution Measured By Introducing a Cut of Increasing Depth while the Change of Strain is Recorded by Strain Gages on the Back Face.....	B-3
Figure B-3 Finite Element Mesh for the Specimen Containing Weld H8 to Model a Cut through the Thickness of the Shroud Support Plate	B-5
Figure B-4 Strain Readings Recorded when σ of Progressively Increasing Depth Introduced to Weld H8	B-5
Figure B-5 Residual Radial Stress Distribution (σ_x) for Weld H8 as a Function of the Distance Normalized by the Thickness of the Shroud Support Plate.....	B-6
Figure B-6 Specimen Configuration and Finite Element Mesh for Weld H10	B-7
Figure B-7 Strain Readings Recorded when a Cut of Progressively Increasing Depth Introduced to Weld H10	B-8
Figure B-8 Residual Axial Stress Distribution (σ_z) for Weld H10 as a Function of the Distance Normalized by the Thickness of the Shroud Support Cylinder.....	B-8
Figure B-9 Finite Element Mesh for the Specimen Containing Weld H9. The Residual Axial Stress Distribution σ_x is Measured through the Thickness of the Shroud Support Plate. Also Shown is the Location of the Near Surface Measurement No. 1.....	B-9
Figure B-10 Strain Readings Recorded when a Cut of Progressively Increasing Depth Introduced to Weld H9 through the Thickness of the Shroud Support Plate.....	B-10
Figure B-11 Residual Radial Stress Distribution (σ_x) as a Function of the Distance Normalized by the Thickness of the Shroud Support Plate (Baffle Plate) for Weld H9...	B-10

Figure B-12 Finite Element Mesh for the Specimen Containing Weld H9. The Residual Axial Stress Distribution (σ_z) is Measured through the Thickness of the Vessel Wall. Also Shown is the Location of the Near Surface Measurement No. 2	B-11
Figure B-13 Strain Readings Recorded when a Cut of Progressively Increasing Depth Introduced to Weld H9 through the Thickness of the Vessel Wall	B-12
Figure B-14 Residual Axial Stress Distribution (σ_z) as a Function of the Distance Normalized the Thickness of the Vessel Wall for Weld H9	B-12
Figure B-15 Finite Element Mesh for the Specimen Containing the Shroud Support Leg Weld (H12)	B-13
Figure B-16 Strain Readings Recorded when a Cut of Progressively Increasing Depth Introduced through the Thickness of the Shroud Support Leg Weld (H12).....	B-14
Figure B-17 Residual Stress Distribution (Normal to the Plane of Cut) for Weld H12 as a Function of the Distance Normalized by the Thickness of the Shroud Support Leg Weld on the Plane of Cut	B-14
Figure B-18 Near Surface Residual Stress Distribution as a Function of the Distance Measured at the Location Shown in Figure B-9 for Weld H9	B-15
Figure B-19 Near Surface Residual Stress Distribution in the Weld as a Function of the Distance Measured at the Location Shown in Figure B-12 for Weld H9	B-16
Figure D-1 Reactor Vessel and Shroud Support Model.....	D-2
Figure D-2 Model Weld Geometry	D-3
Figure D-3 Weld H8 Weld Sequence and Approximate Mesh.....	D-10
Figure D-4 Weld H9 Weld Sequence and Approximate Mesh.....	D-10
Figure D-5 Weld H10 Weld Sequence and Approximate Mesh.....	D-11
Figure D-6 Weld H11 Weld Sequence and Approximate Mesh.....	D-12
Figure D-7 Weld H12 Weld Sequence and Approximate Mesh.....	D-13
Figure D-8 Weld H8 After Welding Radial Stress (SX)	D-18
Figure D-9 Weld H8 After Welding Circumferential Stress (SY)	D-18
Figure D-10 Weld H9 After Welding Radial Stress (SX)	D-19
Figure D-11 Weld H9 After Welding Circumferential Stress (SY)	D-19
Figure D-12 Weld H10 After Welding Vertical Stress (SZ)	D-20
Figure D-13 Weld H10 After Welding Circumferential Stress (SY)	D-20
Figure D-14 Weld H11 After Welding Vertical Stress (SZ)	D-21
Figure D-15 Weld H11 After Welding Circumferential Stress (SY)	D-21
Figure D-16 Weld H12 After Welding Perpendicular Stress (SZ)	D-22
Figure D-17 Weld H12 After Welding Circumferential Stress (SY)	D-22
Figure D-18 Weld H10 After Welding Upper HAZ (from Above) Vertical Stress (SZ).....	D-23
Figure D-19 Weld H10 After Welding Lower HAZ (from Below) Vertical Stress (SZ)	D-24
Figure D-20 Weld H11 After Welding Upper HAZ (from Above) Vertical Stress (SZ).....	D-24
Figure D-21 Weld H11 After Welding Lower HAZ (from Below) Vertical Stress (SZ)	D-25
Figure D-22 Weld H12 After Welding Upper HAZ (from Above) Perpendicular Stress (SZ)	D-25

Figure D-23 Weld H12 After Welding Lower HAZ (from Below) Perpendicular Stress (SZ) ...	D-26
Figure D-24 Weld H8 After PWHT Radial Stress (SX)	D-27
Figure D-25 Weld H8 After PWHT Circumferential Stress (SY)	D-27
Figure D-26 Weld H9 After PWHT Radial Stress (SX)	D-28
Figure D-27 Weld H9 After PWHT Circumferential Stress (SY)	D-28
Figure D-28 Weld H10 After PWHT Vertical Stress (SZ).....	D-29
Figure D-29 Weld H10 After PWHT Circumferential Stress (SY)	D-29
Figure D-30 Weld H11 After PWHT Vertical Stress (SZ).....	D-30
Figure D-31 Weld H11 After PWHT Circumferential Stress (SY)	D-30
Figure D-32 Weld H12 After PWHT Perpendicular Stress (SZ).....	D-31
Figure D-33 Weld H12 After PWHT Circumferential Stress (SY)	D-31
Figure D-34 H8 Support Cylinder HAZ After Welding – Leg Centerline	D-33
Figure D-35 H8 Support Cylinder HAZ After Stress Relief – Leg Centerline	D-33
Figure D-36 H8 Support Plate HAZ After Welding – Leg Centerline	D-34
Figure D-37 H8 Support Plate HAZ After Stress Relief – Leg Centerline	D-34
Figure D-38 H8 Weld Centerline After Welding – Leg Centerline.....	D-35
Figure D-39 H8 Weld Centerline After Stress Relief – Leg Centerline.....	D-35
Figure D-40 H9 Reactor Vessel HAZ After Welding – Leg Centerline	D-36
Figure D-41 H9 Reactor Vessel HAZ After Stress Relief – Leg Centerline.....	D-36
Figure D-42 H9 Support Plate HAZ After Welding – Leg Centerline	D-37
Figure D-43 H9 Support Plate HAZ After Stress Relief – Leg Centerline	D-37
Figure D-44 H9 Weld Centerline After Welding – Leg Centerline.....	D-38
Figure D-45 H9 Weld Centerline After Stress Relief – Leg Centerline.....	D-38
Figure D-46 H10 Upper HAZ After Welding – Leg Centerline	D-39
Figure D-47 H10 Upper HAZ After Stress Relief – Leg Centerline	D-39
Figure D-48 H10 Lower HAZ After Welding – Leg Centerline	D-40
Figure D-49 H10 Upper HAZ After Stress Relief – Leg Centerline	D-40
Figure D-50 H10 Weld Centerline After Welding – Leg Centerline.....	D-41
Figure D-51 H10 Weld Centerline After Stress Relief – Leg Centerline.....	D-41
Figure D-52 H11 Upper HAZ After Welding – Leg Centerline	D-42
Figure D-53 H11 Upper HAZ After Stress Relief – Leg Centerline	D-42
Figure D-54 H11 Lower HAZ After Welding – Leg Centerline	D-43
Figure D-55 H11 Lower HAZ After Stress Relief – Leg Centerline	D-43
Figure D-56 H11 Weld Centerline After Welding – Leg Centerline.....	D-44
Figure D-57 H11 Weld Centerline After Stress Relief – Leg Centerline.....	D-44
Figure D-58 H12 Upper HAZ After Welding – Leg Centerline	D-45
Figure D-59 H12 Upper HAZ After Stress Relief – Leg Centerline	D-45
Figure D-60 H12 Lower HAZ After Welding – Leg Centerline	D-46
Figure D-61 H12 Lower HAZ After Stress Relief – Leg Centerline	D-46

Figure D-62 H12 Weld Centerline After Welding – Leg Centerline	D-47
Figure D-63 H12 Weld Centerline After Stress Relief – Leg Centerline.....	D-47
Figure D-64 H8 Cut Line Residual Stresses Perpendicular to Cut Line	D-49
Figure D-65 H9 Cut Line Residual Stresses Perpendicular to Cut Line	D-50
Figure D-66 H10 Cut Line Residual Stresses Perpendicular to Cut Line – Large Weld Cap on Backgouge.....	D-51
Figure D-67 H12 Cut Line Residual Stresses Perpendicular to Cut Line – After Removal of Bottom Weld.....	D-52
Figure D-68 Residual Stress through RPV Wall Below H9 Weld.....	D-53
Figure D-69 Weld H8 Residual Stress (S_x) – Stresses on Cut Line – Crack Propagating from Bottom to Top	D-55
Figure D-70 Weld H9 With PWHT Residual Stress (S_x) – Stresses on Cut Line – Crack Propagating from Top to Bottom	D-56
Figure E-1 Reactor Vessel and Shroud Support Model.....	E-3
Figure E-2 Model Weld Geometry	E-4
Figure E-3 Weld H8 Section Line Definitions.....	E-8
Figure E-4 Weld H9 Section Line Definitions.....	E-9
Figure E-5 Weld H10 Section Line Definitions.....	E-10
Figure E-6 Weld H11 Section Line Definitions.....	E-11
Figure E-7 Weld H12 Section Line Definitions.....	E-12
Figure E-8 Weld H8 After Welding Radial Stress (S_X) (Run A-Alt. Sequence With H12 Geometry)	E-13
Figure E-9 Weld H8 After Welding Circumferential Stress (S_Y) (Run A-Alt. Sequence With H12 Geometry)	E-13
Figure E-10 Weld H9 After Welding Radial Stress (S_X) (Run A-Alt. Sequence With H12 Geometry)	E-14
Figure E-11 Weld H9 After Welding Circumferential Stress (S_Y) (Run A-Alt. Sequence With H12 Geometry)	E-14
Figure E-12 Weld H10 After Welding Vertical Stress (S_Z) (Run A-Alt. Sequence With H12 Geometry).....	E-15
Figure E-13 Weld H10 After Welding Circumferential Stress (S_Y) (Run A-Alt. Sequence With H12 Geometry)	E-15
Figure E-14 Weld H11 After Welding Vertical Stress (S_Z) (Run G-Alt. Sequence With H11 Geometry).....	E-16
Figure E-15 Weld H11 After Welding Circumferential Stress (S_Y) (Run G-Alt. Sequence With H11 Geometry)	E-16
Figure E-16 Weld H12 After Welding Perpendicular Stress (S_Z) (Run A-Alt. Sequence With H12 Geometry)	E-17
Figure E-17 Weld H12 After Welding Circumferential Stress (S_Y) (Run A-Alt. Sequence With H12 Geometry)	E-17
Figure E-18 Weld H8 After Welding Radial Stress (S_X) (Run D-Orig. Sequence With H12 Geometry)	E-18

Figure E-19 Weld H8 After Welding Circumferential Stress (SY) (Run D-Orig. Sequence With H12 Geometry)	E-18
Figure E-20 Weld H9 After Welding Radial Stress (SX) (Run D-Orig. Sequence With H12 Geometry)	E-19
Figure E-21 Weld H9 After Welding Circumferential Stress (SY) (Run D-Orig. Sequence With H12 Geometry)	E-19
Figure E-22 Weld H10 After Welding Vertical Stress (SZ) (Run D-Orig. Sequence With H12 Geometry).....	E-20
Figure E-23 Weld H10 After Welding Circumferential Stress (SY) (Run D-Orig. Sequence With H12 Geometry)	E-20
Figure E-24 Weld H11 After Welding Vertical Stress (SZ) (Run H-Orig. Sequence With H11 Geometry).....	E-21
Figure E-25 Weld H11 After Welding Circumferential Stress (SY) (Run H-Orig. Sequence With H11 Geometry)	E-21
Figure E-26 Weld H12 After Welding Perpendicular Stress (SZ) (Run D-Orig. Sequence With H12 Geometry)	E-22
Figure E-27 Weld H12 After Welding Circumferential Stress (SY) (Run D-Orig. Sequence With H12 Geometry)	E-22
Figure E-28 Weld H9 After Welding Radial Stress (SX) (Run A-Alt. Sequence With H12 Geometry)	E-23
Figure E-29 Weld H9 After Welding Radial Stress (SX) (Run B-Alt. Sequence With H12 Geometry and Weld H9 Reversed)	E-23
Figure E-30 Weld H12 After Welding Perpendicular Stress (SZ) (Run A-Alt. Sequence With H12 Geometry)	E-24
Figure E-31 Weld H12 After Welding Perpendicular Stress (SZ) (Run C- Alt. Sequence With H12 Geometry and Weld H12 Reversed)	E-24
Figure E-32 Weld H9 After Welding Radial Stress (SX) (Run D- Orig. Sequence With H12 Geometry).....	E-25
Figure E-33 Weld H9 After Welding Radial Stress (SX) (Run E- Orig. Sequence With H12 Geometry and Weld H9 Reversed)	E-25
Figure E-34 Weld H12 After Welding Perpendicular Stress (SZ) (Run D- Orig. Sequence With H12 Geometry)	E-26
Figure E-35 Weld H12 After Welding Perpendicular Stress (SZ) (Run F- Orig. Sequence With H12 Geometry and Weld H12 Reversed)	E-26
Figure E-36 H8 Cut Line Residual Stresses Perpendicular to Cut Line (Run A)	E-28
Figure E-37 H9 Cut Line Residual Stresses Perpendicular to Cut Line (Run A)	E-29
Figure E-38 H10 Cut Line Residual Stresses Perpendicular to Cut Line (Run A)	E-29
Figure E-39 H12 Cut Line Residual Stresses Perpendicular to Cut Line (Run A)	E-30
Figure E-40 H8 Cut Line Residual Stresses Perpendicular to Cut Line (Run B)	E-30
Figure E-41 H9 Cut Line Residual Stresses Perpendicular to Cut Line (Run B)	E-31
Figure E-42 H10 Cut Line Residual Stresses Perpendicular to Cut Line (Run B)	E-31
Figure E-43 H12 Cut Line Residual Stresses Perpendicular to Cut Line (Run B)	E-32
Figure E-44 H8 Cut Line Residual Stresses Perpendicular to Cut Line (Run C)	E-32

Figure E-45 H9 Cut Line Residual Stresses Perpendicular to Cut Line (Run C)	E-33
Figure E-46 H10 Cut Line Residual Stresses Perpendicular to Cut Line (Run C)	E-33
Figure E-47 H12 Cut Line Residual Stresses Perpendicular to Cut Line (Run C)	E-34
Figure E-48 H8 Cut Line Residual Stresses Perpendicular to Cut Line (Run D)	E-34
Figure E-49 H9 Cut Line Residual Stresses Perpendicular to Cut Line (Run D)	E-35
Figure E-50 H10 Cut Line Residual Stresses Perpendicular to Cut Line (Run D)	E-35
Figure E-51 H12 Cut Line Residual Stresses Perpendicular to Cut Line (Run D)	E-36
Figure E-52 H8 Cut Line Residual Stresses Perpendicular to Cut Line (Run E)	E-36
Figure E-53 H9 Cut Line Residual Stresses Perpendicular to Cut Line (Run E)	E-37
Figure E-54 H10 Cut Line Residual Stresses Perpendicular to Cut Line (Run E)	E-37
Figure E-55 H12 Cut Line Residual Stresses Perpendicular to Cut Line (Run E)	E-38
Figure E-56 H8 Cut Line Residual Stresses Perpendicular to Cut Line (Run F).....	E-38
Figure E-57 H9 Cut Line Residual Stresses Perpendicular to Cut Line (Run F).....	E-39
Figure E-58 H10 Cut Line Residual Stresses Perpendicular to Cut Line (Run F).....	E-39
Figure E-59 H12 Cut Line Residual Stresses Perpendicular to Cut Line (Run F).....	E-40
Figure E-60 H8 Cut Line Residual Stresses Perpendicular to Cut Line (Run G).....	E-40
Figure E-61 H9 Cut Line Residual Stresses Perpendicular to Cut Line (Run G).....	E-41
Figure E-62 H10 Cut Line Residual Stresses Perpendicular to Cut Line (Run G).....	E-41
Figure E-63 H11 Cut Line Residual Stresses Perpendicular to Cut Line (Run G).....	E-42
Figure E-64 H8 Cut Line Residual Stresses Perpendicular to Cut Line (Run H)	E-42
Figure E-65 H9 Cut Line Residual Stresses Perpendicular to Cut Line (Run H)	E-43
Figure E-66 H10 Cut Line Residual Stresses Perpendicular to Cut Line (Run H)	E-43
Figure E-67 H11 Cut Line Residual Stresses Perpendicular to Cut Line (Run H)	E-44
Figure E-68 H8 Cut Line Residual Stresses Perpendicular to Cut Line 3 (Runs A to H)	E-44
Figure E-69 H9 Cut Line Residual Stresses Perpendicular to Cut Line 4 (Runs A to H)	E-45
Figure E-70 H10 Cut Line Residual Stresses Perpendicular to Cut Line 5 (Runs A to H)	E-45
Figure E-71 H11 Cut Line Residual Stresses Perpendicular to Cut Line 3 (Runs G and H)	E-46
Figure E-72 H12 Cut Line Residual Stresses Perpendicular to Cut Line 4 (Runs A to F)	E-46
Figure E-73 H11 and H12 Cut Line Residual Stresses Perpendicular to Cut Line 4 (No Weld Reversal).....	E-47
Figure E-74 H8 Cut Line Residual Stresses Perpendicular to Cut Line 1 (Run D) vs. Appendix D Work	E-49
Figure E-75 H9 Cut Line Residual Stresses Perpendicular to Cut Line 2 (Run D) vs. Appendix D Work	E-50
Figure E-76 H10 Cut Line Residual Stresses Perpendicular to Cut Line 3 (Run D) vs. Appendix D Work	E-51
Figure E-77 H12 Cut Line Residual Stresses Perpendicular to Cut Line 1 (Run D) vs. Appendix D Work	E-52

LIST OF TABLES

Table 3-1 Assembly and Welding Sequences Considered in the Integrated Model (from Appendix E).....	3-23
Table 3-2 Strain Measurement for Grand Gulf Support Legs	3-24
Table 6-1 Crack Growth Evaluation Input	6-2
Table 6-2 Crack Growth Evaluation Results	6-2
Table A-1 Pilgrim Nozzle Cracking Data.....	A-5
Table A-2 Lists of Plants With Nozzle/Safe End Cracking	A-6
Table A-3 Summary of Access Hole Cover Cracking in U.S. Plants.....	A-7
Table A-4 GENE Efforts in Evaluating and Dispositioning Cracking in Alloy 182 Welds	A-14
Table A-5 Field Cracking Data for Nozzle-to-Safe End Alloy 182 Initial Inspection	A-16
Table A-6 Field Cracking Data for Nozzle-to-Safe End Alloy 182 After Re-Inspection	A-17
Table A-7 Field Cracking Data for Nozzle-to-Safe End Alloy 182 After Second Re-Inspection.....	A-17
Table B-1 Material Properties Used in Computation.....	B-6
Table B-2 Configuration and Strains Measured for Near Surface Stress Measurement No. 1 of Weld H9.....	B-17
Table B-3 Configuration and Strains Measured for Near Surface Stress Measurement No. 2 of Weld H9.....	B-18
Table D-1 Temperature-Dependent Material Properties Used in Finite Element Analysis	D-7
Table D-2 Peak Residual Stresses	D-32
Table H-1 Revision Details	H-2

1

INTRODUCTION

1.1 Background

The nickel based austenitic alloys, wrought alloy 600 and the weld metals alloy 82 and 182, have been used extensively in boiling water reactor (BWR) application where excellent material toughness, compatibility with vessel material properties and resistance to stress corrosion cracking (SCC) are required. Included in those structural applications are vessel internals components such as:

- access hole covers
- safe ends
- shroud head bolts
- shroud support structure
- vessel attachment brackets

Although the performance of these alloys has generally been excellent in these and other BWR structural applications, some modest incidents of intergranular stress corrosion cracking (IGSCC) have occurred. These cracking incidents, combined with laboratory data illustrating susceptibility of these alloys to IGSCC initiation and growth, have resulted in major research activities sponsored by the Electric Power Research Institute (EPRI), vendors and contractors such as General Electric Company (GE), research groups and the Nuclear Regulatory Commission (NRC) to understand and mitigate the cracking problem in these alloys.

The BWR Vessel and Internals Project (BWRVIP) has prepared a safety assessment of BWR internals [1] addressing issues requiring resolution affecting vessel internals components. Among the issues requiring resolution are the issues of crack growth rates among the various structural materials comprising the vessel internals. An earlier BWRVIP report developed IGSCC crack growth correlations for austenitic stainless steel as a function of water quality, electrochemical potential (ECP) and stress or stress intensity [2]. The methodology utilized in the austenitic stainless steel activity was to determine the crack growth rate as a function of stress intensity for various water purity and ECP conditions, assess the state of applied and residual stress (including weld residual stress) on the core shroud by analytical and experimental methods and develop stress intensity models for which crack growth rates could be determined. Because of the differences in performance of nickel based alloys relative to stainless steel and the differences in the structural configurations for which these materials are used in the RPV internals, it is necessary to develop an independent crack growth model for application to nickel based alloys.

1.2 Susceptibility of Nickel Based Components in the BWR Environment

The objective of this report is to provide the methodology to disposition a flaw in a nickel based component in the BWR environment. To that end, the susceptibility of these materials to IGSCC must be provided. Of specific importance to a flaw disposition evaluation is the crack growth rate of the material. The susceptibility of these materials to crack initiation, while important to the overall reliability of these components, is not the specific charter of this document.

The materials of the shroud support structures are mainly nickel based alloys 600, 82, and 182. The performance of these alloys in BWR service has been quite good. In some instances, IGSCC has initiated in these materials where crevices or weld root defects have been observed. These locations include creviced thermal sleeve attachment to nozzle safe ends, a feedwater nozzle where a weld root defect initiated IGSCC and access hole covers (AHC) where partial penetration welding was sometimes performed. In these instances, the cracking has occurred predominately in Alloy 182, the nickel base flux-coated electrode used for welding these components. Some limited cracking has also been observed in the Alloy 182 welds where crevices or weld root defects were not obviously present. These incidences include cracking in a recirculation system outlet nozzle to safe end butter in a domestic BWR and in steam dryer assembly attachment brackets in two foreign BWRs. In most instances where IGSCC has occurred, the cracking was limited in extent, involving multiple short cracks. Some were circumferential, such as in access hole covers and in nozzle to safe end welds. Some were axial, crossing a weld bead as observed in nozzle to safe end welds. In most documented cases of IGSCC in the BWR, the cracking initiated in the Alloy 182 weld metal, propagating in some instances into the Alloy 600 wrought material or progressing slightly into the low alloy steel nozzle to which the Alloy 182 was welded.

The mechanism for IGSCC in nickel based alloys in the BWR environment appears to be similar to that for austenitic stainless steel. The generally accepted factors responsible for IGSCC of these alloys are sufficient tensile stress, thermal sensitization and a sufficiently oxidizing environment. As in the case of austenitic stainless steels, additional aggravating factors include the presence of crevices.

The following paragraphs describe briefly the susceptibility of each of the nickel base alloys to IGSCC initiation and propagation. More details of the susceptibility of these alloys to IGSCC in the BWR environment are provided in References [3, 4 and 5].

- Alloy 600

Alloy 600 has been used extensively as the structural material of the shroud support in the BWR. The IGSCC performance of Alloy 600 in the absence of crevices has been excellent. Recent in-reactor and laboratory testing sponsored by EPRI [3] has confirmed the high IGSCC initiation resistance of this alloy. In these in-reactor tests, investigators reported that following two years of exposure of bolt loaded specimens loaded to a 0.25 mm deflection, crack initiation was observed in only one of twenty-six specimens. Laboratory crack propagation tests using continuous reversing direct current (DC) electrical measurements of Alloy 600, in a BWR “clean” NWC environment, revealed that some modest crack propagation occurred in constant load tests. The data clearly show that the crack growth rate for Alloy 600 is lower than that for Alloy 182 and lower than that predicted by NUREG-0313, Revision 2 [6] for sensitized stainless steel.

Alloy 600 has, however, exhibited cracking in locations where crevices are involved, such as reactor inlet nozzle safe-ends, access hole covers (AHCs), and shroud head bolts.

- Alloy 182

Alloy 182 is typically utilized within the reactor pressure vessel for limited vessel cladding application, vessel attachment pad buildups, the shroud support plate to vessel pad weld, the shroud support gusset welds, the shroud support leg welds, the shroud support to shroud weld and the access hole cover to shroud support plate weld.

Recent in-reactor and laboratory testing has confirmed the IGSCC crack growth can occur in Alloy 182 material in the BWR environment [3]. Crack propagation tests on Alloy 182 in a “clean” NWC environment in the laboratory demonstrated significant crack growth. The highest crack growth rate in this material approximates that of the NUREG-0313, Revision 2 [6] curve for Type 304 stainless steel.

In the HWC environment, one group of investigators has determined that IGSCC growth, once initiated in Alloy 182, does continue, but at a rate which is roughly one order of magnitude slower than that in the NWC environment [3]. Another investigation found that in the HWC environment, particularly with noble metal chemical addition, crack growth was further reduced to Alloy 600 levels [7]. Both of these investigations demonstrate that crack growth is significantly reduced in the HWC environment for Alloy 182.

The use of Alloy 182 weld material in the fabrication of the shroud support structure makes the shroud support welds susceptible to IGSCC in the normal BWR environment. However, because of the residual stress distribution expected in these welds (see Section 3), and the inherent IGSCC initiation resistance of these alloys in the BWR, cracking is expected to be limited in extent.

- Alloy 82

Alloy 82 is a bare filler wire which is used in BWRs where very high quality gas tungsten arc-welding (GTAW) is employed. It has been widely used as a welding insert for butt welds, and is used for the root and hot passes of many structural welds. This alloy is higher in chromium and lower in carbon than Alloy 182 and, therefore, has improved resistance to IGSCC initiation and growth in the BWR environment compared to Alloy 182. EPRI-sponsored testing has verified the excellent resistance of this alloy to IGSCC, and the NRC has identified this material as an IGSCC resistant alloy in NUREG-0313, Revision 2 [6]. In the HWC environment, the IGSCC resistance of Alloy 82 is further enhanced.

1.3 BWR Plant Operating Experience

The operating experience with nickel based alloys in the BWR environment has been excellent, provided no design or metallurgical crevice is present (such as a weld defect). A total of 34 domestic BWRs have had either visual or UT inspection performed of their nickel based wrought materials and weld metal [8]. As a result of these inspections, the only cracking associated with the core shroud in nickel based alloys occurred in the shroud support at Nine Mile Point, Unit 1 (NMP-1). The inspection performed during the 1996 outage at NMP-1, revealed one short crack in the Alloy 182 weld metal. A subsequent inspection performed in 1997 revealed that this indication had not changed.

The indications reported in the steam dryer bracket attachment of a foreign BWR as noted earlier in Section 1.2 of this report were removed prior to return to service. No new indications have been reported at that plant. The cracking in the recirculation system outlet nozzle to safe end reported in Section 1.2 of this report was removed and the component was rewelded with corrosion resistant Alloy 82 and returned to service.

In summary, the performance of Alloy 182 and the other nickel based alloys used as structural materials in the BWR has been good, when crevices or weld root defects are absent. Crack initiation in uncreviced components has been limited in extent in these materials as noted above. Where crack initiation has occurred, the crack extension on the surface appears to have been limited, consistent with the observation that crack initiation is difficult in these materials. This observation has also been confirmed by laboratory testing which has demonstrated the difficulty in initiating IGSCC in nickel based alloys in simulated BWR environments where crevices or weld root defects are absent.

1.3.1 Surface Crack Growth Rates of Nickel Base Alloys

As highlighted above, only limited crack initiation has been observed in non-creviced nickel base alloys in BWR service. The three plants having reported indications noted that the extent of surface cracking was limited. In each case, the defects were allowed to remain during one or more additional operating cycles. Little or no surface crack extension was observed in the plants where the cracking had been observed. In the foreign plant, the indications were observed for three years before removal. In one of the domestic BWRs, the indications are still being monitored. The cracked component was removed and rewelded in the other domestic BWR.

The field observations support several conclusions. For these internal components and their welds, the stresses are almost entirely attributable to residual stresses. The observations show that under these conditions, un-creviced nickel base alloys are more resistant to crack initiation in the BWR environment than austenitic stainless steels. Therefore, one would expect little new crack initiation in regions adjacent to any detected crack and would expect that the measured rate of length extension would be the same as the rate for through-wall crack growth.

1.4 Objectives and Approach

The objective of this report is to formalize the methodology for determination of nickel base austenitic alloy crack growth rates, based on empirical data that account for parameters that are known to affect crack propagation in the BWR. These crack growth rates (CGR) will then be available for use in the evaluation, inspection and repair criteria for BWR RPV internal components. The scope of CGR influencing factors will be tied to material susceptibility, water environment, and stress-state parameters associated with the core support structure welds. A model is presented that incorporates the effects of the important factors into a conservative, yet realistic, crack growth disposition curves for nickel based alloys in the BWR internals. The model developed in this report is developed for through-thickness crack growth based upon available test data and is based upon analysis of available test data. The model has been formulated with material, environment, and stress data which result from laboratory and in-plant test programs. It is then tested against field data and found to provide realistic upper bound estimates of growth rates observed over the BWR operating regime.

Although several different structural configurations for the core support structure have been used in BWRs, the present study focuses on the structural configuration of a BWR-6 because it is believed that this configuration can be used to bound the BWR-3 and 4s. Other work done by the BWRVIP on the core shroud and the reactor pressure vessel addresses the welds of the other core shroud support structures. The motivation for choosing a BWR-6 design for this study lies in the fact that components from two plants of that design (River Bend Nuclear Station and Grand Gulf Nuclear Station) were readily available for experimental measurements of residual stresses. The analytical studies used in this report were benchmarked against the experimental residual stress measurements and once benchmarked and found to be valid, can be used generically. The present study focuses on five welds of a BWR-6. These are welds H8, H9, H10, H11 and H12. Experimental measurements were performed only on welds H8, H9, H10 and H12 since no weld exists for the H11 location at River Bend or at Grand Gulf. However the analytical evaluations are also extended to Weld H11.

The following sections of this report describe the work undertaken within this project to understand the state of stress, and material variability on the crack growth rates of nickel base alloys in the core shroud support structure. Section 2 provides a description of the various core shroud support structure designs in the BWR industry and the materials used in the fabrication of the structure. The IGSCC susceptibility of these materials and their field performance is also discussed in this section. Section 3 provides the operating and residual stress data for the core support structure welds. Fracture mechanics methods employed in determining the stress intensity factors associated with the applied and residual stresses are presented in Section 4. Section 5 presents a compilation and assessment of crack growth data produced by laboratories and in field testing. This collection of data provides a compiled database for use in determining crack growth rates as a function of environment and stress intensity in nickel base austenitic alloys. This section also provides crack growth rate disposition curves developed using material, environment and stress information. Section 6 presents crack growth evaluation methodology for estimation of crack growth rates in the through-thickness direction for BWR shroud support structure welds.

1.5 Implementation Requirements

In accordance with the implementation requirements of Nuclear Energy Institute (NEI) 03-08, *Guideline for the Management of Materials Issues*, the crack growth rate disposition equations described in Section 7 are considered “needed” when performing flaw evaluation on the materials covered by this report. The remaining sections of the report are provided for information only.

2

BWR SHROUD SUPPORT WELD CONFIGURATIONS

The shroud support structures for most BWRs are defined as those structural regions below the H7 weld in the core shroud (Figure 2-1). The shroud support consists generally of the support plate and cylinder and generally includes either gussets or legs. The shroud support structure is typically fabricated from Alloy 600 although in some plants Type 304 stainless steel was used. For all nickel alloy welds, the weld metal used was either Alloy 82 or 182.

The purpose for the shroud support is to provide support for the core plate, jet pumps, core shroud, top guide, core spray spargers and annulus piping and the shroud head/steam separator dryer assembly. The shroud support also supports the weight of peripheral fuel bundles, and provides lateral restraint to the fuel during seismic or other dynamic events. The shroud support also forms part of the core coolant envelope in the event of a recirculation system line break (loss of coolant accident).

There are several shroud support designs, varying from one BWR model to another and even within a BWR model design. The basic four designs are identified as follows:

- Conical Shroud Support Plate (BWR-2)
- Thick Shroud Support Plate (Hatch Unit 2)
- Shroud Support Plate with Legs
- Shroud Support Plate with Gussets

Detailed descriptions of these designs are provided in Reference [9]. For completeness, abbreviated descriptions from the Reference [9] report are repeated in the following sections.

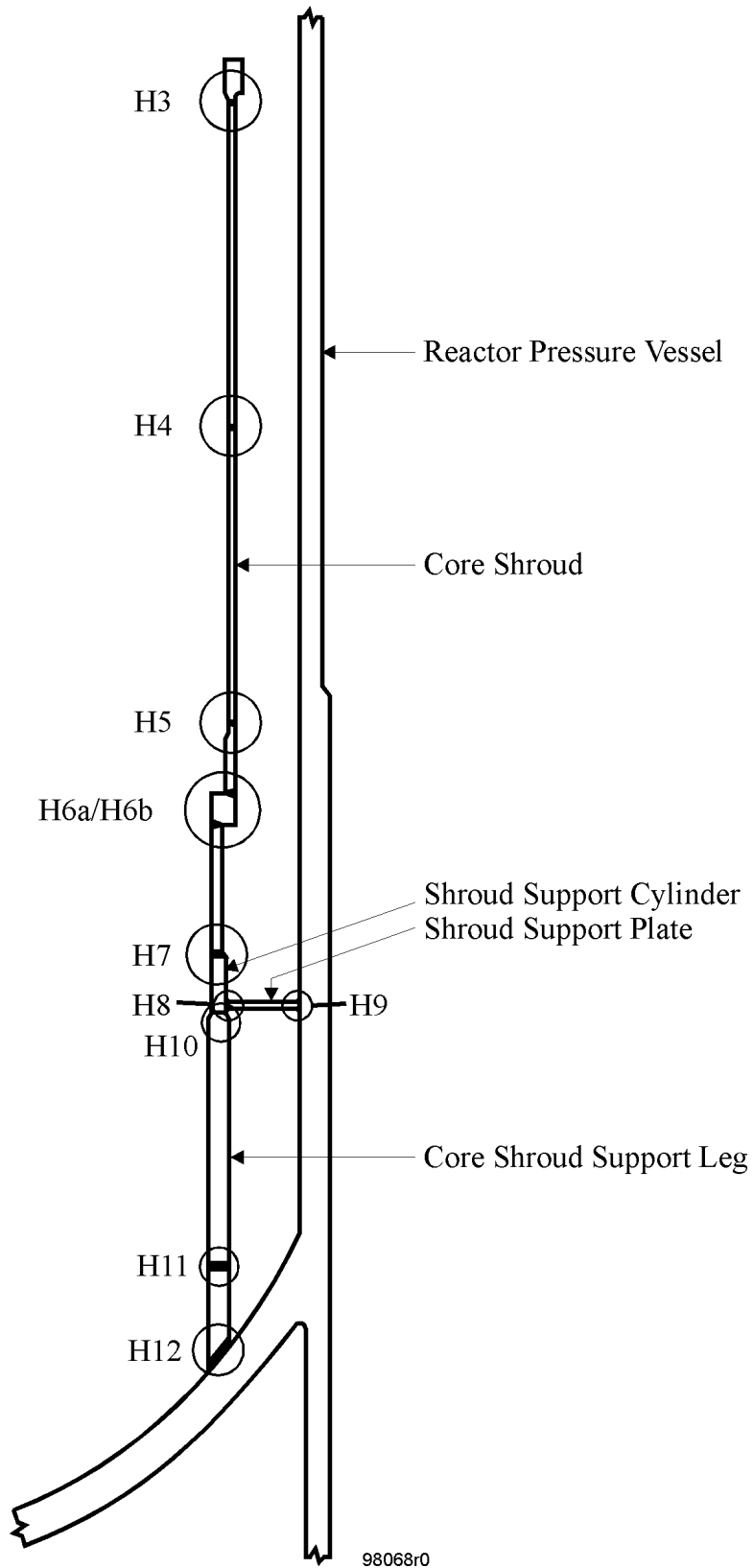


Figure 2-1
Typical Arrangement of Core Shroud and Support Structure (BWR-6)

2.1 Conical Shroud Support Plate (BWR-2)

The shroud support in the two operating U.S. BWR-2 plants (Nine Mile Point Unit 1 and Oyster Creek) is a 1.5 inch thick conical design fabricated by Combustion Engineering (CE). This configuration is shown in Figure 2-2. The conical shroud support plate is fabricated from Alloy 600 material, with Alloy 82/182 welds connecting it to the low alloy steel RPV wall (H9 weld) and the Type 304 stainless steel shroud support ring (H8 weld). The Oyster Creek shroud support structure possesses thirty-six lug/clevis pin assemblies at the H8 weld (shown by the dotted lines in Figure 2-2). These lug/clevis pin assemblies were installed during vessel construction as a result of cracking detected in the shroud support ring after fabrication, and were designed to structurally replace the H8 weld.

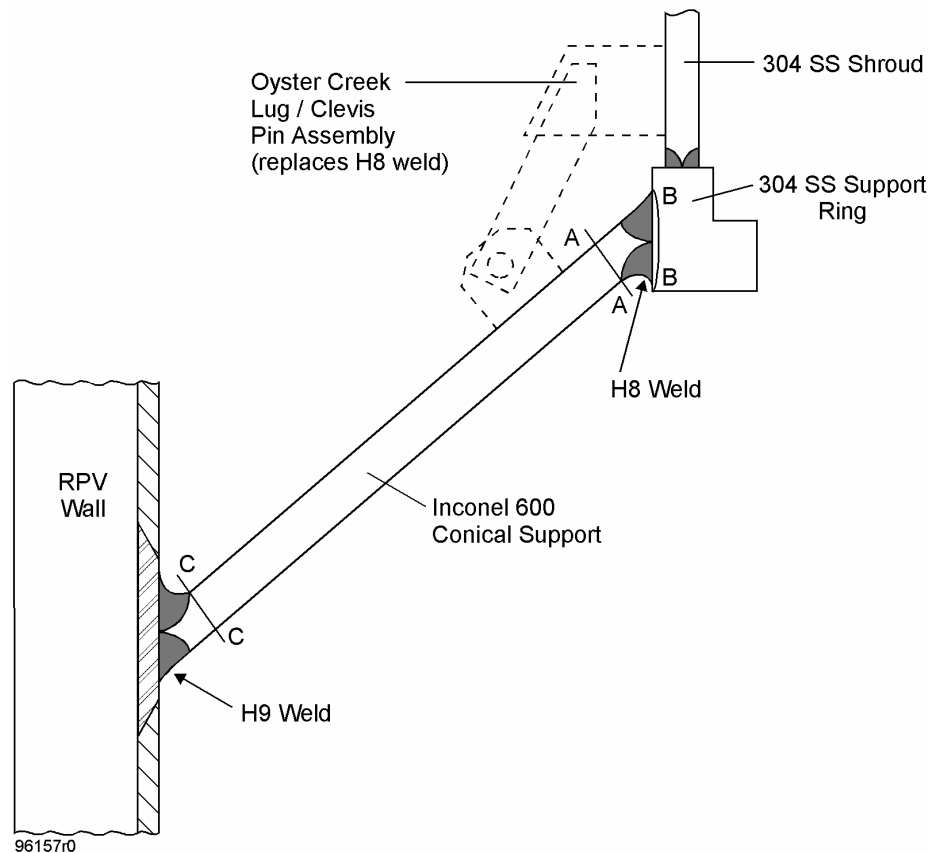


Figure 2-2
BWR-2 Shroud Support Configuration

2.2 Thick Shroud Support Plate (Hatch Unit 2)

The shroud support design in the Hatch Unit 2 plant (BWR-4) is an 8.8 inch thick flat plate design fabricated by CE. This configuration is shown in Figure 2-3. The shroud support plate is fabricated from low alloy steel material, with a low alloy steel weld connecting it to the low alloy steel RPV wall (H9 weld), and an Alloy 82/182 weld connecting it to the Alloy 600 shroud support cylinder (horizontal H8 weld). The top surface of the shroud support plate is clad with Alloy 82/182 material, and the bottom surface is clad with Type 304 stainless steel.

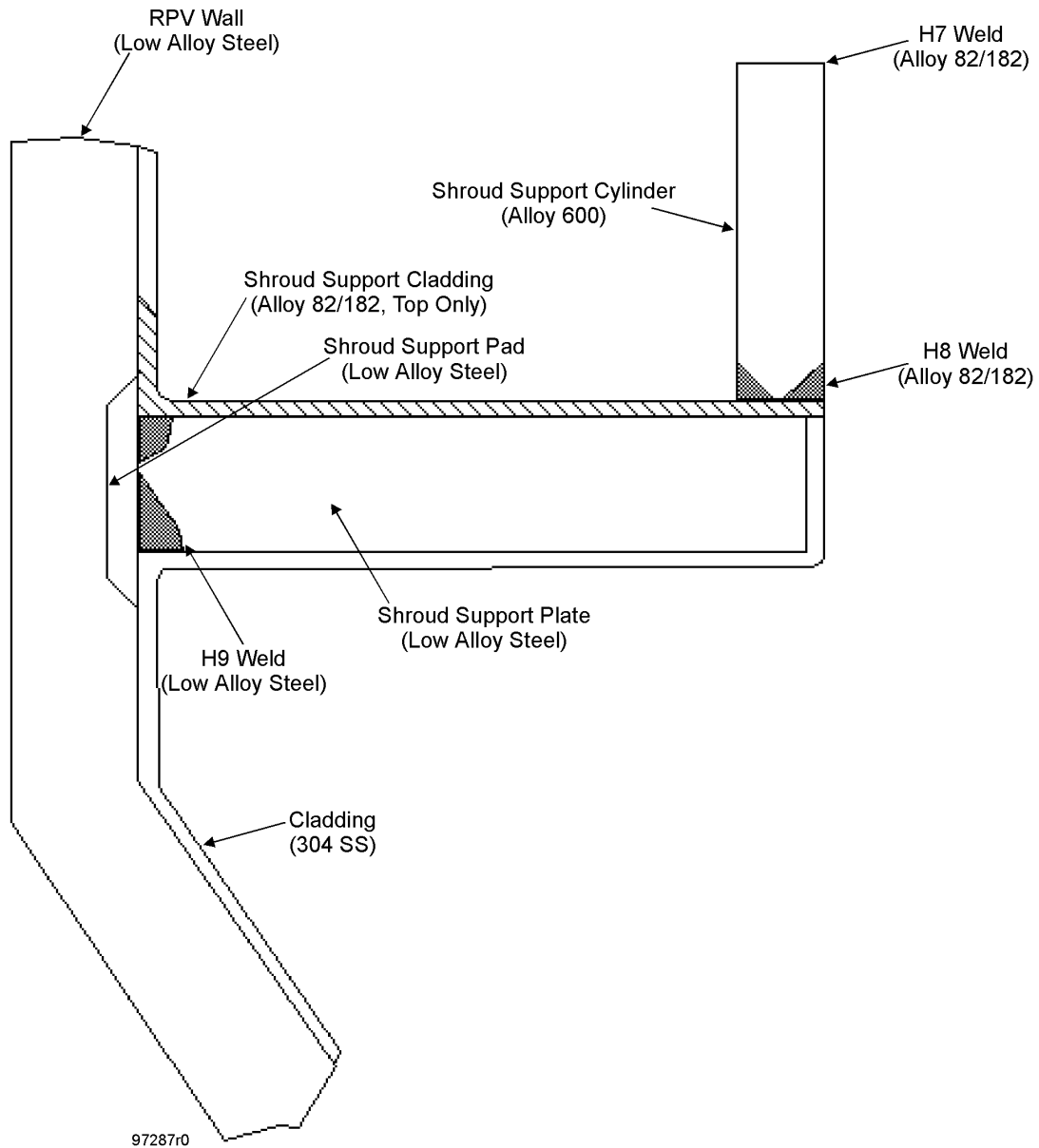


Figure 2-3
Hatch Unit 2 Shroud Support Configuration

2.3 Shroud Support Plate With Legs

The shroud support design implemented at the majority of the BWR-3, 4, 5 and 6 plants, in particular the Babcock & Wilcox (B&W) and Chicago Bridge & Iron Nuclear (CBIN) constructed RPVs, is a flat plate design with support legs that connect to the RPV bottom head. At some plants, an Alloy 600 stub tube is welded to an attachment pad on the inside of the RPV lower head, and the leg is welded to the top of the stub and to the bottom face of the shroud support cylinder (Figure 2-4). At other plants, the legs are welded directly to the attachment pad on the inside surface of the RPV lower head (Figure 2-5). At some plants, the legs are reinforced with stiffeners, which run vertically and are welded to the middle of the inner and outer (radial) surfaces of each leg (Figure 2-5).

The support legs vary in both size and quantity between plants. They are fabricated from Alloy 600 material (except for WNP-2, which has low alloy steel legs clad with Type 304 stainless steel) with multiple Alloy 82/182 welds joining the various leg sections to each other, and joining the legs to the low alloy steel RPV and the Alloy 600 shroud support cylinder (refer to Figures 2-4 and 2-5). There are generally six to fourteen legs for this design. The leg welds of interest, are the welds attaching the leg to the support cylinder, attaching the leg to the RPV, and a third intermediate weld in some designs. The two variations of this configuration are also shown in Figures 2-4 and 2-5.

The shroud support plate ranges from approximately 2 to 2.5 inches in thickness, is fabricated from Alloy 600 material, and is connected to the low alloy steel RPV wall (H9 weld) and to the Alloy 600 shroud support cylinder (vertical H8 weld) using Alloy 82/182 welds.

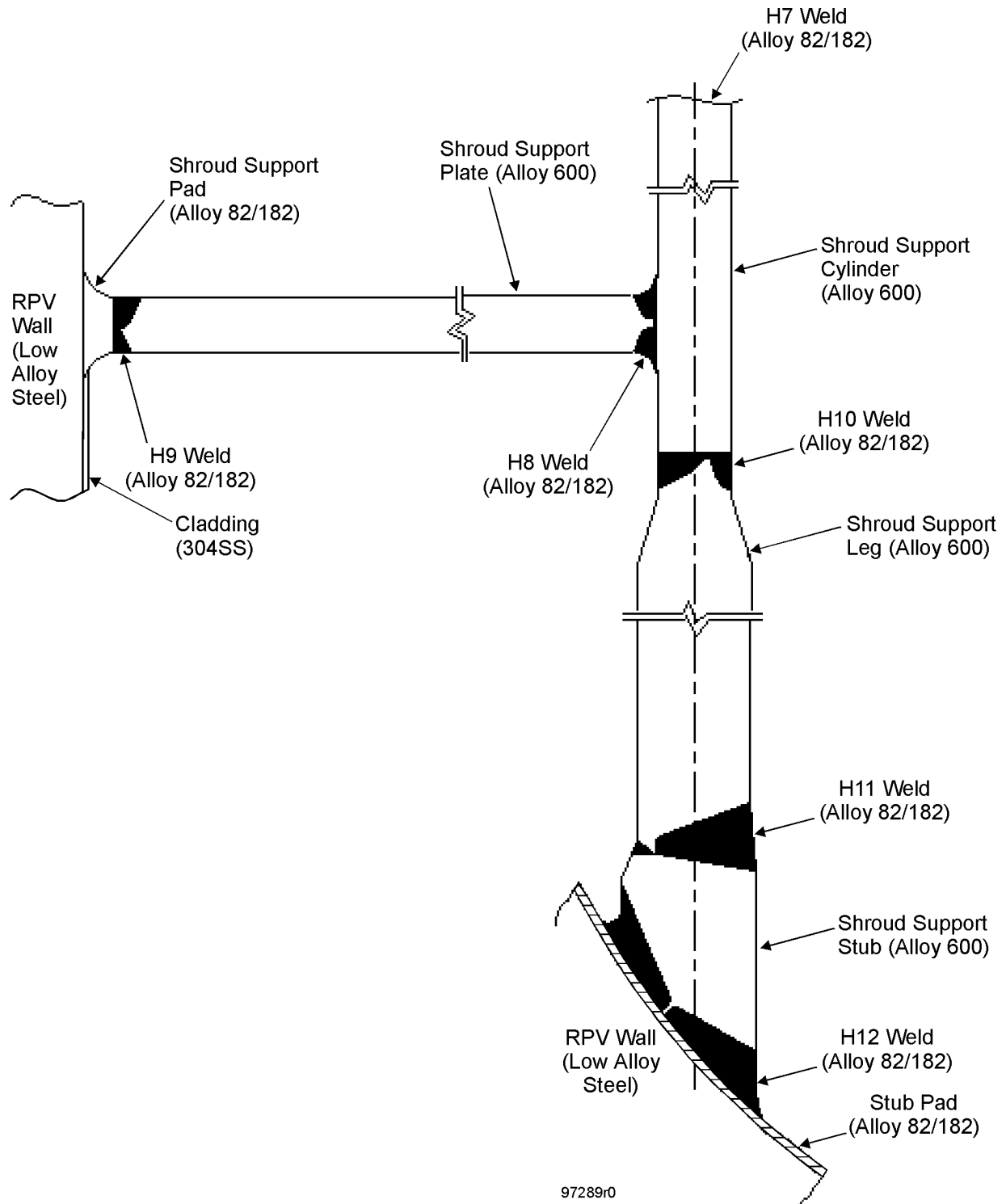


Figure 2-4
Shroud Support Plate With Legs (CBIN BWR-4, 5, 6 Design)



Figure 2-5
Shroud Support Plate With Legs (B&W BWR-3, 4 Design)

2.4 Shroud Support Plate With Gussets

The shroud support design used at a number of BWR-3, 4 and 5 plants, the CE-fabricated plants, is a cantilevered plate design with twenty-two support gussets, rather than support legs, that connect to the RPV wall. The gussets vary in size and thickness among plants, and are fabricated from Alloy 600 material. The welds of interest are the welds attaching the gusset to the support plate and the gusset to the vessel. This is shown in Figure 2-6.

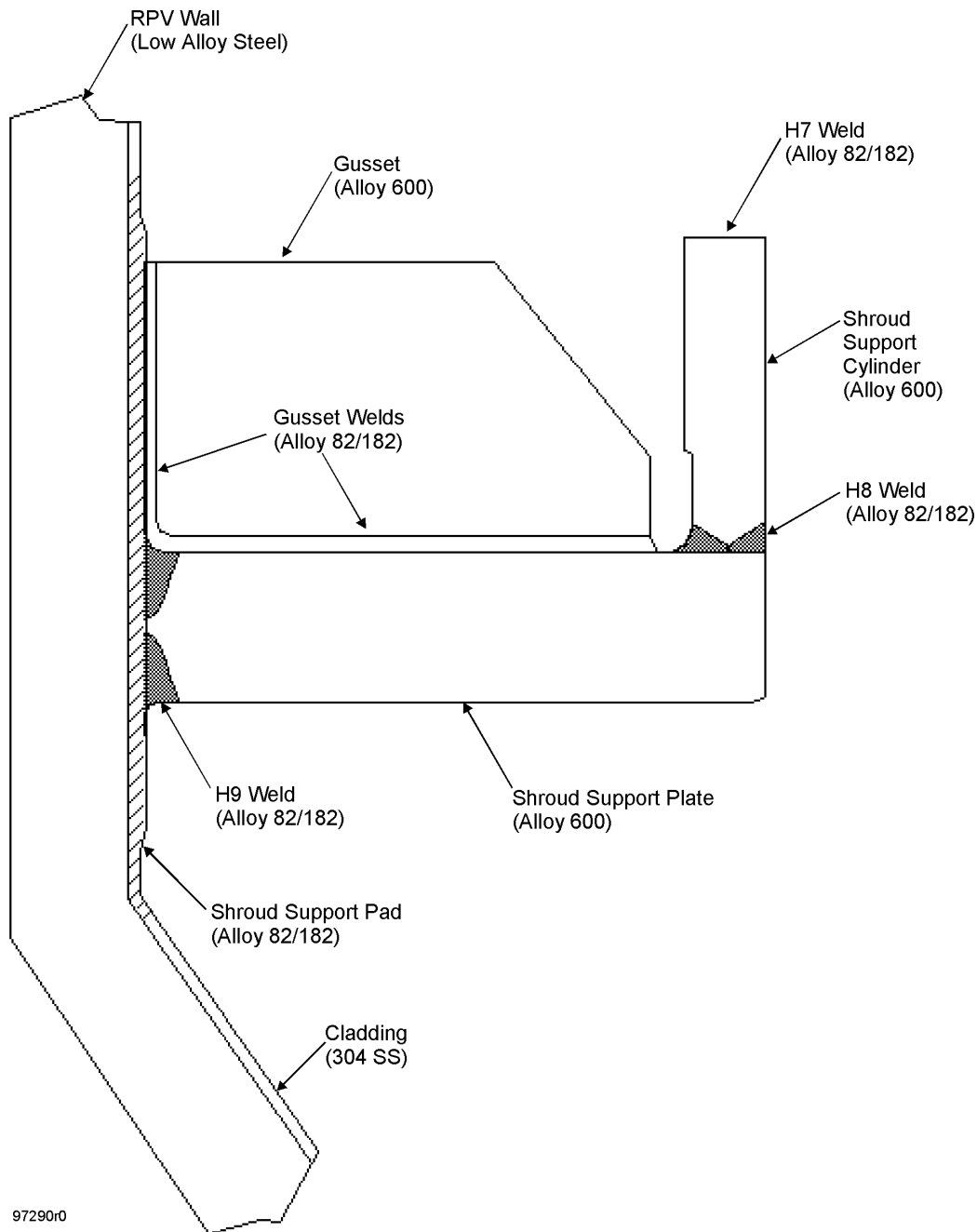


Figure 2-6
Shroud Support Plate With Gussets Configuration (CE BWR-3, 4, and 5 Design)

The shroud support plate ranges from 2 to 2.5 inches in thickness, is fabricated from Alloy 600 material, and is fabricated with Alloy 82/182 welds connecting it to the low alloy steel RPV wall (H9 weld) and the Alloy 600 shroud support cylinder (horizontal H8 weld).

2.5 Shroud Support Structure Used in this Study and Applicability to Other Shroud Support Structures

The study described in this report was conducted on a BWR-6 design. The choice of a BWR-6 for this study is motivated in part by the fact that the spare vessel at River Bend, a BWR-6 was available to be used for experimental residual stress measurements to supplement the analytical evaluation to be presented in this report. It is believed, however, that with the exception of the BWR-2 design shown in Figure 2-2 (limited to only Nine Mile Point Unit 1 and Oyster Creek), the present study and results of other work performed by the BWRVIP for the core shroud [2] and the reactor vessel attachment welds [10] can be used to address the welds of all the remaining core shroud support structure configurations shown in Figures 2-3 through 2-6. Weld H8 for Hatch Unit 2 core support structure (Figure 2-3) and the gusset design (Figure 2-6) are essentially circumferential welds in the core shroud and has been addressed by the work done in Reference [2]. Weld H9 for these configurations which are attachment welds to the reactor pressure vessel are addressed separately in Reference [10]. The B&W BWR-3, 4 design shown in Figure 2-5 is very similar to the CBIN BWR-5, 6 design (Figure 2-4) used in the present study except that the legs are thinner in the BWR-3, 4 design. As will become evident in Section 3 of this report, the thinner legs of the BWR-3, 4 design will result in less constraint and therefore smaller residual stresses in the welds of this structure. Hence, the residual stresses determined for the BWR-5, 6 design can be conservatively used for the BWR-3, 4 design.

The dimensions of the River Bend Support Structure are shown in Figure 2-7. The experiment study will focus on welds H8, H9, H10 and H12 since weld H11 is not present in the core support structure at River Bend. However, weld H11 will be addressed as part of the analytical effort. In order to provide details of these welds for the analytical studies, photomacrographs of these welds were taken so that the details could be included in the modeling process. The photomacrograph are shown in Figures 2-8 through 2-11 for the four welds considered in the experimental study.

**Content Deleted -
EPRI Proprietary Information**

**Figure 2-7
Geometry and Dimensions of the Core Support Structure at River Bend**

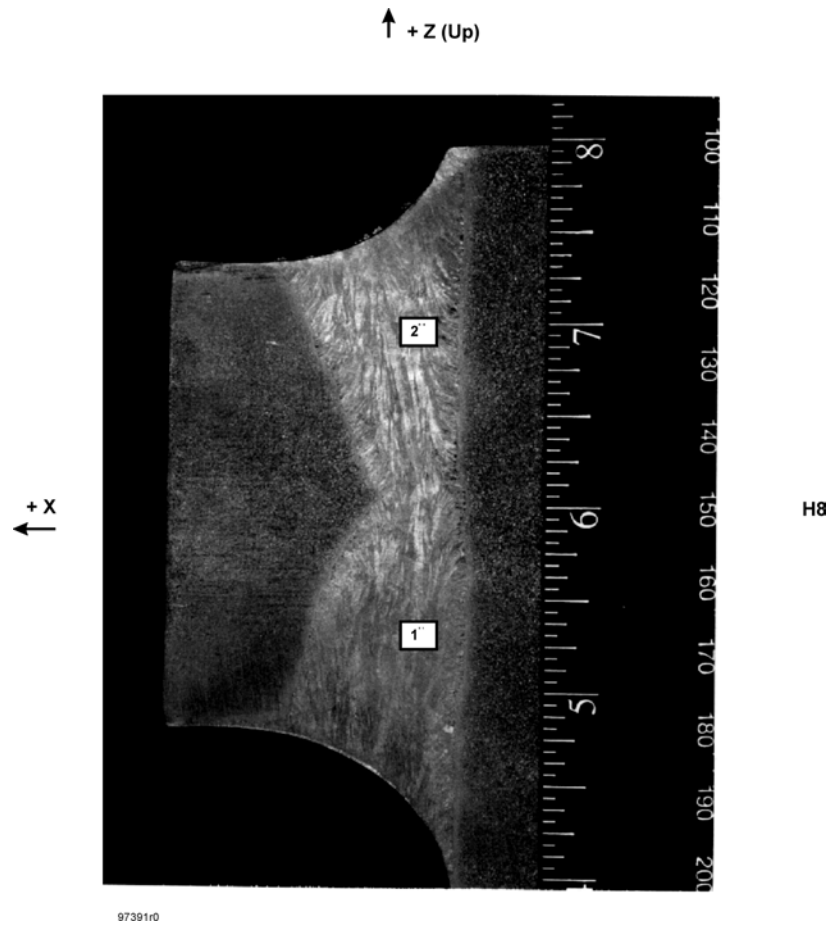


Figure 2-8
Photomacrograph of Weld H8 at River Bend

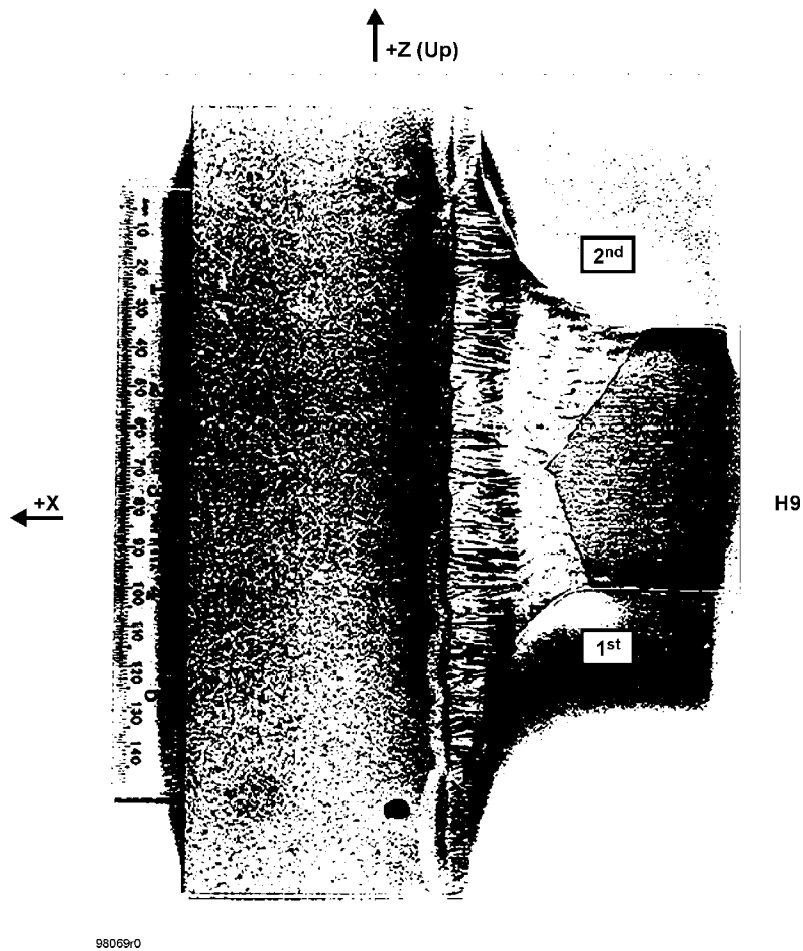


Figure 2-9
Photomacrograph of Weld H9 at River Bend

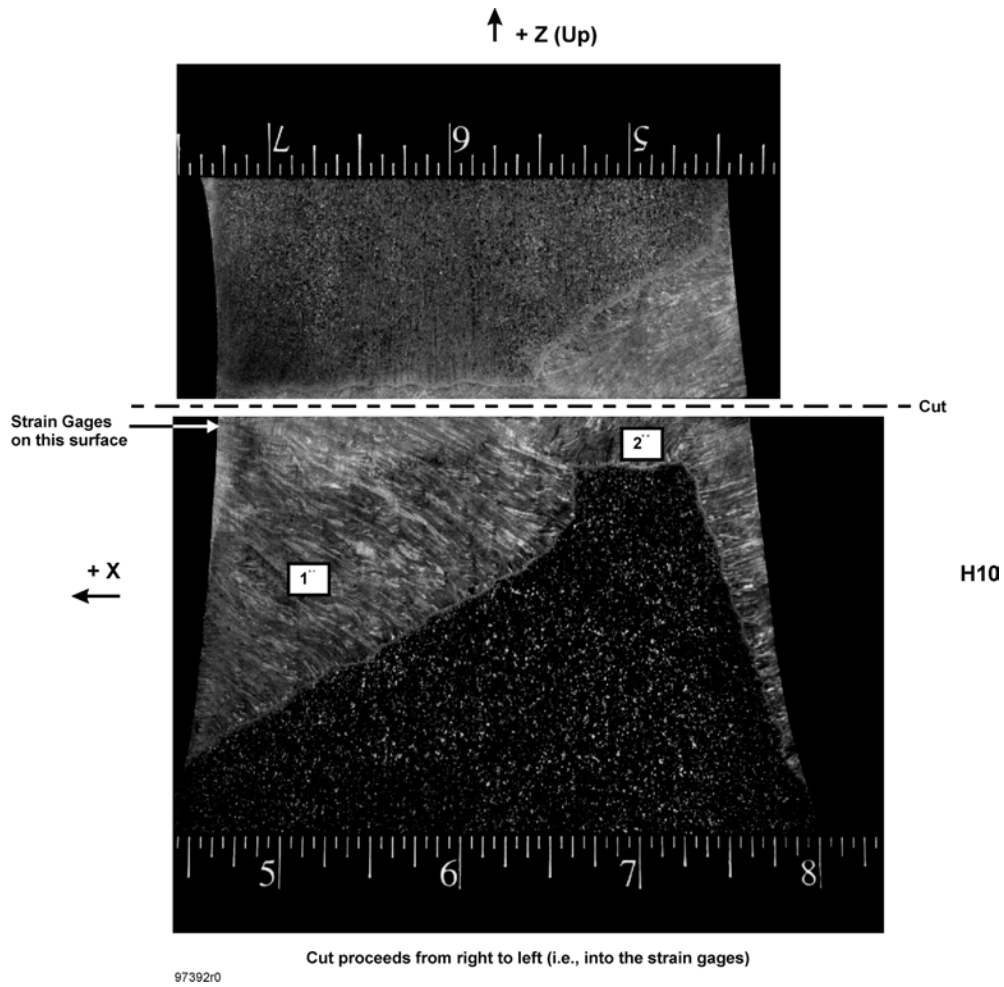


Figure 2-10
Photomacrograph of Weld H10 at River Bend

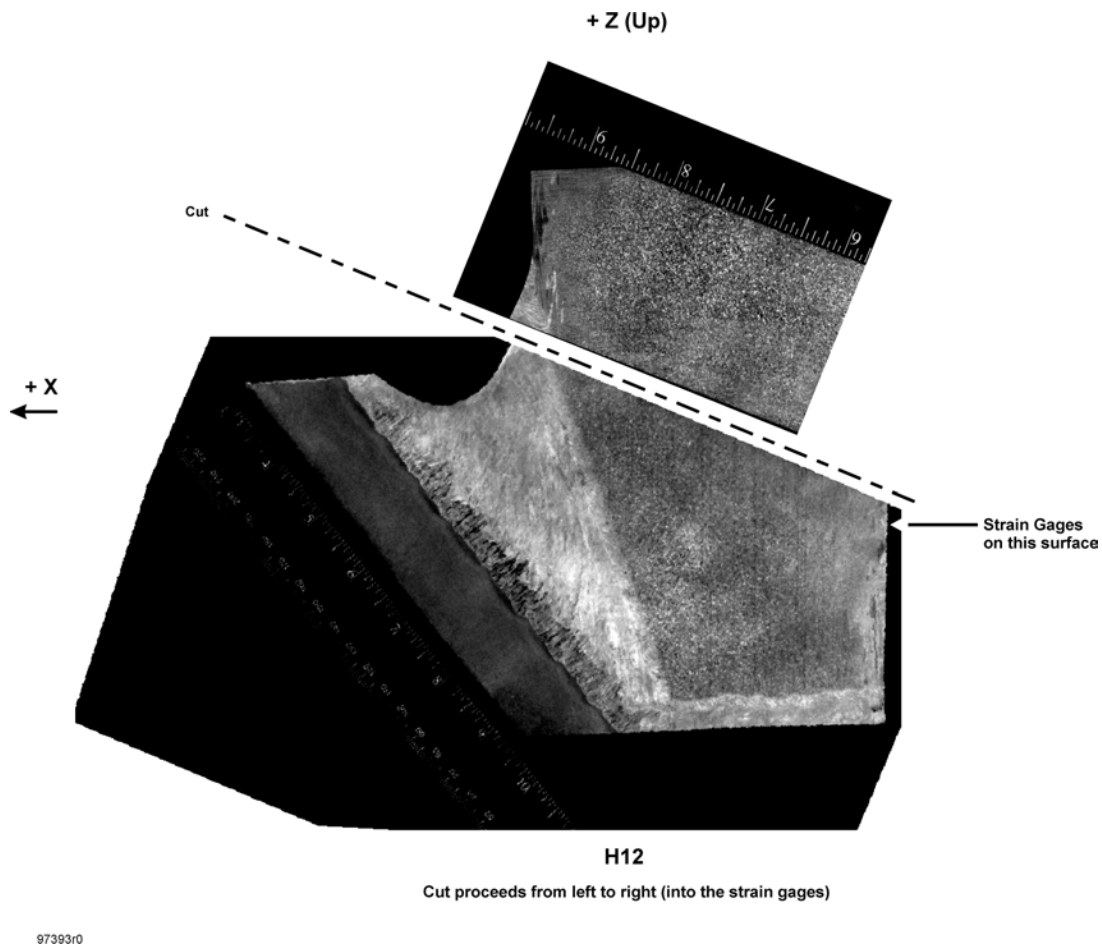


Figure 2-11
Photomacrograph of Weld H12 at River Bend

2.6 Weld Sequence During Fabrication of Shroud Support Structure

In the initial evaluation of the shroud support structure, a fabrication sequence obtained from one set of CBIN drawings was used. This sequence is described as follows:

- The shroud support cylinder is first attached to the shroud support plate via weld H8. This weld is performed in the shop prior to any field fabrication of subsequent joints.
- The shroud support legs are then connected to the vessel lower head, either by welding directly to the reactor vessel (weld H12) or to a pedestal built up on the lower head prior to vessel stress relief (weld H11). The shroud support legs are assumed to be laterally restrained at their upper ends during welding to prevent gross misalignment caused by weld shrinkage stresses.
- The shroud support cylinder is then placed on the shroud support legs, and the legs are connected to the shroud support cylinder by weld H10.
- Finally, the shroud support plate is attached to the reactor vessel shell at weld H9.

Subsequent to this initial work, it was discovered that a number of reactor vessels manufactured by Chicago Bridge and Iron Nuclear (CBIN), including River Bend, had their shroud support structures assembled in a significantly different sequence. This alternate sequence is understood to be as follows:

- The shroud support cylinder is attached to the shroud support plate via weld H8. This weld is performed in the shop prior to any field fabrication of subsequent joints.
- The shroud support cylinder is temporarily supported in position, and the shroud support plate is attached to the reactor vessel shell at weld H9.
- The shroud support legs are then fit between the shroud support cylinder and the vessel lower head, and welded into the lower head and support cylinder simultaneously. The weld at the upper end of the legs is H10, and the connection to the lower head is made using either an H11 or an H12 weld, depending on whether the optional pedestal was used. Destructive examination of the River Bend 2 shroud support structure revealed that the H12 weld was used in that application.

3

OPERATING AND RESIDUAL STRESSES

Stresses in the core shroud support welds can be divided into two broad categories. The first category is associated with stresses arising from plant operation. The second is associated with stresses which develop in the component during the fabrication process. Major contributors to the fabrication stresses are the weld residual stresses caused by the thermo-plastic strains associated with the welding and the locked-in or fit-up stresses due to restraint of various parts of the structure during fabrication.

3.1 Operational Stresses

A detailed description of the operational loads acting on the shroud support structure and the load combinations for the various service levels can be found in the vessel stress reports for the plants. The primary loads consist of pressure, deadweight, buoyancy, seismic and hydrodynamic loads. Secondary stresses result from loadings associated with thermal and pressure expansion of the RPV.

In general, the upset condition (including operating basis earthquake loads) is the limiting load from a structural standpoint. A review of several stress reports showed that for most cases, total membrane plus bending stresses are relatively low for the core shroud support structure welds.

3.2 Weld Residual Stresses

Unlike piping butt welds in which the residual stresses are essentially independent of the fabrication sequence due to the flexibility in the system, the residual stresses in the shroud support structure are affected by the fabrication process. This is because the support structure arrangement produces a highly constrained structure and the manner in which the structure is restrained during the welding process is expected to play a key role in determining the final state of the residual stresses. For the River Bend vessel which was considered in this evaluation, two weld sequences were considered in the evaluation as detailed in Section 2.6. In the first sequence, the legs were welded to the RPV lower head with the H11 or H12 weld before installation of the support structure in the vessel. For River Bend, the H12 weld was fabricated first since the H11 weld does not exist in this plant. Also, the H8 weld was also fabricated separately before the support structure was installed. The H10 weld was then fabricated followed by the H9 weld. During the fabrication of the H11, H12, H10 and H9 welds, it is expected that the leg and the support structure was constrained to some degree in order to maintain the tolerances specified in the drawings. For instance, the top of the leg had to be restrained from horizontal translation while the H11 or H12 weld was made. The restraints were subsequently removed after attachment was made at the H10 weld. This restraining process is expected to have introduced some forces and moments into the leg structure which undoubtedly will affect the final residual stress state of the welds depending on the degree of restraint. Hence unlike piping

welds, the residual stresses in the core shroud support structure welds are affected not only by the thermo-plastic strains associated with the welding process, but also by the forces and moments developed as a result of the restraint introduced into the structure during the fabrication process. The degree of restraint is expected to vary from plant to plant and from one fabricator to the other. Hence, in determining the residual stresses and the fracture mechanics parameters in the next section, sensitivity analysis is performed to determine how the degree of restraint from different welding sequences influences the final residual stress state.

In addition to the fabrication sequence, other factors that affect the residual stresses in the support structure welds include heat input during the welding process, welding sequence for each particular weld, weld starts and stops, cooling time between phases, base/weld metal mechanical properties, local weld repairs and post weld heat treatment (PWHT). Although all these parameters can play a role in the final residual stress state, it is believed that their effect is overshadowed by the contribution due to constraint effects of the support structure. One effect which was investigated in the study is post weld heat treatment even though records indicate that CBIN practice was to stress relieve the vessel prior to the installation of the shroud support structure. For fabricators who performed a PWHT after installation, it is expected that in general, the weld residual stresses will be reduced as discussed in Appendix D Section D.3.2. In this report, the potential benefit of PWHT was not considered in order to provide a conservative, bounding evaluation.

Both experimental and analytical studies were performed to determine the magnitude and distribution of the weld residual stresses in the River Bend support structure. The purpose of determining the residual stresses using both methods is to use the experimental measurements to benchmark the analytical study such that the analytical approach can be used with confidence to determine the residual stresses at other critical locations of the shroud support structure welds for River Bend and also to determine the stresses associated with other shroud support structure configurations discussed in Section 2 of this report without the need for additional experimental measurements. As discussed in Section 2, it is believed that with the exception of only a few cases, the residual stresses for the shroud support structure used in this study together with other BWRVIP work done for shroud and the RPV attachment welds can be used to represent the welds of the other shroud support structures.

3.2.1 Through-Thickness Residual Stress Measurements at River Bend Nuclear Station

Through-wall residual stress measurements of the shroud support structure welds H8, H9, H10 and H12 at River Bend were performed by University of California, Berkeley personnel using the crack compliance method (Appendix B). Specimens containing all the four welds were cut out from coupons removed from the core shroud support structure and the vessel. Photomacrographs of the welds are presented in Figure 2-8 through 2-11. The cutting process of the coupons from the support structure is provided in Reference [11]. As discussed earlier, it is expected that the residual stresses are influenced by the forces and moment developed in the constrained structure during fabrication. Cutting out of the specimens from the support structure released the part of the residual stresses associated with the constraint of the structure. Hence the measurements of the residual stresses presented herein only account for that part of the local residual stress associated with the thermo-plastic strains during the welding that are locally balanced with no resultant external loads.

The theoretical background of the crack compliance method and details of the methodology in application to the measurements of the shroud at River Bend are provided in Appendix B of this report. In summary, the method involves installing a strain gage at an optimal location of a specimen containing the weld.

An electrical discharge wire machining (EDWM) is used to introduce a thin cut of increasing depth in the specimen. The strain distribution during the cutting process is measured. The relationship between the stress released and the measured strain is given by:

$$\epsilon(a) = \sum_{i=0}^n \frac{\sigma_i}{E'} C_i(a) \quad \text{Equation 3-1}$$

The unknown residual stress distribution is represented by a series:

$$\sigma(x) = \sum_{i=0}^n \sigma_i P_i(x) \quad \text{Equation 3-2}$$

where: $P_i(x)$ = the surface traction

σ_i = the amplitude factor for the i^{th} term $P_i(x)$

E' = an elastic constant

$C_i(n)$ = the crack compliance function for $P_i(x)$

The crack compliance functions were obtained by using fracture mechanics solutions in the literature of finite element analysis. When a number $m > n+1$ of strain measurements are made, a least square fit can be used to minimize the average errors involved in the measurement and estimation resulting in $n+1$ linearly independent equations given as:

$$\frac{\partial}{\partial \sigma_i} \sum_{j=1}^m \left[\epsilon(a_j) - \sum_{k=0}^n \sigma_k C_k(a_j) \right]^2 = 0 \quad i = 0, \dots, n \quad \text{Equation 3-3}$$

from which the unknown σ_i can be solved.

The above procedure was used to determine the through-wall residual stress distribution in the shroud for welds H8, H9, H10 and H12. The geometry of the specimens that were used to obtain the measurements and the weld profiles as well as location of the measurements are shown in Figures 3-1 through 3-4. The strain and the through-wall residual stress distributions are presented in Appendix B of this report.

**Content Deleted -
EPRI Proprietary Information**

Figure 3-1
Through-Thickness Measured Residual Stress Distribution (σ_x) for Weld H8

**Content Deleted -
EPRI Proprietary Information**

Figure 3-2
Through-Thickness Measured Residual Stress Distribution (σ_x) for Weld H9

**Content Deleted -
EPRI Proprietary Information**

**Figure 3-3
Through-Thickness Measured Residual Stress Distribution (σ_x) for Weld H10**

**Content Deleted -
EPRI Proprietary Information**

Figure 3-4
Through-Thickness Measured Residual Stress Distribution (σ_x) for Weld H12

3.2.2 Analytical Determination of Residual Stresses

In addition to the experimental determination of the weld residual stress for the various welds of the shroud support structure at River Bend, finite element analyses were performed by Dominion Engineering Inc. to analytically determine the weld residual stresses. The objective of performing analytical and experimental studies on equivalent welds was to allow the analytical results to be benchmarked against experimental results for actual BWR components. Because of the fact that experimental measurements were made on samples that represent only a small fraction of the total weld and the simplifying assumptions that must be used to make analysis tractable, exact agreement between the analytical and experimental results is not expected. However, the experimental and analytical results are generally in agreement with regard to the magnitudes of peak stresses and the shapes of the through thickness variations in stress. This reasonable agreement provides a basis for using analysis to determine residual stress distributions at other locations of the shroud support structure welds at River Bend and also to provide confidence in the use of the analytical approach to determine stresses in other shroud support structure configurations for which experimental results are unavailable.

Two different analytical approaches were used at different times to obtain the weld residual stresses for the shroud support structure weld.

3.2.2.1 Initial Analyses With Discrete Weld Models

The initial analyses were performed during the 1997 to 1998 time frame. These original analyses were performed using a number of separate models of the individual welds with the effects of subsequent welding on the locked-in moments predicted in welds produced earlier in the assembly sequence compensated for by use of superposition. This initial analysis is presented in this report to serve the useful purpose of comparing the results with the experimental results. As will be discussed in Section 3.2.2.2, updated analyses were performed for both the initial and subsequent fabrication sequences using a more representative integrated model.

The analyses were performed using the geometrical data of the core support structure configuration at River Bend in order to provide consistent and comparable results with the experimental stress measurements performed at River Bend. The analysis followed the initial fabrication sequences described in Section 2.6. This necessitated using a three-dimensional finite element model of a 15° segment of the RPV and the shroud support structure which contains all the welds. For completeness sake, weld H11 was included as part of the model even though this weld is not present in the support structure at River Bend. Consequently, no measurements are made for this weld. However, since it is a possible BWR-6 configuration, it is believed that the data may prove useful to other BWR-6 utilities with support structure configurations containing H11. In the finite element simulation, weld H11 was made first, followed by H8, H10 and H9 in that order. The analysis of the H12 weld was done separately from the other welds.

The weld residual stress analyses were performed using the ANSYS finite element Code [12] with a 15° segment of the RPV and the support structure. The 15° segment model includes an opening to represent one of the ten jet pumps and two access hole cover openings in the shroud support plate. The relatively high temperature associated with the welding process and the resulting high strains necessitated the use of temperature-dependent material properties. Other than the yield stress which was made higher for the weld metal than the corresponding base

material, all material properties were essentially the same for the base and weld metals. It was assumed that both the base and weld metals behave as elastic-perfectly plastic materials. For simplicity of the simulation, the welding process was modeled by assuming an entire weld layer to be deposited at the same time. Weld passes are modeled with two elements through the thickness of the layer and four elements across the width of the weld. The material properties used in the finite element analysis are presented in Appendix D.

The simulation of the welding process consisted of three stages. In the first stage, a thermal analysis was performed. This involved application of appropriate thermal boundary conditions followed by simulation of each welding pass. Weld passes were simulated by successively activating the elements that make up each weld pass, applying a uniform heat generation rate to all the elements in the pass and then allowing the weld metal and shroud to cool to room temperature. Temperature distributions were calculated at a number of points in time during each weld pass and saved for use with the structural model. The second stage involved the structural analyses which was performed by the application of the temperature distribution to a structural model. Residual stresses were then determined by sequentially imposing the temperature distributions at each time step as loads on the structural model and then solving for the resultant stresses. In the final stage of the modeling process, the shroud support structure was subjected to a post weld heat treatment modeled by ramping the temperature of the entire model from 70°F to 1150°F in 300 seconds and back again to 70°F in the next 300 seconds. The 300 second ramp rate was chosen for numerical stability in the analysis. The analysis results are independent of the ramp rate used because only time independent plasticity is included in the model, and thermal stresses are avoided by forcing the model to have a uniform temperature for each step of the stress relief cycle. The stress relief effect that is simulated by this procedure is lowering of the residual stresses because of the reduction of yield strength at the stress relief temperature. Creep relaxation of stresses in the nickel base alloy components and welds is not expected to be significant at the stress relief temperature, which is designed for stress relief of the low alloy steel pressure vessel.

Details of these initial analyses and the analyses results for all the welds in the core shroud support structure are presented in Appendix D of this report . The results are presented in terms of contour plots as well as through-wall distribution of hoop and axial stresses at key locations of the weldments including the locations where the experimental measurements were taken to provide the basis for comparison. Since the analysis results indicate that there is variation of stresses along the leg of the support structure, the through-wall stress distribution is presented for several discrete locations along the leg. This is even more so for the H8 and H9 welds because in addition to the discrete legs, the jet pump and the access hole cover holes interact with the H8 and H9 welds. Results of the through-wall stress distributions for welds H8, H9, H10 and H12 for the as-welded as well as the stress relieved conditions are presented in Appendix D. Through-wall residual stress distribution was obtained at only one section corresponding to where the experimental data was obtained for each weld.

3.2.2.2 Updated Analyses With Integrated Model

As a result of improvements in computational capabilities, an integrated model that incorporated all the four welds was developed in 2002-2003 time frame. This model eliminated the need to perform the individual analyses on the welds and the use of superposition to combine all of them as described in Section 3.2.2.1. This integrated model made it possible to rerun all the cases considered in the initial sequence and also to consider the alternate welding sequence described in Section 2.6. With this integrated model, it was then possible to investigate the impact of assembly sequence, weld sequence, and assumed crack plane location on the stresses that are used in the fracture mechanics evaluations in Section 4.

There is a fairly large analysis space that could be investigated by permuting all possible weld assembly sequences (legs first vs. last), configurations (H11 or H12 geometry), and reversal of each of the four weld locations, for a total of 64 unique cases. This analysis space was limited in this study by considering the reversal of only welds H9 (which is similar in nature to H8) and H12 (which is the most constrained weld configuration on the legs), and only reversing these welds one at a time. This produced an eight-case matrix, as shown in Table 3-1. Limiting the evaluations to the cases shown in Table 3-1 allowed for a reasonable sensitivity study to be performed without the need for generating overwhelming amounts of data.

In the initial analyses described in Section 3.2.2.1, the through-wall residual stress distribution for each weld was obtained only at locations corresponding to the strain gauge locations used to obtain the experimental results. These locations do not necessarily correspond to the most conservative and critical locations for the through-wall stress distributions. Hence, in these updated analyses with the integrated model, several additional cut lines were selected to determine the bounding through-wall residual stress distribution to use for the various welds. The locations of the cut lines for the various welds are shown in Figure 3-5. The cut lines corresponding to the locations that the experimental data was taken from are also indicated in Figure 3-5. The directions in which the through-wall stress distributions were obtained are also indicated on the cut lines. These directions are consistent with those of the experimental measurements and the evaluations in Appendix D, except for weld H8, where the through-wall stress direction shown in Appendix E is opposite to the experimental measurements and Appendix D. Hence, for comparison with Appendix D and the experimental results, the direction of the Appendix E through-wall stress for weld H8 will be reversed.

The analytical approach for determination of the residual stresses for the River Bend shroud support structure welds from this updated analyses is very similar to that described for the initial analyses in Section 3.2.2.1, except that a combined integrated model was used and hence there was no need to perform linear superposition of the various weld models as was done in Appendix D. The analyses were performed using ANSYS Finite Element Code, Revision 5.7 on an HP J6700 workstation. Details of the analytical modeling and results from these analyses are presented in Appendix E.

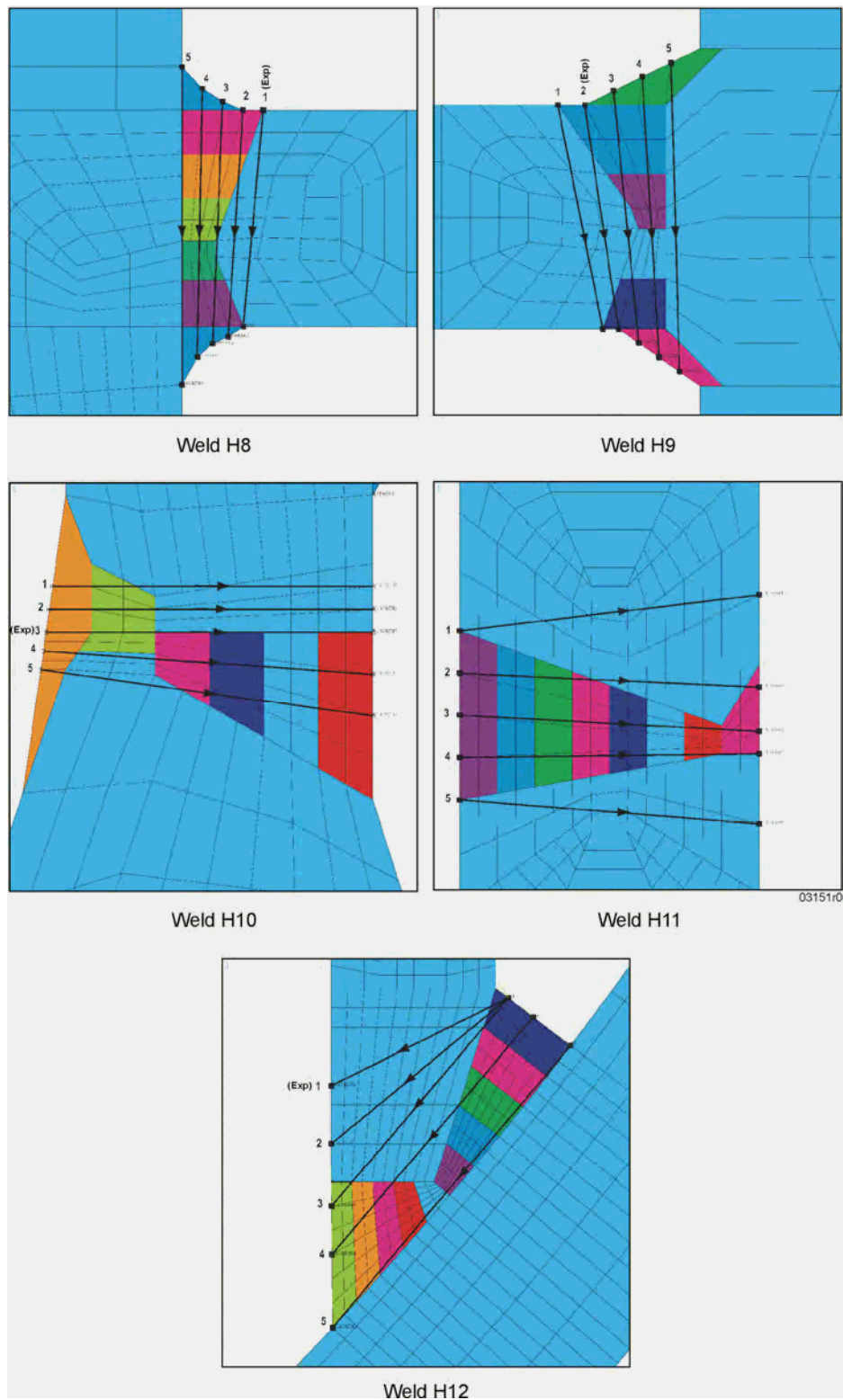


Figure 3-5
Weld Section Line Definitions in Updated Analyses With Integrated Model

3.2.2.3 Summary of Analytical Results

The following presents the summary of the observation made on the analytical results detailed in Appendices D and E.

**Content Deleted -
EPRI Proprietary Information**

3.2.3 Comparison of Initial and Updated Analytically Predicted Residual Stresses With Experimental Measured Data

The through-wall residual stress measurements reported earlier are compared with the analytical predictions (both the initial and updated analyses) for all the welds (with the exception of H11) with the purpose of establishing consistency between experiment and analysis, and to provide a recommendation for appropriate distributions which should be used in crack growth evaluation. The comparison is made by considering the trends and peak magnitudes rather than point by point numerical comparisons because, as discussed earlier, the final state of residual stress in each weld or portion of weld is affected significantly by the degree of constraint imposed by the remainder of the structure during fabrication and this is likely to be different from plant to plant and from point to point on the weld. It is also recognized that there are several designs of shroud support structures as discussed in Section 2 of this report and residual stress measurements for all is not possible. Hence, if the analytical predictions are supported by the measured values, it will provide a basis for using only analytical means to determine the residual stresses in the future for other core shroud support structure configurations.

The comparisons of the analytically predicted (from both the initial and updated analyses) and measured residual stresses are presented in Figures 3-6 to 3-9. The comparisons are made at the same locations where the stress measurements were taken to make them meaningful. It should be recalled that when the experimental data were obtained, the specimens had been cut from the RPV and, hence, all the locked-in stresses due to the constraint of the structure had been released. Hence the net moments and forces that are present in the analytical model were not present in the specimens used for the experimental data.

In order to provide a more meaningful comparison between analysis and experiment, the residual forces and moments in the analytical models were mathematically relaxed to zero to simulate the release of stress from cutting the samples from the structure. The relaxed stress distributions are termed “FEA Adjusted” in Figures 3-6 to 3-9. The following conclusions can be drawn by examining Figures 3-6 to 3-9.

**Content Deleted -
EPRI Proprietary Information**

The reasonable agreement between measured data and adjusted analytical results indicates that the analytical approach used for the calculations gives a satisfactory simulation of the welding process with respect to generation of residual stresses. Thus, analysis can be used to obtain reasonable estimates of weld residual stress distributions in other shroud support structure configurations where no experimental data are available. The comparison also demonstrates

the importance of knowing the degree of constraint in the core shroud support structure during fabrication because locked-in forces and moments significantly affect the final residual stress distributions. For cases where constraints on the components during fabrication were small (i.e., could not produce large forces or moments) the residual stress distributions should approach those determined by the experimental measurements. However, if the components were restrained by rigid structures during fabrication, total residual stresses at the welds will approach the analytical values without any adjustment. The FEA analyses in the initial analysis in Appendix D assumed fully effective restraints on deflections of the components during welding by enforcing zero rigid body displacements. This generally provides a conservative upper bound to the residual stresses. The high degree of restraint is probably realistic for the final H9 weld because the structure is complete and capable of withstanding large locked in forces and moments at that time. The fully effective restraint is less realistic, and excessively conservative for the leg welds H10, H11, and H12 as discussed below.

To estimate the degree of restraint and the associated locked-in stresses, both deflection and strain measurements were performed on a three legs of a spare core shroud structure at Grand Gulf Station after a cut was made just below the H10 weld. The location of the cut and the strain gages are shown in Figure 3-10. The displaced shape of one of the support legs after the cutting process is shown in Figure 3-11.

**Content Deleted -
EPRI Proprietary Information**

**Content Deleted -
EPRI Proprietary Information**

Figure 3-6
Comparison of Results from Initial and Updated Models (Initial Analysis) With Measured Residual Stress for Weld H-8

**Content Deleted -
EPRI Proprietary Information**

Figure 3-7
Comparison of Analytical Results from Initial and Updated Models With Measured Residual Stress for Weld H-9

**Content Deleted -
EPRI Proprietary Information**

Figure 3-8
Comparison of Analytical Results from Initial and Updated Models With Measured Residual Stress for Weld H10

**Content Deleted -
EPRI Proprietary Information**

Figure 3-9
Comparison of Analytical Results from Initial and Updated Models With Measured Residual Stress for Weld H12

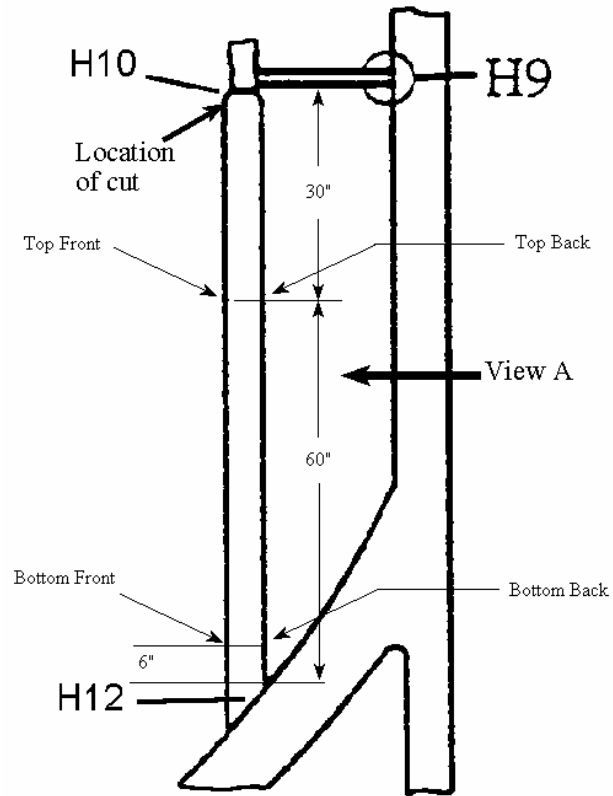


Figure 3-10
Strain Gage and Cut Locations During Measurement at Grand Gulf



Figure 3-11
Deflection (Towards Vessel Wall) of Support Leg After Cutting

**Content Deleted -
EPRI Proprietary Information**

Figure 3-12
Change in Axial Strain in the Support Legs at Grand Gulf After Cutting

**Content Deleted -
EPRI Proprietary Information**

Figure 3-13
Change in Transverse Strains in the Support Legs at Grand Gulf After Cutting

Table 3-1
Assembly and Welding Sequences Considered in the Integrated Model (from Appendix E)

Run ID	Run Description
A	The base assembly case using the H12 weld for the alternate welding sequence believed to have been used for River Bend 2 (H8 first, then H9, finally H10 and H12 simultaneously).
B	Identical to Run A, but with weld H9 welded top first, then bottom.
C	Identical to Run A, but with weld H12 welded inside first, then outside.
D	The base assembly case using the H12 weld for the assembly sequence originally used in Appendix D (H8 first, then H10 and H12, and finally H9), and using the base case weld pass sequences.
E	Identical to Run D, but with weld H9 welded top first, then bottom.
F	Identical to Run D, but with weld H12 welded inside first, then outside.
G	Identical to Run A, but using an H11 geometry rather than H12.
H	Identical to Run D, but using an H11 geometry rather than H12.

3.2.4 Critical Sections Selected for Further Analyses

The reasonably good comparison between the experimental and analytical results gives confidence to the fact that the results from the integrated model can be used to select the critical sections from all the cut line results presented in Appendix E for fracture mechanics evaluation in the subsequent sections. Through-wall stress distributions for the most critical sections for the most critical welds considering all the appropriate runs listed in Table 3-1 are shown in Figures 3-14 through 3-18 for the individual welds. Because the sequence of welding is difficult to establish on a plant unique basis, it will be assumed that the flaw started on the surface which yields the most conservative through-wall stress distributions. Hence, the stress distributions in Figures 3-14 through 3-18 will be used on the surface where the crack is expected to initiate which corresponds to the surface which yields the higher K distribution. As such, for Weld H-9, the stress distribution shown in Figure 3-15 corresponds to Run E, Section 4 of Figure E-35 in Appendix E with the crack propagating from right to left in Figure E-35 (bottom to top). Therefore, Figure 3-15 is a mirror image of Figure E-35.

Table 3-2
Strain Measurement for Grand Gulf Support Legs

**Content Deleted -
EPRI Proprietary Information**

**Content Deleted -
EPRI Proprietary Information**

Figure 3-14
Critical Residual Stress Distribution for Weld H8 from Updated Analyses (Run E, Section 3)

**Content Deleted -
EPRI Proprietary Information**

Figure 3-15
Critical Residual Stress Distribution for Weld H9 from Updated Analyses (Run E, Section 4)

**Content Deleted -
EPRI Proprietary Information**

Figure 3-16
Critical Residual Stress Distribution for Weld H10 from Updated Analyses (Run C, Section 5)

**Content Deleted -
EPRI Proprietary Information**

Figure 3-17
Critical Residual Stress Distribution for Weld H11 from Updated Analyses (Run G, Section 3)

**Content Deleted -
EPRI Proprietary Information**

Figure 3-18
Critical Residual Stress Distribution for Weld H12 from Updated Analyses (Run B, Section 4)

4

FRACTURE MECHANICS CONSIDERATIONS

The fracture mechanics parameter which is key in the crack growth evaluation of components is the stress intensity factor (K_I). In this section, the derivation of the stress intensity factor for all the core shroud support structure welds is discussed. Separate fracture mechanics models are used to determine the K_I distribution for the completely 360° weld configuration cracks (H8 and H9) and for the leg welds with finite length cracks (H10, H11 and H12). In performing the fracture mechanics evaluations, the most critical residual stress distributions from the updated analyses results presented in Figures 3-14 through 3-18 for the various welds are used.

4.1 Stress Intensity Factor for Welds H8 and H9

Welds H8 and H9 extend around the entire circumference of the shroud and RPV respectively. Because the possibility of a crack extending completely around the circumference is very unlikely, finite length flaws were considered in the derivation of K_I for these components. Although both welds are welded to relatively rigid structures (the core shroud and the RPV), the methodology for determination of K_I in ASME Code Section XI, Appendix A for vessels [13] involving the assumption of a flat plate structure was used to derive the K_I distribution. It is believed that this will provide a reasonable conservative estimate of K_I . In this case a semi-elliptical flaw shape is assumed for a surface flaw. The methodology involves representing the stress distribution by a polynomial fit over the flaw depth using the following relationship:

$$\sigma = A_0 + A_1\left(\frac{x}{a}\right) + A_2\left(\frac{x}{a}\right)^2 + A_3\left(\frac{x}{a}\right)^3 \quad \text{Equation 4-1}$$

where

x = distance through the wall measured from the flawed surface

a = crack depth

$A_0 A_1 A_2 A_3$ = constants

The stress intensity factor K_I is calculated from the above cubic polynomial stress relations by the following equation:

$$K_I = [(A_0 + A_p) G_0 + A_1 G_1 + A_2 G_2 + A_3 G_3] \sqrt{\pi a / Q} \quad \text{Equation 4-2}$$

where

- a = flaw depth
- A_0, A_1, A_2, A_3 = coefficients from Equation 4-1 that represent the stress distribution over the flaw depth, $0 \leq x/a \leq 1$. When calculating K_I as a function of flaw depth, a new set of coefficients A_0 through A_3 is determined for each new value of flaw depth.
- G_0, G_1, G_2, G_e = free surface correction factors from Tables A-3320-1 and A-3320-2 of Reference [13]

The flaw shape parameter Q is calculated using the following equation:

$$Q = 1 + 4.593 (a/\ell)^{1.65} - q_y \quad \text{Equation 4-3}$$

where

- ℓ = the major axis of the flaw
- a/ℓ = the flaw aspect ratio $0 \leq a/\ell \leq 0.5$
- q_y = the plastic zone correction factor calculated using the following equation:
- $$q_y = [(A_0 G_0 + A_1 G_1 + A_2 G_2 + A_3 G_3) / \sigma_{ys}]^2 / 6$$

where

σ_{ys} is the material yield strength.

The technical basis for the above stress intensity factor formulation is provided in Reference [14]. The methodology requires that the residual stresses determined for welds H8 and H9 be curve fit on an incremental basis. In deriving K_I for these welds, the stresses were curve fit over the entire thickness such that one set of coefficients was used to derive stress intensity factor. This is reasonable since adequate curve fit was obtained for the entire distribution through the thickness. The polynomial fits to the stress distributions are shown in Figures 3-14 and 3-15.

The results of the K_I determination for welds H8 and H9 using the stress distributions in Figures 3-14 and 3-15 are shown in Figures 4-1 and 4-2 for aspect ratios 0.1 to 0.5. Smaller aspect ratios, though possible, are considered very unlikely. For aspect ratios less than 0.1, a plant specific evaluation is required. Alternatively, the bounding K-independent crack growth correlation discussed in Sections 5 and 6 can be used for the evaluation. The K_I distribution shown in Figures 4-1 and 4-2 correspond to the worst-case through-wall stress distribution shown in Figures 3-14 and 3-15. It should be noted that the K_I distribution is normalized with respect to thickness, and therefore to obtain the actual K_I , the ordinate values should be multiplied to \sqrt{t} , where t is the thickness of the component. As indicated in Section 3, stress relief has only a minor effect on the residual stress distribution and therefore, the K_I distribution is not expected to be very different (in fact, slightly more favorable) than the as-welded case. It is observed from Figures 4-1 and 4-2 that as the aspect ratio increases, K_I becomes progressively smaller.

**Content Deleted -
EPRI Proprietary Information**

Figure 4-1
 K_I Distribution for Weld H8 in As-Welded Condition

**Content Deleted -
EPRI Proprietary Information**

Figure 4-2
 K_I Distribution for Weld H9 in As-Welded Condition

4.2 Stress Intensity Factor Determination for Welds H10, H11 and H12

Welds H10, H11 and H12 are considered separately since they are leg welds and as such, they have a finite width. The maximum through-wall residual stress distributions shown in Figures 3-16 through 3-18 are used in the evaluation. The stress intensity factor was determined using a single edge-cracked beam model.

It is well known that the stress intensity factor for a single edge-cracked beam increases rapidly with the increase of the crack size when subjected to a resultant force and/or a resultant moment. For an edge crack located near welds H10 and H12 the solution for an edge-cracked beam will overestimate K_I since the support leg is welded to the vessel wall at the bottom and to the core shroud at the top. That is, the presence of the displacement conditions at the ends of the leg, as shown in Figure 4-3, will greatly reduce the loading on the plane of the crack for a deep crack.

Using the solution obtained in Reference [15], the stress intensity factor can be obtained for an arbitrary loading on the faces of an edge crack in a beam with nonuniform thickness and fixed ends. The stress intensity factor K_I in this case is given by the expression

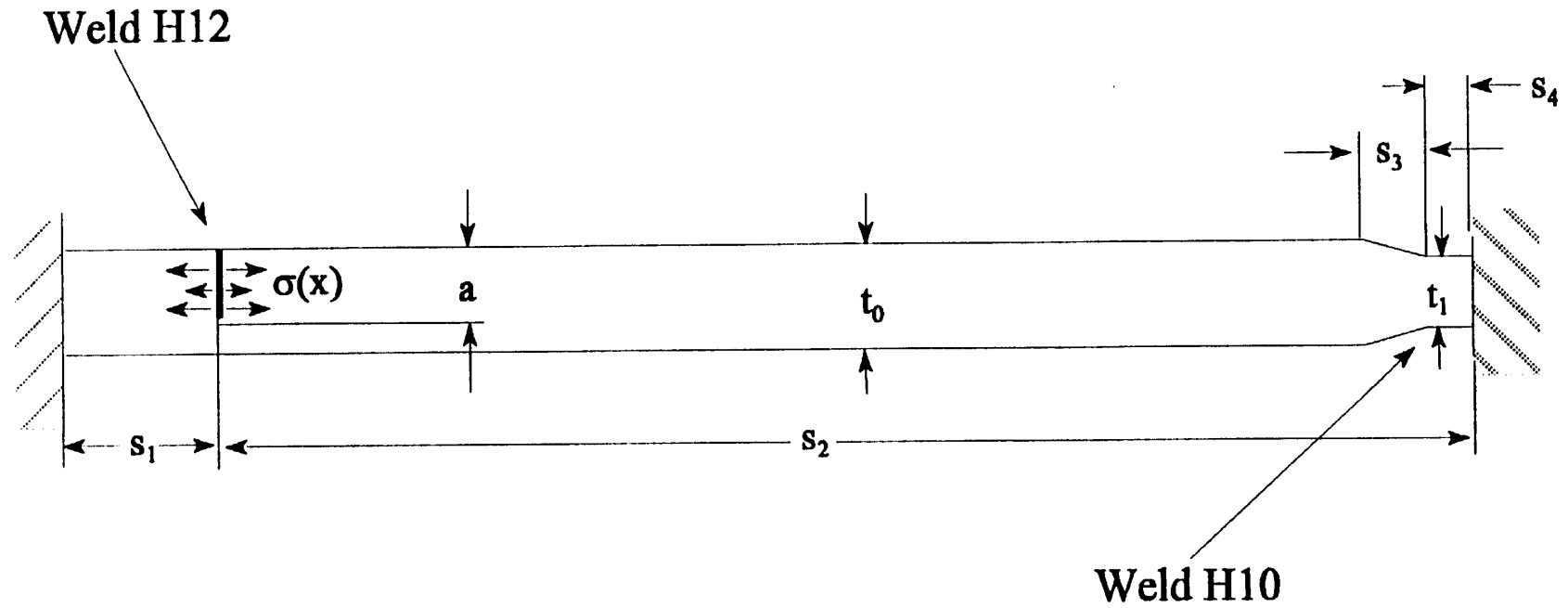
$$K_I = K_I^\sigma - K_I^m - K_I^f \quad \text{Equation 4-4}$$

where K_I^σ , K_I^m and K_I^f are the stress intensity factors for an edge-cracked beam with free ends subjected respectively to a surface stress $\sigma(y)$, moment (M), or axial loading (F). Equation 4-4 can be expanded as

$$K_I = \sqrt{\pi a} \left[\sigma f^\sigma(a/t) - \frac{6M}{t^2} f^m(a/t) - \frac{F}{t} f^f(a/t) \right] \quad \text{Equation 4-5}$$

where σ is a reference stress associated with the magnitude of $\sigma(y)$ on crack faces, a and t are the crack length and thickness. Also, f^σ , f^m and f^f are respectively the finite thickness corrections of the stress intensity factors K_I^σ , K_I^m and K_I^f as a function of a/t . Solutions for, f^σ , f^m and f^f are provided in Reference [15].

The K_I distribution for Welds H10, H11 and H12 obtained with the relationship in Equation 4-5 are shown in Figures 4-4, 4-5, and 4-6, respectively. It should be noted once again that the K_I distributions are normalized and therefore to obtain the actual K_I , the ordinate in these figures should be multiplied by \sqrt{t} , where t is the thickness.



Dimensions: $s_1 = 7.9"$, $s_2 = 80"$, $s_3 = 4"$, $s_4 = 1"$, $t_0 = 5"$ and $t_1 = 3"$

Figure 4-3
An Edge-Cracked Beam With Non-Uniform Thickness and Fixed Ends

**Content Deleted -
EPRI Proprietary Information**

Figure 4-4
Normalized K_I Computed for Weld H10

**Content Deleted -
EPRI Proprietary Information**

Figure 4-5
Normalized K_I for Weld H11

**Content Deleted -
EPRI Proprietary Information**

Figure 4-6
Normalized K_I for Weld H12

5

CRACK GROWTH DISPOSITION CURVES

Beginning in the 1970s and continuing to the present, General Electric Nuclear Energy (GENE) has performed studies of the behavior of Alloy 182 and Alloy 600 structural materials that are used throughout the BWR. These studies have included laboratory stress corrosion tests, crack initiation tests, crack growth tests involving the measurement of crack growth rates in the laboratory and in reactor site testing systems. GENE has also evaluated field cracking and performed failure analyses. GENE has provided IGSCC updates to the NRC on a regular basis to aid in the dissemination of data and understanding of the technical issues. Over the past 15 years, GENE has accumulated data bases on field behavior of these materials and has continually been involved with evaluating plant cracking.

Using this historical foundation coupled with current understanding about SCC, disposition crack growth rate curves for use with Alloy 182 weld metal and Alloy 600 can be defined. Appendix A brings together these different elements and presents the comprehensive basis for these curves. These elements include the laboratory data used by GENE in disposition efforts, data used to discuss the SCC behavior of Ni-base alloys with the NRC, field cracking data, crack growth data from other laboratories and the fundamental PLEDGE model based on stress corrosion principles. This chapter presents the key information from Appendix A and presents the Disposition Curves to be used in the analysis of crack deepening.

5.1 Review of Alloy 182 Disposition Efforts

In response to the cracking in the nozzle-to-safe-end locations and the access hole covers, several utilities required disposition actions to evaluate the consequences of crack growth on the structural margin of the component [16-18]. These analyses were plant specific and directed at the particular cracking conditions found in the components. In some cases, a generic methodology was also invoked. These included a generic report that was prepared for the BWR Owner's Group for Access Hole Covers as well as several specific analyses of nozzle-to safe-end cracking [19-20]. In each analysis the basis for the crack growth rates was presented. Specific discussions of crack growth rates for Alloy 182 and Alloy 600 wrought materials were given. Analyses based on crack growth rates at or below 5×10^{-5} in/hr were used to support operation for additional fuel cycles. These evaluations are useful not only because of the field experience documentation, but also because of the precedent of NRC acceptance of the crack growth rate basis.

5.2 Rates Determined from Field Cracking Events

As stated, cracking has been detected in several different plants in BWR piping components constructed with Alloy 182. Many of the safe ends were overlayed or repaired immediately. Appendix A gives the UT determined crack depth data for many of the crack indications in the different nozzle-to-safe-end welds. Data is also presented for the limited number of re-inspections. The total data base is quite large and can be used to estimate average crack growth rates.

Using the nozzle-to-safe-end cracking incidents, crack growth rates can be estimated by making assumptions on crack initiation time or using reinspection data. Since many of the Alloy 182 cracks are associated with weld defects or weld repairs, the crack initiation time is negligible and field data on crack depths can be used to estimate crack growth over the actual hot operating time. The rate calculations include the initial inspection data as well as the data from the nozzles that were re-inspected. The UT estimated depths and crack growth rates are given in Appendix A. These results provide actual estimates of average crack growth rates under actual plant operating environments. Since many of the cracks were found in plants that had poor conductivity in the first five operating cycles the assumption of very early initiation is reasonable. The data establishes that even for axial crack indications, the average rates are below the 5×10^{-5} in/hr that has been used to disposition indications in the stainless steel reactor internals.

5.3 Review of Recent Data

As a significant part of crack growth assessment efforts, GENE made use of CAVS data to support specific disposition efforts as well as to continually benchmark/validate the conservative nature of its proposed crack growth rates for Alloy 182 and Alloy 600. There have also been continuing efforts to compile laboratory crack growth rate data that have been measured throughout the industry. This compilation now includes data from ABB, Studsvik, VTT, Toshiba and GE CR&D which complements the other existing GENE data. These data are compared with the previous GENE efforts in the second section. The CAVS data has continued to be useful in benchmarking the behavior of Alloy 182 under plant water chemistry conditions. The conductivity level, the specific anionic species and the types of oxidizing species which are present in the in-reactor environment tests have been difficult to reproduce in most laboratory settings.

The EPRI/BWRVIP has recently spent significant effort collecting and reviewing much of the Alloy 182 data from the different testing laboratories to better assess the rates of crack growth. The data covers a large range of conductivity, corrosion potential, cyclic loading conditions and applied K level. It is appropriate that this data also be reviewed for consistency with any proposed disposition curve. Applying the appropriate screens (to exclude data for conditions that are outside the range expected in plant operation) which included conductivity level, constant load conditions, limitation on applied K and limitations on data with large post-test corrections, the data set is consistent with the GENE laboratory and CAVS data. Crack growth data taken under low corrosion potential conditions (typical of HWC) are observed to be significantly below the NWC results. Alloy 600 data follows these trends and are somewhat below the Alloy 182 data for both NWC and HWC environments.

5.4 Modeling Assessments

The working hypothesis for the crack propagation process for IGSCC of Ni-base alloys is widely acknowledged to be similar to that for type 304/316 austenitic stainless steel in high temperature water. For Alloy 182 weldments, the weld residual stress, the Alloy 182 material susceptibility, and the oxygenated water environment are factors that lead to IGSCC cracking. The GE PLEDGE model makes use of these fundamental inputs and has been used to evaluate crack growth and factors of improvement based on environmental parameters.

5.5 Disposition Crack Growth Rate Approach

Using all of this background understanding, the disposition curves incorporate two additional considerations. First there is a clear recognition that the coolant environment, particularly its corrosion potential and conductivity directly influence crack growth rates. Therefore, curves are developed for three different environments: (1) Normal Water Chemistry at or below EPRI Action Level 1 conditions, (2) high purity Normal Water Chemistry with conductivity restricted to 0.15 $\mu\text{S}/\text{cm}$ or better and sulfate and chloride levels below 5 ppb consistent with EPRI Action Level 1 and (3) Hydrogen Water Chemistry that meets EPRI guidelines. The second key element in the methodology for these proposed disposition curves is an approach similar to that proposed in BWRVIP-14 for dispositioning stainless steel. For each environment, this report provides the detailed curves for a disposition curve with K dependent crack growth rate up to a stress intensity level of 25 $\text{ksi}\cdot\text{in}^{1/2}$ and a K independent rate beyond that stress intensity level. The K dependence requires specific knowledge of the stress state for the location of interest. Each curve can be used for the appropriate environment without any other consideration. The methodology acknowledges that plants may also use a specific crack growth rate that would factor in plant environmental and material parameter inputs.

5.6 Specific Curves

Based on all of the past and current information, Disposition Crack Growth Rate Curves are proposed for the evaluation Alloy 182 crack growth for each of three different environments: (1) normal water chemistry (NWC) that meets the EPRI Water Chemistry Guidelines, (2) a more restrictive NWC with conductivity at or better than 0.1 $\mu\text{S}/\text{cm}$ and (3) hydrogen water chemistry (HWC) that meets EPRI guidelines. These curves are to be used for through thickness growth.

5.6.1 Normal Water Chemistry Below EPRI Guidelines Action Level 1

Figure 5-1 displays the proposed curve for use under these NWC conditions.

**Content Deleted -
EPRI Proprietary Information**

**Content Deleted -
EPRI Proprietary Information**

**Figure 5-1
Proposed Disposition Curve for NWC at or Below Action Level 1**

**Content Deleted -
EPRI Proprietary Information**

5.6.2 Normal Water Chemistry With Conductivity at or Below 0.15 $\mu\text{S}/\text{cm}$

**Content Deleted -
EPRI Proprietary Information**

5.6.3 Hydrogen Water Chemistry Within EPRI Guidelines

**Content Deleted -
EPRI Proprietary Information**

5.6.4 Crack Growth Rates for Assessing Crack Lengthening

**Content Deleted -
EPRI Proprietary Information**

5.7 Effect of Fluence on Crack Growth

BWRVIP has performed fluence calculations based on BWRVIP-45 [21, 22] that show that the fluence at the shroud support weld is very low ($\sim 1.2 \times 10^{11} \text{ n}/\text{cm}^2$). At such a low fluence, there should be no effect of fluence on IGSCC of the Alloy 82/182 welds of the shroud support welds.

**Content Deleted -
EPRI Proprietary Information**

**Figure 5-2
Proposed NWC Disposition Curve CAVS Data and Old GENE Lab Data**

**Content Deleted -
EPRI Proprietary Information**

**Figure 5-3
NWC Disposition Curve vs. Screened BWRVIP Alloy 182 Data**

**Content Deleted -
EPRI Proprietary Information**

**Figure 5-4
Comparison of NWC Curve With Field Inspection Field Data**

**Content Deleted -
EPRI Proprietary Information**

**Figure 5-5
Proposed High Purity NWC Disposition Curve**

**Content Deleted -
EPRI Proprietary Information**

Figure 5-6
Comparison of High Purity NWC Disposition Curve With Screened Lab and CAV Data

**Content Deleted -
EPRI Proprietary Information**

Figure 5-7
HWC Disposition Curve Compared With CAVS and Lab Data Under HWC Conditions

6

CRACK GROWTH EVALUATION

In this section, crack growth evaluation is performed for all the various welds of the core shroud support structure of a BWR-6 using the crack growth disposition curves provided in Section 5 and the K distribution for the individual welds determined in Section 4. The basic formulation of the crack growth disposition curve for any of the water chemistry conditions provided in Section 5 is given by

$$\frac{da}{dt} = C_o K^n \quad \text{for } K \leq 25 \text{ ksi } \sqrt{\text{in}}$$

$$\frac{da}{dt} = C_1 \quad \text{for } K > 25 \text{ ksi } \sqrt{\text{in}}$$

C_o , C_1 and n are constants depending on the water chemistry condition which have been provided in Section 5. In the crack growth evaluation, only the normal water chemistry (NWC) and hydrogen water chemistry (HWC) conditions are considered. To perform the evaluation, the appropriate normalized K distribution from Section 4 is determined for the weld. Using the thickness information provided in Figure 2-7 for each weld, the actual K distribution through the wall can be determined. The above equation can then be integrated to determine the crack growth with time. The input into the analysis is provided in Table 6-1. The most conservative aspect ratio of 0.1 is selected for the K distribution for welds H8 and H9. Results of the crack growth evaluation are provided in Appendix C for the various welds.

The results of the evaluation are presented in Table 6-2. The following provides a summary of the observations on the evaluation results.

**Content Deleted -
EPRI Proprietary Information**

**Content Deleted -
EPRI Proprietary Information**

**Table 6-1
Crack Growth Evaluation Input**

Weld	Thickness (in)	K Distribution	Crack Growth Disposition Curve	Initial Flaw Size (in)
H8	2.5	Figure 4-1	NWC (Fig. 5-1) HWC (Fig. 5-7)	0.25
H9	2.5	Figure 4-2	NWC (Fig. 5-1) HWC (Fig. 5-7)	0.25
H10	3.0	Figures 4-4	NWC (Fig. 5-1) HWC (Fig. 5-7)	0.30
H11	5.0	Figure 4-5	NWC (Fig. 5-1) HWC (Fig. 5-7)	0.50
H12	5.0	Figure 4-6	NWC (Fig. 5-1) HWC (Fig. 5-7)	0.50

**Table 6-2
Crack Growth Evaluation Results**

**Content Deleted -
EPRI Proprietary Information**

7

SUMMARY AND CONCLUSION

The following provides a summary and conclusions of the work performed in this report to support crack growth evaluation of the nickel base austenitic alloy core shroud support welds H8, H9, H10, H11 and H12.

**Content Deleted -
EPRI Proprietary Information**

**Content Deleted -
EPRI Proprietary Information**

8

REFERENCES

1. *BWR Vessel and Internals Project, Safety Assessment of BWR Reactor Internals (BWRVIP-06)*. EPRI PROPRIETARY, October 1995. EPRI Report No. TR-105707.
2. *BWR Vessel and Internals Project, Evaluation of Crack Growth in BWR Stainless Steel RPV Internals (BWRVIP-14)*. EPRI PROPRIETARY, March 1996. EPRI Report No. TR-105873.
3. *Stress Corrosion Cracking of Alloys 600 and 182 in BWRs*. September 1994. EPRI Report No. TR-104972.
4. *Stress Corrosion Cracking in Alloy 600 and 690 and Weld Metals No. 82 and 182 in High-Temperature Water*. September 1982. EPRI Report No. NP-2617.
5. *Stress Corrosion Cracking Resistance of Alloys 600 and 690 and Compatible Weld Metals in BWRs*. July 1988. EPRI Report no. NP-5882M.
6. NUREG-0313, Revision 2, "Technical Report on Material Selection and Processing Guidelines for BWR Coolant Pressure Boundary Piping," U.S. Nuclear Regulatory Commission, January 1988.
7. Hettiarachchi, S. et.al., "The Concept of Noble Metal Chemical Addition Technology for IGSCC Mitigation of Structural Materials," NACE International, Seventh International Symposium on Environmental Degradation of Materials in Nuclear Power Systems - Water Reactors, August 7-10, 1995, Breckenridge, CO.
8. *BWRVIP Document, Vessel Internals Inspection Summaries*. EPRI PROPRIETARY, April 1997.
9. *BWR Vessel and Internals Project, BWR Shroud Support Inspection and Flaw Evaluation Guidelines (BWRVIP-38)*. EPRI PROPRIETARY, September 1997. EPRI Report No. TR-108823.
10. *BWR Vessels and Internals Project, Evaluation of Stress Corrosion Crack Growth Rate in Low Alloy Steel Vessel Materials in the BWR Environment (BWRVIP-60)*. EPRI PROPRIETARY. March 1999. EPRI Report No. TR-108709.
11. EPRI Repair and Replacement Application Center, "Stress Analysis of River Bend Unit 2 Reactor Pressure Vessel and Alloy 600 Weld Components".
12. ANSY Finite Element Program, Revision 5.3, Swanson Analysis Systems, Inc.
13. ASME Boiler and Pressure Vessel Code, Section XI, 1995 Edition.
14. Cipolla, R. C., "Technical Basis for the Revised Stress Intensity Factor Equation for Surface Flaws in ASME Section XI Appendix A," Proceedings of ASME Pressure Vessels and Piping Conference, PVP-Vol. 313-1, July 1995.
15. Cheng, W., "Determination of the Stress Intensity Factor for an Edge-Cracked Beam with Fixed Ends" to be submitted to Engineering Fracture Mechanics.

References

16. General Electric Nuclear Energy report SASR 89-18, "Brunswick Nozzle Cracking," February 1989.
17. General Electric Nuclear Energy report SASR 89-22: "Evaluation of the Indication in the Limerick Unit 1 H2H Safe End to Nozzle Weld," August 1989.
18. General Electric Nuclear Energy report SASR-89-37: "Evaluation of the Indication in the River Bend Feedwater Nozzle to Safe End Weld," May 1989.
19. General Electric Nuclear Energy report PMWG-G-537, "Update of Nozzle/Alloy 182 Butter Cracking," 1989.
20. General Electric Nuclear Energy report 523-107-0892: "BWR Access Hole Cover Radial Cracking Evaluation," October 1992.
21. *BWR Vessel and Internals Project, Weldability of Irradiated LWR Structural Components (BWRVIP-45)*. September 1997. EPRI TR-108707.
22. E-mail Communication from Ken Watkins to Ken Wolfe, "Shroud Support Weld Fluence," Thursday March 16, 2006 7:17 pm.
23. *BWR Vessel and Internals Project, Evaluation of Crack Growth in BWR Nickel-Base RPV Internals (BWRVIP-59)*. December, 1998. EPRI Report TR-108710.
24. Letter from C. E. Carpenter (NRC) to C. Terry, (BWRVIP Chairman), Proprietary Request for Additional Information – On EPRI TR-108710, "Evaluation of Crack Growth in BWR Nickel Base Austenitic Alloys in RPV Internals (BWRVIP-59)", (TAC No. MA4467), November 29, 1999, Correspondence File Number 99-491).
25. Letter from C. Terry (BWRVIP) to C. E. Carpenter (NRC), "BWRVIP Response to NRC Request for Additional Information on BWRVIP-59," December 4, 2000. (BWRVIP Correspondence File Number 2000-335).
26. Letter from C. Terry (BWRVIP) to C. E. Carpenter (NRC), "BWRVIP Request for NRC Approval of an Interim Crack Growth Rate of 2.5×10^{-5} in/hr for Nickel Base Austenitic Alloys in BWR Plants Under Hydrogen Water Chemistry (HWC) and Noble Metal Chemical Application (NMCA) Conditions," February 19, 2001. (BWRVIP Correspondence File Number 2001-040).
27. Letter from W. H. Bateman (NRC) to C. Terry (BWRVIP Chairman), "Safety Evaluation of the BWR Vessel and Internals Project BWRVIP-59 Report (TAC No. M94975" and enclosure, July 31, 2001. (BWRVIP Correspondence File Number 2001-247A).
28. Letter from W. H. Bateman (NRC) to C. Terry (BWRVIP Chairman), "Clarification to NRC Letter Regarding BWRVIP Response to BWRVIP-59 Safety Evaluation" (TAC No. MA4467), January 29, 2002. (BWRVIP Correspondence File Number 2002-037).
29. Letter from W. A. Eaton (BWRVIP) to M. Khanna (NRC), "BWRVIP Response to NRC Safety Evaluation of BWRVIP-59," Including CD with Revised BWRVIP-59 Report, December 20, 2004. (BWRVIP Correspondence File Number 2004-535).
30. Letter from M. A. Mitchell (NRC) to W. A. Eaton (BWRVIP Chairman), "Safety Evaluation of EPRI Report, BWR Vessel and Internals Project, Evaluation of Crack Growth in BWR Nickel Base Austenitic Alloys in Reactor Pressure Vessel Internals (BWRVIP-59)", and enclosure, July 14, 2006. (BWRVIP Correspondence File Number 2006-386).

A

NICKEL BASE CRACK GROWTH DISPOSITION CURVES

**Content Deleted -
EPRI Proprietary Information**

**Content Deleted -
EPRI Proprietary Information**

A.1 Background

**Content Deleted -
EPRI Proprietary Information**

A.2 Report Outline

**Content Deleted -
EPRI Proprietary Information**

A.3 Review of Previous Efforts to Evaluate Alloy 182 Cracking in Operating BWRs

**Content Deleted -
EPRI Proprietary Information**

**Table A-1
Pilgrim Nozzle Cracking Data**

**Content Deleted -
EPRI Proprietary Information**

Table A-2
Lists of Plants With Nozzle/Safe End Cracking

**Content Deleted -
EPRI Proprietary Information**

Table A-3
Summary of Access Hole Cover Cracking in U.S. Plants

**Content Deleted -
EPRI Proprietary Information**

A.3.1 Review of Alloy 182 Disposition Efforts

**Content Deleted -
EPRI Proprietary Information**

A.3.2 Historical Disposition Crack Growth Discussion

A.3.2.1 Limerick 1: First Disposition Effort: 1989

**Content Deleted -
EPRI Proprietary Information**

**Content Deleted -
EPRI Proprietary Information**

**Figure A-1
Alloy 182 Crack Growth Rate Dependency [A-15–A-18]**

**Content Deleted -
EPRI Proprietary Information**

**Figure A-2
Alloy 182 Crack Growth Rate Dependency With Conductivity**

A.3.2.2 Hatch Access Hole Cover Disposition

**Content Deleted -
EPRI Proprietary Information**

**Content Deleted -
EPRI Proprietary Information**

**Figure A-3
Crack Growth Rates for Alloy 182 (<0.5 $\mu\text{S}/\text{cm}$) [A-19–A-28]**

**Content Deleted -
EPRI Proprietary Information**

Figure A-4
SCC Crack Growth Rates for Alloy 182 (<0.5 μ S/cm and >0.5 μ S/cm: [A-19–A-26])

**Content Deleted -
EPRI Proprietary Information**

**Figure A-5
SCC Crack Growth Rates for Nickel Base Alloys as a Function of Conductivity [A-29]**

**Content Deleted -
EPRI Proprietary Information**

**Figure A-6
SCC Crack Growth Rates for Alloy 600**

A.3.2.3 Limerick 1: Follow-Up Disposition Effort: 1990

**Content Deleted -
EPRI Proprietary Information**

A.4 Discussions With the U.S. NRC on Alloy 182 Crack Growth Rates

**Content Deleted -
EPRI Proprietary Information**

**Table A-4
GENE Efforts in Evaluating and Dispositioning Cracking in Alloy 182 Welds**

**Content Deleted -
EPRI Proprietary Information**

A.4.1 IGSCC Technology Update Meeting for NRC: June 9, 1987

**Content Deleted -
EPRI Proprietary Information**

A.4.2 IGSCC Technology Update Meeting for the NRC: March 22, 1989

**Content Deleted -
EPRI Proprietary Information**

A.5 Rates Determined from Field Cracking Events

**Content Deleted -
EPRI Proprietary Information**

Table A-5
Field Cracking Data for Nozzle-to-Safe End Alloy 182 Initial Inspection

**Content Deleted -
EPRI Proprietary Information**

Table A-6
Field Cracking Data for Nozzle-to-Safe End Alloy 182 After Re-Inspection

**Content Deleted -
EPRI Proprietary Information**

Table A-7
Field Cracking Data for Nozzle-to-Safe End Alloy 182 After Second Re-Inspection

**Content Deleted -
EPRI Proprietary Information**

**Content Deleted -
EPRI Proprietary Information**

**Figure A-7
CAVS Alloy 182 Data: Limerick 1**

**Content Deleted -
EPRI Proprietary Information**

**Figure A-8
CAVS Data from Various Plants [A-19–A-25]**

**Content Deleted -
EPRI Proprietary Information**

**Figure A-9
Comparison of the Predicted and Observed Rates vs. Stress Intensity for Data on Alloy
182 [A-19–A-25]**

**Content Deleted -
EPRI Proprietary Information**

Figure A-10
Field Inspection Crack Growth Rate Data (as a Function of Time when Inspection was Performed)

**Content Deleted -
EPRI Proprietary Information**

Figure A-11
Inspection Field Data: Axial and Circumferential Nozzle Cracking

A.6 Review of Recent Data

**Content Deleted -
EPRI Proprietary Information**

A.6.1 Recent CAV Data

**Content Deleted -
EPRI Proprietary Information**

A.6.2 Recent Crack Growth Rate Data

**Content Deleted -
EPRI Proprietary Information**

**Content Deleted -
EPRI Proprietary Information**

**Figure A-12
GENE Lab and CAV Data vs. K Level**

**Content Deleted -
EPRI Proprietary Information**

**Figure A-13
CAVS Data Along With GENE Disposition Band**

**Content Deleted -
EPRI Proprietary Information**

**Figure A-14
Alloy 600 CAVS Data (All ECP Conditions)**

**Content Deleted -
EPRI Proprietary Information**

**Figure A-15
Full BWRVIP Alloy 182 Data Base**

**Content Deleted -
EPRI Proprietary Information**

**Figure A-16
BWRVIP Alloy 182 Data Screened by GE**

A.6.3 Recent GENE Crack Growth Rates Efforts

**Content Deleted -
EPRI Proprietary Information**

**Content Deleted -
EPRI Proprietary Information**

**Figure A-17
CAVS Data Under HWC Conditions**

**Content Deleted -
EPRI Proprietary Information**

**Figure A-18
Alloy 600 CAVS Data (ECP < -230mV, she)**

A.7 Modeling Assessments

**Content Deleted -
EPRI Proprietary Information**

**Content Deleted -
EPRI Proprietary Information**

**Figure A-19
Crack Growth Rates for Alloy 182 Compared With PLEDGE Predictions**

**Content Deleted -
EPRI Proprietary Information**

**Figure A-20
PLEDGE Calculations vs. Proposed NWC Disposition Curve**

A.8 Proposed Interim Disposition Curves

A.8.1 Review of Basis for Approach

**Content Deleted -
EPRI Proprietary Information**

A.8.2 Specific Curves

**Content Deleted -
EPRI Proprietary Information**

A.8.2.1 Normal Water Chemistry Below EPRI Guidelines Action Level 1

**Content Deleted -
EPRI Proprietary Information**

**Content Deleted -
EPRI Proprietary Information**

**Figure A-21
Proposed Disposition Curve for NWC at or Below Action Level 1**

**Content Deleted -
EPRI Proprietary Information**

Figure A-22
Proposed NWC Disposition Curve vs. GENE CAV and Lab Data

**Content Deleted -
EPRI Proprietary Information**

**Figure A-23
NWC Disposition Curve vs. Screened BWRVIP Alloy 182 Data**

**Content Deleted -
EPRI Proprietary Information**

**Figure A-24
Comparison of NWC Curve With Field Inspection Field Data**

A.8.2.2 Normal Water Chemistry With Conductivity Below 0.15 $\mu\text{S}/\text{cm}$

**Content Deleted -
EPRI Proprietary Information**

A.8.2.3 Hydrogen Water Chemistry Within EPRI Guidelines

**Content Deleted -
EPRI Proprietary Information**

A.8.3 Comparison With PLEDGE and the SKI Disposition Curves

**Content Deleted -
EPRI Proprietary Information**

**Content Deleted -
EPRI Proprietary Information**

**Figure A-25
Proposed High Purity NWC Disposition Curve**

**Content Deleted -
EPRI Proprietary Information**

**Figure A-26
Proposed NWC Disposition Curved With CAVS Data and Old GENE Curves**

**Content Deleted -
EPRI Proprietary Information**

Figure A-27
Comparison of High Purity NWC Disposition Curve With Screened Lab and CAV Data

**Content Deleted -
EPRI Proprietary Information**

**Figure A-28
Proposed HWC Disposition Curve**

**Content Deleted -
EPRI Proprietary Information**

Figure A-29
HWC Disposition Curve Compared With CAVS and Lab Data Under HWC Conditions

**Content Deleted -
EPRI Proprietary Information**

**Figure A-30
PLEDGE Calculations vs. Proposed Curves**

**Content Deleted -
EPRI Proprietary Information**

**Figure A-31
Proposed Disposition Curves vs. SKI Curves**

A.8.4 Applicability to Alloy 600

**Content Deleted -
EPRI Proprietary Information**

A.9 Conclusions and Recommendations

**Content Deleted -
EPRI Proprietary Information**

A.10 References

**Content Deleted -
EPRI Proprietary Information**

B

THROUGH-THICKNESS RESIDUAL STRESS MEASUREMENT AT RIVER BEND NUCLEAR STATION

Prepared by
W. Cheng
University of California, Berkeley
(Currently with Berkeley Engineering and Research)

Measurements of Residual Stresses in BWR Core Shroud Support Welds

Research Project B301-11

Final Report, December 1997

Prepared by
Weili Cheng
Iain Finnie
University of California, Berkeley
Berkeley, CA 94720

Prepared for
Boiling Water Reactor Vessel & Internals Project and
Electric Power Research Institute
3412 Hillview Avenue
Palo Alto, CA 94304

B.1 Introduction

The presence of residual stresses due to welding has been found to have a significant influence on the intergranular stress corrosion cracking (IGSCC) BWR vessel internals. The objective of the project is to use the crack compliance method to obtain the residual stresses in the BWR core shroud support welds H8, H10 and H9, and H12. A brief overview of the theoretical background and experimental procedures of the method is given in this section. The results of measurement for different welds will then be presented.

B.1.1 Theoretical Background

The crack compliance method is based on linear superposition for the linear elastic deformation which occurs when a thin cut of progressively increasing depth is introduced into a body with residual stresses. That is, the deformation due to releasing residual stresses, as shown in Figure B-1, is the same as that produced by applying the same stress with opposite sign to the faces of the cut.

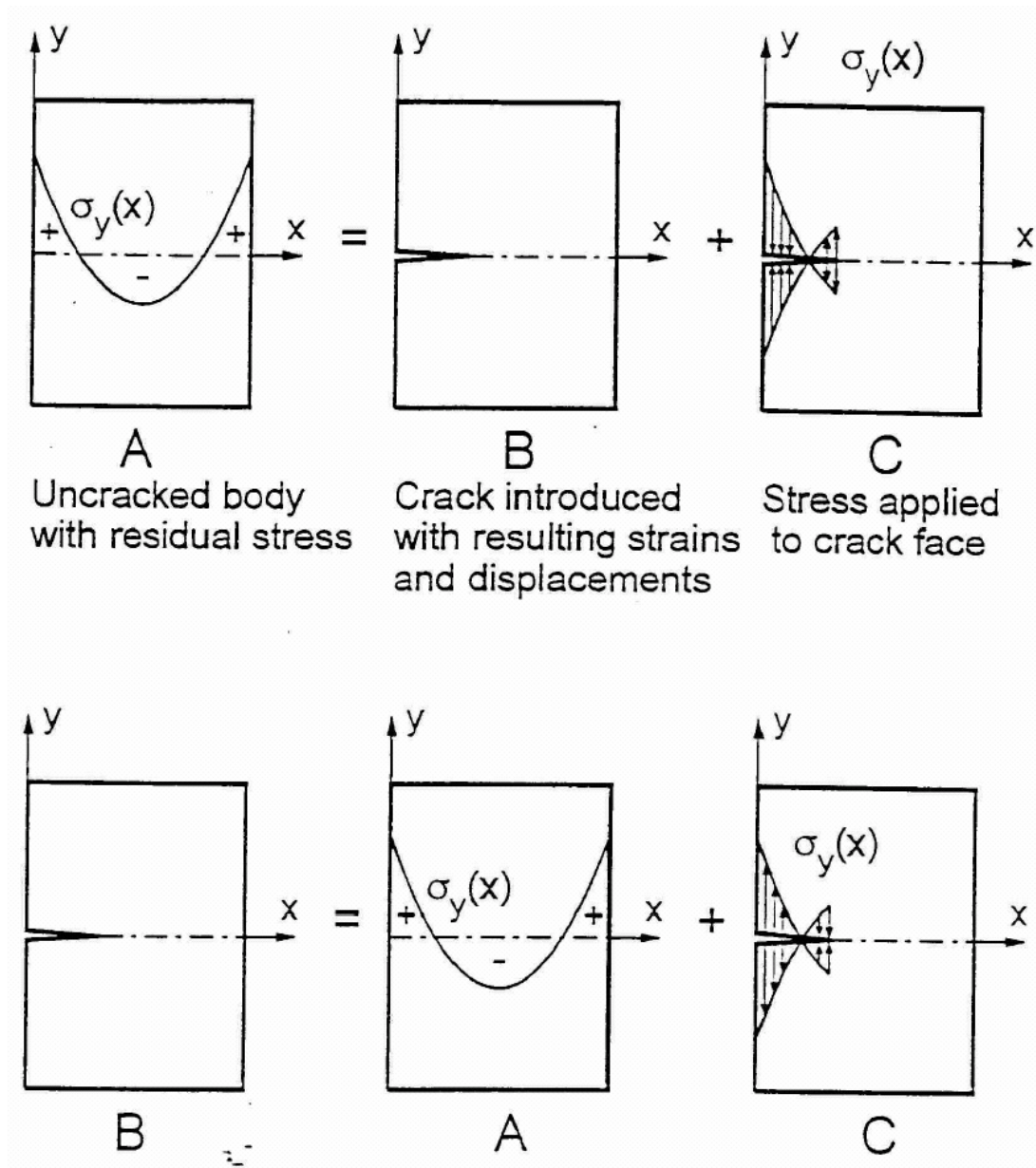


Figure B-1
Illustration of Linear Superposition for Determining Strains Due to Introducing a Crack into Body With Residual Stresses

The unknown residual stress distribution released by cutting is first represented by a series

$$\sigma(x) = \sum_{i=0}^n A_i P_i(x) \quad \text{Equation B-1}$$

in which A_i is the amplitude factor to be determined for the i^{th} term of a prescribed polynomial series $P_i(x)$. When the change of strain ϵ is measured for a given depth of cut a , as shown in Figure B-2, the relation between the stress released and the strain measured may be expressed as

$$\epsilon(a) = \sum_{i=0}^n A_i C_i(a) \quad \text{Equation B-2}$$

where $C_i(a)$, referred to as the crack compliance function, is the strain produced by the surface traction $P_i(x)$ for a depth of cut a . When a number $m > n-1$ of strain measurements are made, a least squares fit can be used to minimize the mean error involved in the measurement and estimation. This procedure leads to a set of $n-1$ linearly independent equations, from which the unknown A_i can be solved.

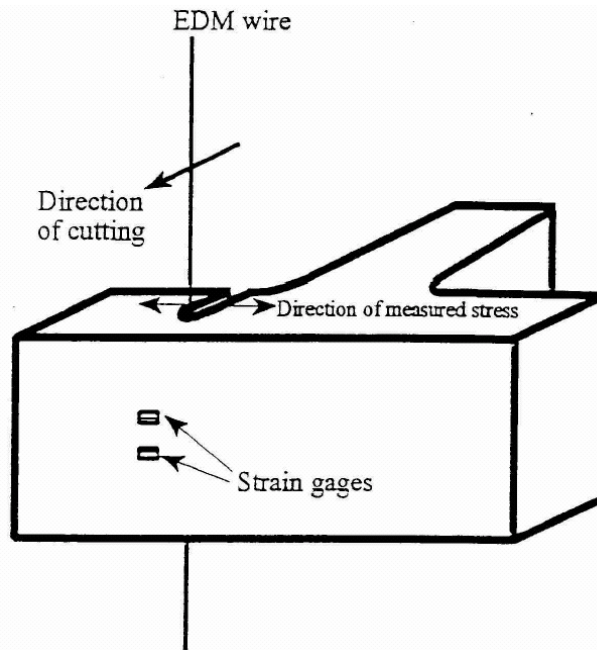


Figure B-2
Residual Stress Distribution Measured By Introducing a Cut of Increasing Depth while the Change of Strain is Recorded by Strain Gages on the Back Face

For through-thickness measurement the cut can be approximated by a crack and the crack compliance functions are obtained for an edge-cracked body subjected to an arbitrary surface traction on the crack faces [1]. To ensure zero resultant force and moment over the thickness, the residual stress distribution is usually approximated by Legendre polynomials of orders larger than one. For a body of a complicated geometry, the finite element method can be used to carry out the required computations.

B.1.2 Experimental Procedures

Strain gages are first installed on specimens at locations optimal for measurement of residual normal stresses. Electrical discharge wire machining (EDWM) is then used to introduce a thin cut of increasing depth as shown in Figure B-2. The test is carried out in a temperature-controlled environment. For through-thickness measurement more than forty strain readings can be recorded and used to estimate the residual stresses over a region about 4% to 96% of the thickness.

B.2 Measurement of Residual Stresses through the Thickness of Welds

Specimens containing welds H8, H10, H9, and H12 (the support leg weld) were cut out from coupons removed from the main body of the shroud and vessel structure. Since the state of residual stress changes as the specimens are cut out from the coupons, the original residual stresses σ consist of two parts

$$\sigma = \sigma_1 + \sigma_2 \quad \text{Equation B-3}$$

in which σ_1 is the stress to be measured in a specimen and σ_2 is the change of the stress when the specimen was cut out. The first part of the stress can be obtained by the crack compliance method while the second part will be estimated by the finite element method based on the strain data recorded when the specimen is cut out from the coupon. In this report the results for the first part of the residual stresses (σ_1) are presented.

For all the specimens the region of the weld surface was found to have been subjected to machining or grinding. Therefore, the residual stresses near the surface are expected to be influenced by machining or grinding as well as welding. Because the surfaces of the as received parts were too rough for attaching strain gages directly, polishing using sand paper was carried out to smooth the surface (standard procedure recommended by strain gage supplier). This process however is expected to have very little influence on the residual stresses in the as received specimens.

B.2.1 Residual Stress Distribution Measured for Weld H8

Weld H8 was located between the shroud support plate (baffle plate) and core shroud. Figure B-3 shows the configuration of the specimen and the finite element mesh used for numerical computations. To ensure a high accuracy of the numerical computation, a very fine mesh using 8-nodes elements is implemented in the region where residual stresses are to be measured. The plane of measurement was located about 7/8" from the core shroud. A cut of progressively increasing depth was made from location o indicated in Figure B-3 while the change of strain was measured by two strain gages (CEA-06-062UW-120) on the back face opposite the cut. Figure B-4 shows the strains measured as a function of the depth of cut. The strain readings of the two gages were stable and consistent throughout the test. The average of the readings from the two strain gages was used to estimate the residual stress.

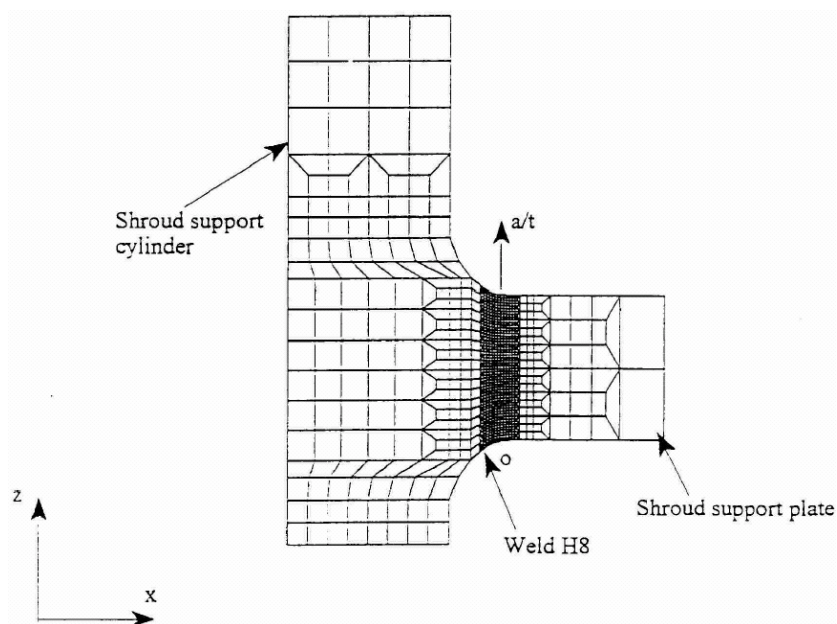


Figure B-3
Finite Element Mesh for the Specimen Containing Weld H8 to Model a Cut through the Thickness of the Shroud Support Plate

**Content Deleted -
EPRI Proprietary Information**

Figure B-4
Strain Readings Recorded when σ of Progressively Increasing Depth Introduced to Weld H8

Only the elastic properties of the material are required for all the stress estimations. It is assumed that the properties for the base and weld metals are identical. Table B-1 lists the material properties used in the computation.

**Content Deleted -
EPRI Proprietary Information**

Figure B-5
Residual Radial Stress Distribution (σ_r) for Weld H8 as a Function of the Distance Normalized by the Thickness of the Shroud Support Plate

Table B-1
Material Properties Used in Computation

Elastic modulus $E = 30 \times 10^6$ psi	Poisson's ratio $\mu = 0.3$
--	-----------------------------

B.2.2 Residual Stress Distribution Measured for Weld H10

Weld H10 joins the core shroud to the shroud support leg. Figure B-6 shows the configuration of the specimen and the finite element mesh used for numerical computations. Again, in this and all other welds a very fine mesh is used in region of the measurement. The plane of measurement was located about 2" from the shroud support plate. A cut of progressively increasing depth was made from location o shown in Figure B-6 while the change of strain was measured by two strain gages (CEA-06-062UW-120) on the back face opposite the cut. Figure B-7 shows the strains measured as a function of the depth of cut. The strain readings of the two gages were stable and consistent through the test. The average of the readings from the two strain gages was used to estimate the residual stress.

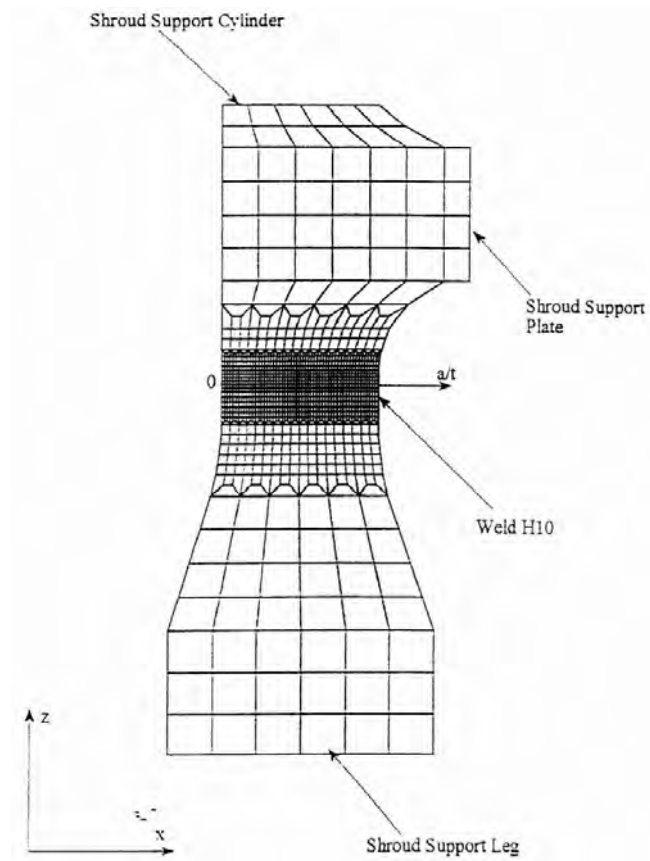


Figure B-6
Specimen Configuration and Finite Element Mesh for Weld H10

**Content Deleted -
EPRI Proprietary Information**

**Content Deleted -
EPRI Proprietary Information**

**Figure B-7
Strain Readings Recorded when a Cut of Progressively Increasing Depth Introduced to
Weld H10**

**Content Deleted -
EPRI Proprietary Information**

**Figure B-8
Residual Axial Stress Distribution (σ_z) for Weld H10 as a Function of the Distance
Normalized by the Thickness of the Shroud Support Cylinder**

B.2.3 Residual Stress Distribution Measured in Shroud Support Plate for Weld H9

Weld H9 joins the shroud support plate to the vessel wall. Residual stresses were measured through the thickness of both the shroud support plate and the vessel wall. For the shroud support plate the measurement was carried out on a plane about 1.1 inch from the vessel wall. Figure B-9 shows the configuration of the specimen and the finite element mesh used for numerical computations. Two strain gages (CEA-06-062UW-120) were installed on the back face opposite the cut. Strains measured during cutting are plotted in Figure B-10 against the depth of cut. Similar to the previous two tests, the readings were stable and consistent throughout the test.

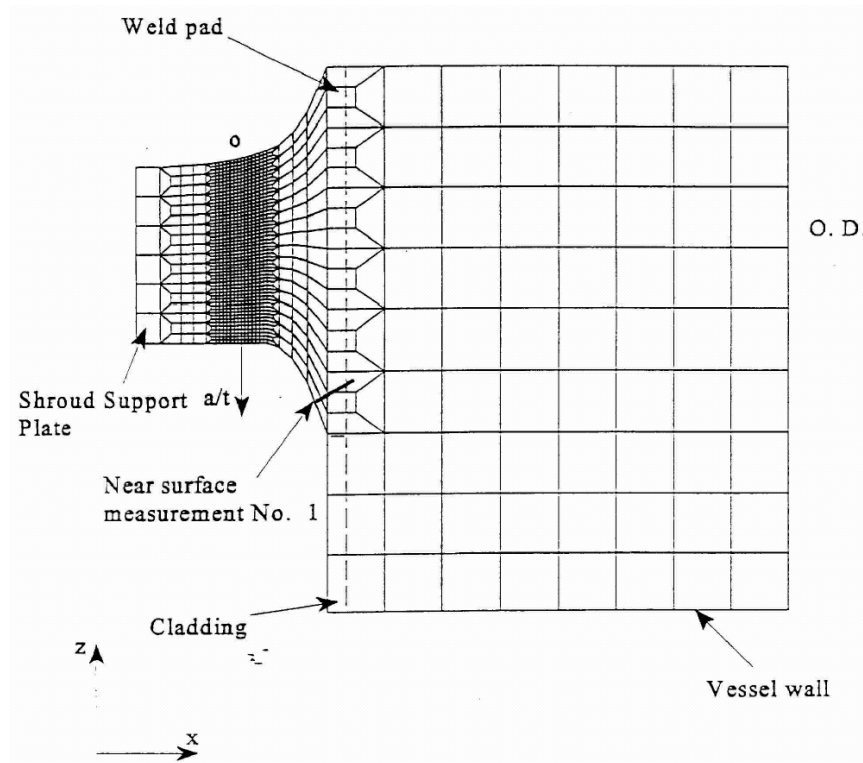


Figure B-9
Finite Element Mesh for the Specimen Containing Weld H9. The Residual Axial Stress Distribution σ_x is Measured through the Thickness of the Shroud Support Plate. Also Shown is the Location of the Near Surface Measurement No. 1

**Content Deleted -
 EPRI Proprietary Information**

**Content Deleted -
EPRI Proprietary Information**

**Figure B-10
Strain Readings Recorded when a Cut of Progressively Increasing Depth Introduced
to Weld H9 through the Thickness of the Shroud Support Plate**

**Content Deleted -
EPRI Proprietary Information**

**Figure B-11
Residual Radial Stress Distribution (σ_x) as a Function of the Distance Normalized
by the Thickness of the Shroud Support Plate (Baffle Plate) for Weld H9**

B.2.4 Residual Stress Distribution Measured in Vessel Wall for Weld H9

For weld H9 on the vessel wall the measurement was carried out on a plane about 5/32 inch from the toe of the weld. Figure B-12 shows the configuration of the specimen and the finite element mesh used for numerical computations. Two strain gages (CEA-06-062UW-120) were installed on the back face opposite the cut. Strains measured during cutting are plotted in Figure B-13 against the depth of cut. Similar to the previous tests, the readings were stable and consistent throughout the test.

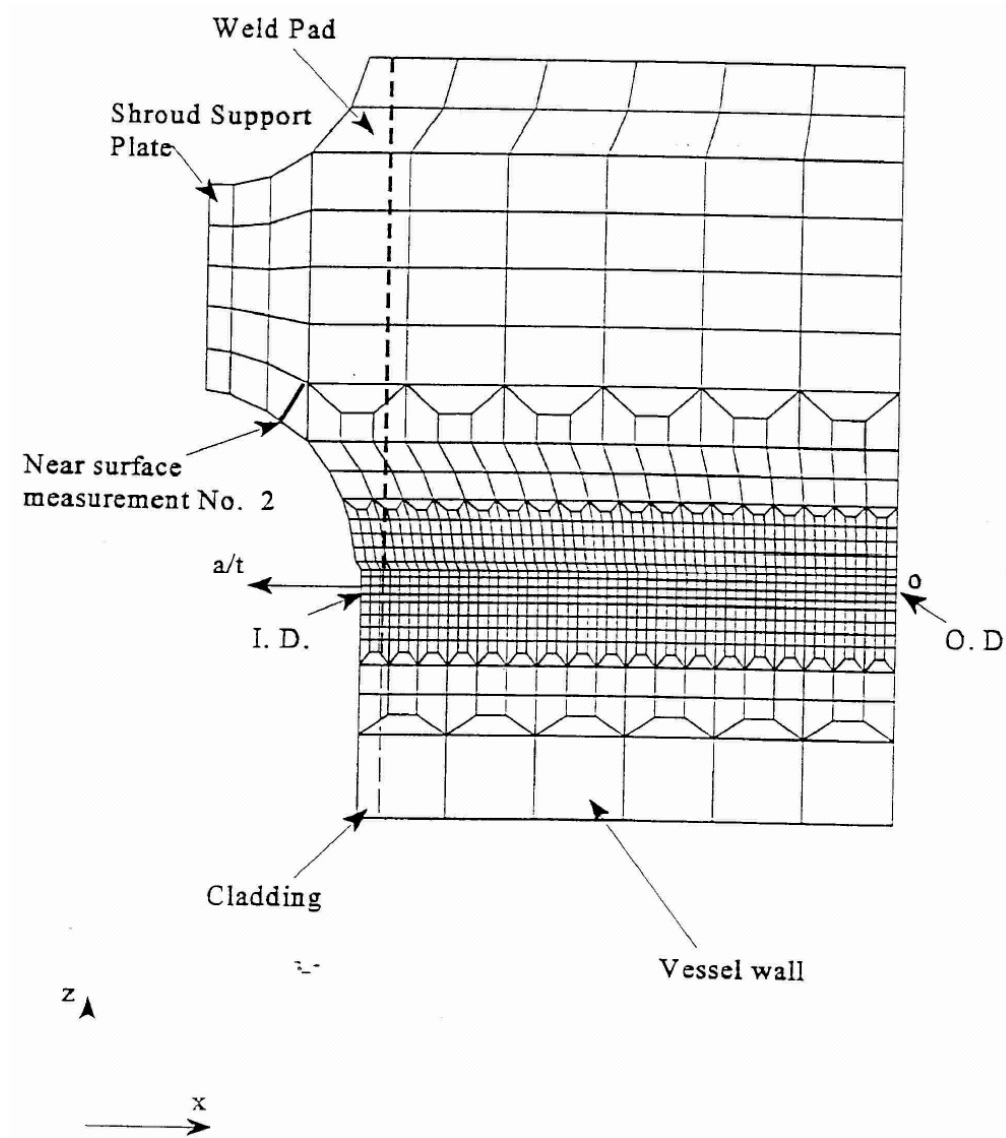


Figure B-12
Finite Element Mesh for the Specimen Containing Weld H9. The Residual Axial Stress Distribution (σ_z) is Measured through the Thickness of the Vessel Wall. Also Shown is the Location of the Near Surface Measurement No. 2

**Content Deleted -
EPRI Proprietary Information**

Figure B-13
Strain Readings Recorded when a Cut of Progressively Increasing Depth Introduced to Weld H9 through the Thickness of the Vessel Wall

**Content Deleted -
EPRI Proprietary Information**

Figure B-14
Residual Axial Stress Distribution (σ_z) as a Function of the Distance Normalized the Thickness of the Vessel Wall for Weld H9

Content Deleted -
EPRI Proprietary Information

B.2.5 Residual Stress Distribution Measured for the Shroud Support Leg Weld (H12)

The shroud support leg and the vessel wall was joined by the shroud support leg weld (H12). The configuration of the specimen, plane of measurement, and the finite element mesh used for numerical computations are shown in Figure B-15. Two strain gages (CEA-06-062UW-120) were installed on the back face opposite the cut. Strains measured during cutting are plotted in Figure B-16 against the depth of cut. Similar to the previous tests, the readings were stable and consistent throughout the test.

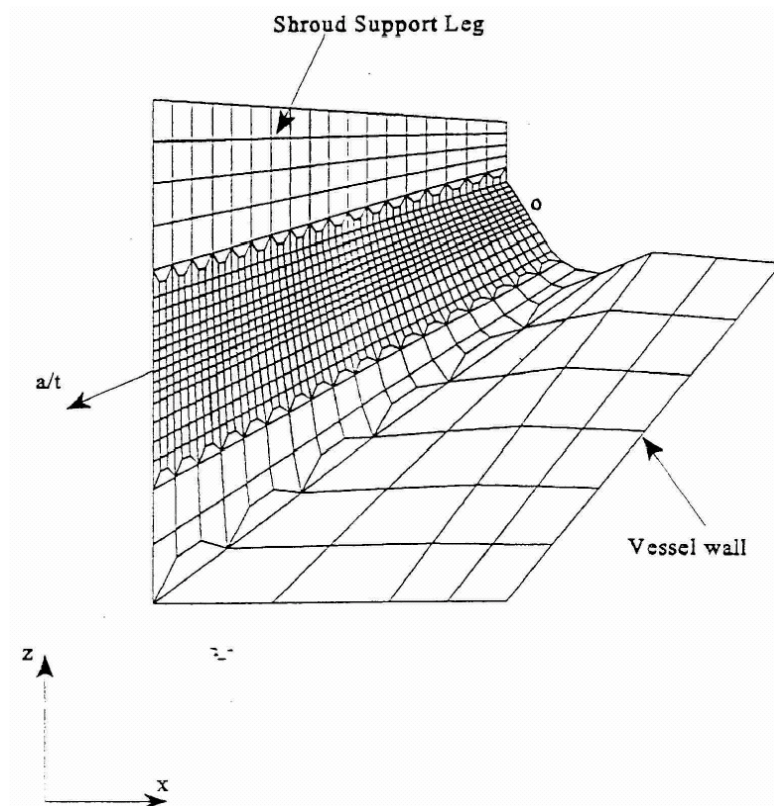


Figure B-15
Finite Element Mesh for the Specimen Containing the Shroud Support Leg Weld (H12)

Content Deleted -
EPRI Proprietary Information

**Content Deleted -
EPRI Proprietary Information**

Figure B-16
Strain Readings Recorded when a Cut of Progressively Increasing Depth Introduced through the Thickness of the Shroud Support Leg Weld (H12)

**Content Deleted -
EPRI Proprietary Information**

Figure B-17
Residual Stress Distribution (Normal to the Plane of Cut) for Weld H12 as a Function of the Distance Normalized by the Thickness of the Shroud Support Leg Weld on the Plane of Cut

B.3 Measurement of Residual Stresses Near the Surface of Weld H9

In addition to the through thickness measurements, near surface stress measurements were also carried out at two locations for weld H9.

In this case the width of the cut introduced to release the residual stresses is no longer negligible when compared with the depth of the cut. For this reason the compliance functions were obtained using the body force method, which is more accurate and convenient to use than the finite element method for a semi-infinite body with a cut of finite width [2].

**Content Deleted -
EPRI Proprietary Information**

Figure B-18
Near Surface Residual Stress Distribution as a Function of the Distance Measured at the
Location Shown in Figure B-9 for Weld H9

**Content Deleted -
EPRI Proprietary Information**

**Figure B-19
Near Surface Residual Stress Distribution in the Weld as a Function of the Distance
Measured at the Location Shown in Figure B-12 for Weld H9**

Table B-2
Configuration and Strains Measured for Near Surface Stress Measurement No. 1
of Weld H9

**Content Deleted -
EPRI Proprietary Information**

B.4 Conclusion

Residual stress distributions in four weld configurations were measured using the crack compliance methods. All tests were carried out by high precision numerical controlled EDWM. Strain data recorded during tests were found to be both stable and consistent. To minimize the influence of measurement error, a least squares fit was used to obtain the residual stresses from the average of the strain readings recorded by two strain gages.

Table B-3
Configuration and Strains Measured for Near Surface Stress Measurement No. 2
of Weld H9

**Content Deleted -
EPRI Proprietary Information**

As shown in Figures B-5, B-8, B-11, B-14, and B-17, residual stresses are found to be tensile near the weld surface and become compressive near the center portion of the thickness. This is expected because the residual stresses in the specimens always satisfy the equilibrium condition in both force and moment.

B.5 References

1. Cheng, W. and Finnie, I., "An Overview of the Crack Compliance Method for Residual Stress Measurement," *Proceedings of Fourth Int. Conf. on Residual Stresses*, pp.449-458, 1994.
2. Cheng, W. and Finnie, I., "A Comparison of the Strains due to Edge Cracks and Cuts of Finite Width With Applications to Residual Stress Measurement," *ASME J. of Eng. Mat. and Tech.*, **115**, pp. 220-226, 1993.
3. Cheng, W., Gremaud, M. and Finnie, I., "The Compliance Method for Measurement of Near surface Residual Stresses - Analytical Background," *ASME J. of Eng. Mat. and Tech.* **116**, pp. 550- 555, 1994.

C

CRACK GROWTH EVALUATION RESULTS

**Entire Appendix Deleted
EPRI Proprietary Information**

D

ANALYTICAL PREDICTION OF RESIDUAL STRESSES IN BWR SHROUD SUPPORT STRUCTURE WELDS

December 1998

Prepared by
A. P. L. Turner
J. E. Broussard
E. S. Hunt

Prepared for
Electric Power Research Institute
3412 Hillview Avenue
Palo Alto, CA 94303

Analytical Prediction of Residual Stresses in Shroud Welds

The purpose of this appendix is to describe a finite element analysis (FEA) which was performed to compute residual stresses in welds of the BWR core shroud support structure design which includes support legs to the lower head of the reactor pressure vessel (RPV).

D.1 Weld Joints Analyzed

BWR core shroud support structures have a number of different designs. The design addressed in this appendix is shown in Figure D-1. The support structure consists of twelve equal size, equally spaced legs between the RPV bottom head and a shroud support cylinder. Lateral support is provided by an annular support plate (baffle plate) between the outside diameter (OD) of the shroud support cylinder and the inside diameter (ID) of the RPV. The baffle plate has holes for mounting the recirculation jet pumps. All components of the shroud support structure are made from nickel Alloy 600. The dimensions used for the model were based on the River Bend reactor, but a similar design is used in a number of plants. The calculated residual stresses are considered to be typical for all plants of similar design.

The River Bend shroud support system is twelve fold symmetric with the exception that access manways replace the jet pumps at two diametrically opposite positions. Thus, there are ten jet pump assemblies and two manways around the circumference of the shroud support assembly. It is considered that the differences between the jet pump and manway locations are negligible in terms of the structural characteristics of the support system. Therefore, a finite element model of a 15-degree segment of the RPV and shroud support structure, as shown in Figure D-2, with mirror boundary conditions on the radial plane boundaries of the model accurately represents the complete vessel and supports.

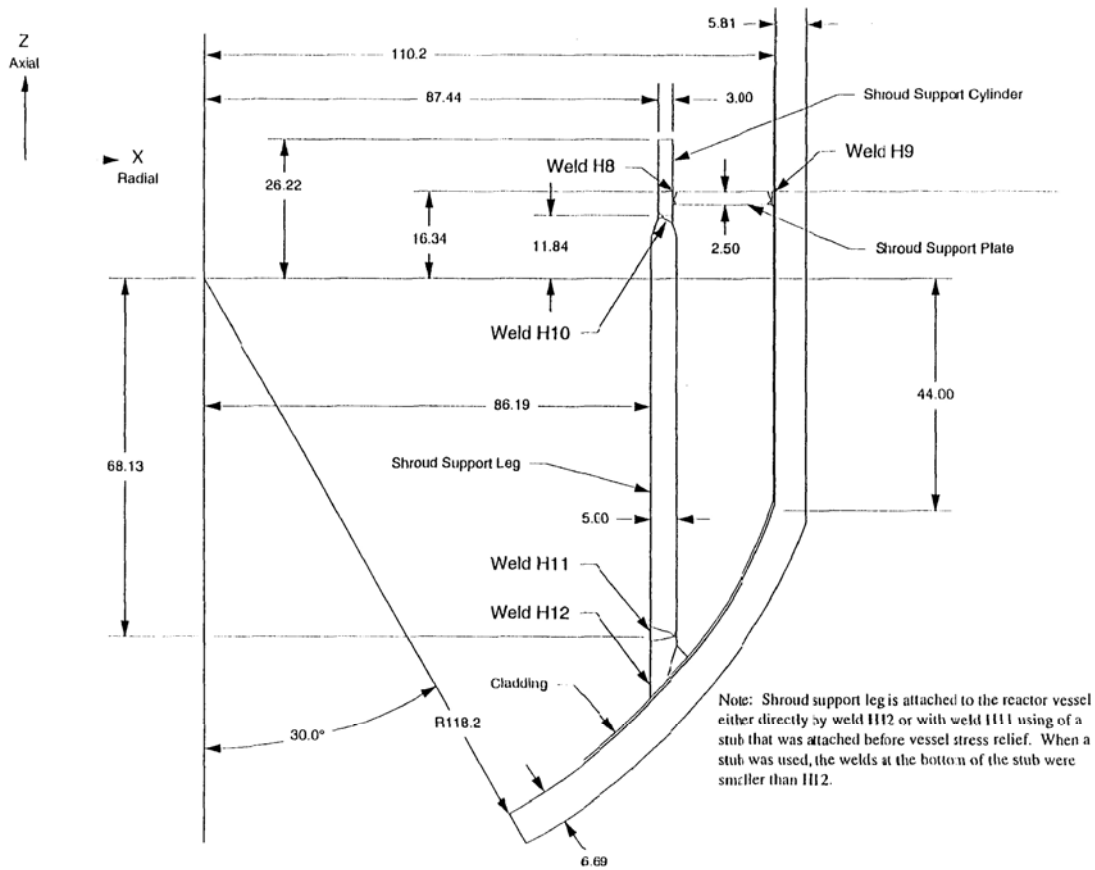


Figure D-1
Reactor Vessel and Shroud Support Model

Five welds were modeled in the finite element analysis. The weld locations are shown in Figure D-1 and are given designations as follows:

- H8 Weld connecting the ID of the shroud support plate to the OD of the shroud support cylinder.
- H9 Weld connecting the OD of the shroud support plate to the ID of the RPV.
- H10 Weld between the top of a support leg and the bottom of the shroud support cylinder.
- H11 Weld between the bottom of a support leg and a pedestal attached to the lower head of the RPV when pedestals are used. The shroud support drawing indicates that pedestals are optional. No pedestals were used with the River Bend legs. Either an H11 or an H12 weld is used to attach the support leg to the lower head of the RPV.
- H12 Weld directly between the bottom of a support leg and the lower head of the RPV (no pedestal used). Either an H11 or an H12 weld is used to attach the support leg to the lower head of the RPV.

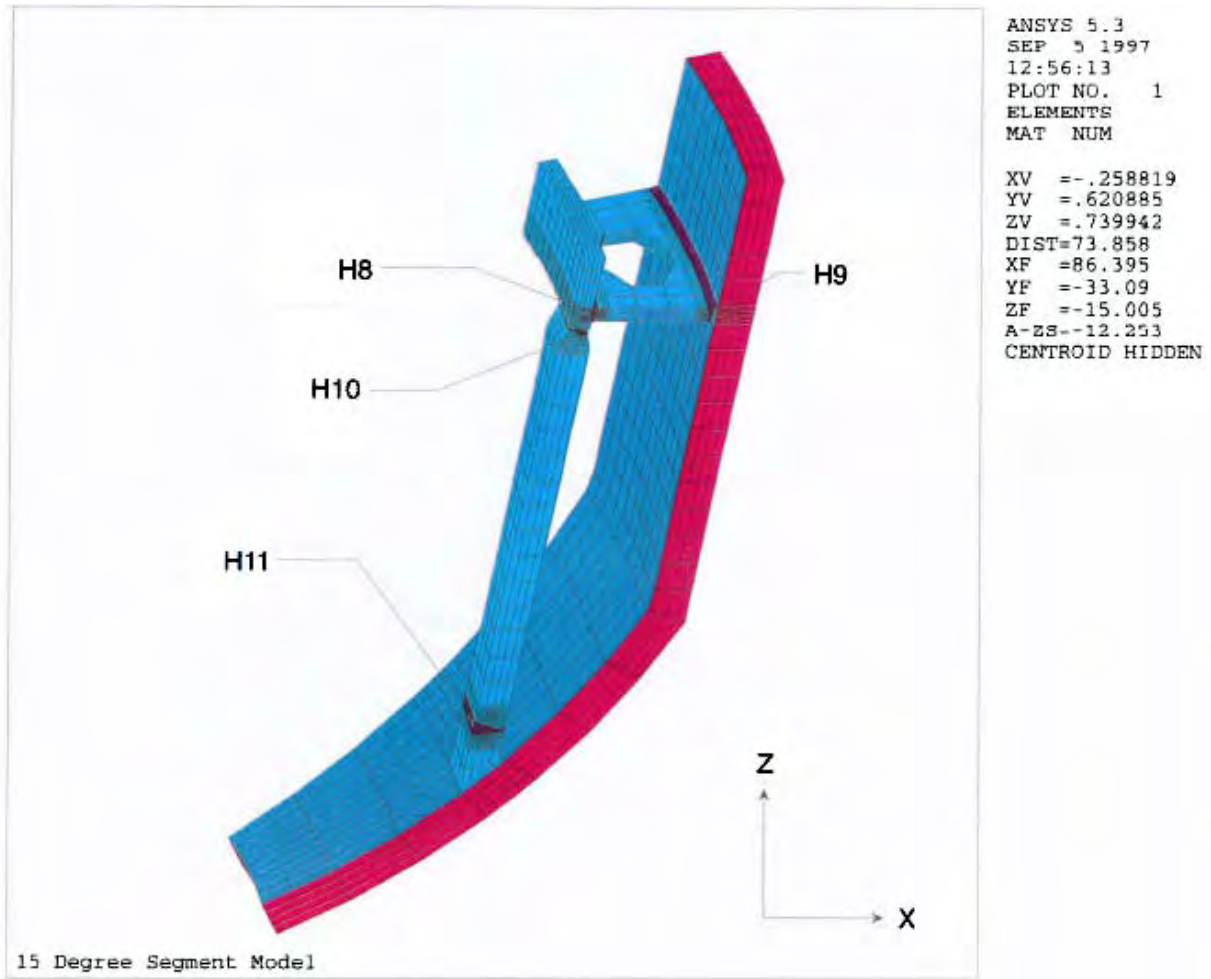


Figure D-2
Model Weld Geometry

Several different companies fabricated BWR reactor vessels and they used different support system designs and fabrication sequences.¹ The weld sequence assumed in this work is as follows: First, the legs were attached to the RPV lower head with the H11 or H12 welds before the support structure was installed in the vessel. The H8 weld was made to fabricate the support ring/baffle plate assembly before it was installed in the RPV. Thus, the H11/H12 and H8 welds were fabricated independently. After installation of the legs, they were trimmed to the proper height, and the support ring/baffle plate assembly was installed and positioned. The H10 welds were completed next. The final weld to be made was the H9 weld. In the finite element model, the welds were made in the sequence H11 or H12, H8, H10, and H9. The top of the leg was restrained from horizontal translation while the H11 weld was made. The restraints were removed after an initial connection was made at the H10 weld location, but before the bulk of the weld metal was inserted. This procedure maintains a shear restraint on the top of the leg throughout fabrication, but there is no bending moment on the top of the leg until the H10 weld is made.

¹ David W. Gandy, et al., "Reactor Pressure Vessel Internals Survey," EPRI Repair Applications Center, June 12, 1989.

Although the welding sequence used in the model assumed the specific sequence described above, calculations were also done where each weld was modeled individually. These calculations indicate that the local weld residual stress patterns in the H11, H8, and H10 welds are affected in only a minor way by making the subsequent welds. However, it was found that the resulting net forces and moments in the components depend on the fabrication sequence and assumptions regarding restraints during fabrication. Adjustments for net force and bending moments can be made by adding uniform and linear stress distributions to the local stress distributions calculated by the FEA. This procedure was used to relax restraints and to account for forces and moments generated by subsequent welds when analyses of individual welds were performed. In general the magnitudes of the uniform and bending stresses were small compared to the peak local stresses so this superposition procedure produced results that are accurate to within other uncertainties from the modeling procedure.

One fabrication step that does have a significant influence on the final residual stresses is a vessel stress relief heat treatment. It is understood² that vessels fabricated by Babcock and Wilcox (B&W) and Combustion Engineering (CE) were stress relieved after the shroud support structure was installed in the vessel. CBIN practice was to stress relieve the vessel prior to installation of the shroud support structure. To assess the benefits of a stress relief heat treatment, a post weld stress relief heat treatment (PWHT) load step was applied to the FEA model after all welds were completed.

Because the configuration of the leg bottom using an H12 welds is not shown on the drawings, which were used as the basis for the FEA, the analysis of the H12 weld was done as a separate analysis from the other welds. Furthermore, etchings of the weld pieces used for experimental residual stress measurements revealed differences between the weld geometry on the drawings and the actual parts. Therefore, additional analyses of individual welds were performed for comparison to the experimental measurements. In order to reduce the time required for new analyses, the H9 and H10 welds were re-done as separate models; the results from these separate models are the ones presented in this appendix. As discussed above, it was determined that, within the uncertainty of the model, the weld local stress results are essentially independent of the fabrication sequence, and forces and moments from other welds can be added to individual analyses by superposition.

Stress data from the FEA analyses were used as inputs for the crack stress intensity predictions described in the main body of this report. While local weld residual stress patterns are independent of fabrication sequence, cross section forces and bending moments, which are the dominant driving force for through crack growth, are not independent of fabrication sequence. Therefore, for the H10 and H12 welds, results from the individual H9, H10, and H12 weld analyses were combined according to the welding sequence to determine the overall residual force and bending moment state after completion of welding. Stresses across the width of the legs at the H10 and H12 welds were averaged, and the average stresses were used in a two-dimensional crack growth analysis. Additionally, for welds H8 and H9, further FEA analyses successively killing elements along a crack path through the weld were performed to simulate the effects of crack growth and determine the extent of relaxation of net residual forces and bending

² David W. Gandy, et al., "Reactor Pressure Vessel Internals Survey," EPRI Repair Applications Center, June 12, 1989.

moments as a crack grows through thickness. Because of the discrete legs and the holes in the shroud support plate for the jet pumps, there is a variation in the bending moments at the H8 and H9 welds around the circumference. Maximum forces and moment occur at azimuth angles through the centers of the legs. Stresses, forces, and moments from these locations were used in the crack growth analyses. The use of the weld FEA analyses in determining crack stress intensities for the different welds is discussed in further detail in section D-5.

D.2 Analysis Approach

Welding residual stresses in the support leg and baffle plate welds were computed using the ANSYS finite element code (Revision 5.3).

D.2.1 Factors which Affect Weld Residual Stresses

The residual stresses in the vicinity of shroud support structure welds depend upon many factors including:

- Dimensions of the components and welds
- Restraints on the weld joint as it cools
- Thermal and mechanical properties of the base metal and weld metal as a function of temperature
- Thermal and physical characteristics of the welding process (e.g., heat input rate, weld rod size, number and distribution of weld passes, welding speed, interpass temperature)
- Fabrication and heat treatment history of the shroud assembly

All of these factors can have a significant impact on the final stresses existing after the last weld pass has cooled.

D.2.2 Key Modeling Assumptions

While all of the factors described in the previous paragraph can affect residual stresses in the parts after welding, many of these variables are difficult to quantify. It is also impractical to model the actual details of the welding process with a finite element analysis. As a result, it is necessary to use a simplified model that incorporates the principal features of the welding process that give rise to residual stresses.

The main assumptions used for the shroud residual stress analyses are listed below.

1. The shroud support structure model is three-dimensional because the structure is not axisymmetric. The RPV and shroud support ring are axisymmetric, but the legs are discrete component with rectangular cross section. The baffle plate was modeled with discrete holes for the jet pumps so that it is not axisymmetric.
2. The welding process was modeled by putting in entire layers of weld at the same time. For the H10, H11 and H12 welds, the layers span the entire width of the leg. For the H8 and H9 welds, layers cover the entire 15 degree segment of the model (and by symmetry the entire 360 degrees of the vessel).

3. The heat input from the welding was modeled as a uniform heat generation rate throughout the layer as it is formed. The heat generation rate is increased linearly over a short period of time, then held constant at a maximum value, then decreased linearly to zero.
4. The maximum heat generation rates and the time history were selected to obtain peak temperatures in the weld metal greater than the liquidus temperature of the alloy (2460°F) and to reach temperatures above 1200°F in a layer of the base metal adjacent to the weld about 50 mils thick, to simulate the heat affected zone (HAZ).
5. Weld layers in the model are approximately 0.5 inches thick. Thus, many actual weld passes are modeled as a single layer in the FEA. The number and thicknesses of weld layers in the model are dictated by the finite element mesh refinement that is practical for the three dimensional reactor vessel and shroud support structure model. Previous analyses for axisymmetric configurations² determined that the residual stresses calculated by a FEA model are not very sensitive to the number of weld layers used provided that there are many layers through the weld thickness.
6. All shroud support structural components are Alloy 600. Welds and weld overlay pads for connections to the RPV are NiCrFe 82 or 182 alloys. These materials are all similar in composition. With the exception of yield strength and coefficient of thermal expansion, physical properties of the weld materials were assumed to be the same as those of the wrought Alloy 600. The RPV is A533, Grade B with a cladding of Type 309L stainless steel on the ID surface. This is based on the specifications for the River Bend RPV, but properties for all pressure vessel steels used in BWR reactor vessels are similar to within heat to heat uncertainties. The RPV and cladding are sufficiently far removed from any of the welds to not experience high temperatures or plastic deformation. In the FEA, the RPV functions as an elastic restraint and a heat sink.
7. All materials were assumed to behave in an elastic-perfectly-plastic manner. That is, once the nominal yield strength has been reached at a given temperature, the material will continue to experience additional strain without an increase in stress. This approximation is considered reasonable for modeling a welding process because most of the plastic strain occurs at high temperatures where metals do not work harden significantly. The amounts of plastic strain that occur at temperatures low enough for strain hardening to persist are limited. Stress-strain relationships that are accurate for plastic deformation that occurs concurrently with rapid changes in temperature (i.e., cooling from the solidification temperature) are not well established and are not easily implemented in the ANSYS code. The elastic-perfectly-plastic model is considered to be more accurate than any of the other available options for the weld simulation problem.
8. The effects of a post weld stress relief included in the model were limited to the reduction in yield strength associated with heating to the stress relief temperature. No time dependent creep effects were included in the analysis.

² "Evaluation of Crack Growth in BWR Stainless Steel RPV Internals," BWR Vessel and Internals Project, Topical Report TR-105873, 2nd Draft Report, November 1995, Appendix H.

D.2.3 Material Properties

The welding process raises the weld metal and portions of the base metal to temperatures above the liquidus temperature (about 2460°F for Alloy 600). In addition, portions of the base metal are heated sufficiently to affect the thermal and mechanical properties of the material. Consequently, the analyses were performed using temperature-dependent material properties. Specific values used in the analysis are reported in Table D-1. To the extent possible, properties are taken from tabulations in the ASME Boiler and Pressure Vessel Code.³

Table D-1
Temperature-Dependent Material Properties Used in Finite Element Analysis

Alloy 600 Components						
Temp. (°F)	Yield Strength (ksi)	Young's Modulus (10⁶ psi)	Thermal Exp. Coeff. (10⁻⁶/°F)	Poisson Ratio	Specific Heat (Btu/lb-°F)	Thermal Conduct. (Btu/hr-ft °F)
Reference	(1)	(2)	(2)	(2)	(2)	(2)
70	36	31.0	6.76	0.29	41.6	8.6
350	34	29.7	7.50	0.29	44.8	9.8
800	30	27.6	8.04	0.29	49.6	12.1
1200	26	25.1	8.60	0.29	54.7	14.3
1600	9.0	22.0	9.10	0.29	58.0	16.5
2300	1.5	1.0	10.0	0.29	60.4	19.4
3500		0.5	11.0	0.29	62.1	23.8
Alloy 182 and 82 Weld Metal						
Reference	(1)	(2)	(1)	(2)	(2)	(2)
70	56	31.0	7.20	0.29	41.6	8.6
350	52	29.7	8.05	0.29	44.8	9.8
800	45	27.6	8.50	0.29	49.6	12.1
1200	40	25.1	8.90	0.29	54.7	14.3
1600	18	22.0	9.30	0.29	58.0	16.5
2300	2.0	1.0	10.0	0.29	60.4	19.4
3500		0.5	11.0	0.29	62.1	23.8

³ ASME Boiler and Pressure Vessel Code, Section II, Part D, 1995 Edition, American Society of Mechanical Engineers, New York, 1995.

Table D-1
Temperature-Dependent Material Properties Used in Finite Element Analysis (Continued)

Temp. (°F)	Yield Strength (ksi)	Young's Modulus (10 ⁶ psi)	Thermal Exp. Coeff. (10 ⁻⁶ /°F)	Poisson Ratio	Specific Heat (Btu/lb-°F)	Thermal Conduct. (Btu/hr-ft °F)
A533 Grade B Steel						
Reference	(2)	(2)	(2)	(2)	(2)	(2)
70	50.0	29.2	7.02	0.29	41.7	22.3
350	44.5	27.7	7.50	0.29	47.8	23.8
800	38.8	23.9	8.05	0.29	58.9	21.7
1200	28.4 ⁴	14.5	8.20	0.29	79.7	18.4
1600	9.0	6.0	8.80	0.29	67.2	15.6
2300	1.5	0.5	9.40	0.29	51.7	12.0
3500		0.2	9.50	0.29	38.8	9.0
Type 309L Stainless Steel						
Reference	(2)	(2)	(2)	(2)	(2)	(2)
70	40.0	28.3	8.81	0.29	46.4	7.8
350	31.6	26.8	9.12	0.29	49.8	9.9
800	26.8	24.1	9.28	0.3	54.1	12.0
1200	21.0	23.0	9.80	0.29	58.0	14.4
1600	16.0	17.0	10.0	0.25	61.8	16.8
2300	2.0	1.0	10.3	0.25	61.8	16.8
3500		0.5	10.6	0.25	61.8	16.8

D.2.4 References

1. Inconel alloy 600, Inco Alloys International, Inc., Huntington, West Virginia 25720, 1985.
2. ASME Boiler and Pressure Vessel Code, Section II, Part D, 1995 Edition, American Society of Mechanical Engineers, New York, 1995.

⁴ This value is applied at 1000°F in the model. All other properties on this row are applied at 1200°F.

For all shroud models, the temperature dependent yield strength of the weld metal is taken from published International Nickel Co. data, which were determined to be consistent with typical weld qualification test results at room temperature. The room temperature yield strength for the weld metal, 56 ksi, is 1.55 times the yield strength used for the Alloy 600 base metal. This means that the base metal is the limiting strength material when the weld has cooled to near ambient temperature. However, because of the steep temperature gradient at the boundary of the weld, the weld metal is hotter and weaker than the base metal for most of the deposition and cooling process.

Little material property information is available for temperatures greater than about 1200°F. For temperatures above 1200°F, properties that behave in a nearly linear fashion at lower temperatures were extrapolated. For temperatures near or above the melting point (i.e., 2300°F and 3500°F), the yield strength and Young's modulus are reduced to low values that are sufficiently large to maintain stability in the FEA solution but limit calculated stresses in the molten pool to very low values. For the cladding, Poisson ratio, specific heat, and thermal conductivity) are assumed to remain constant at their values for 1600°F. Material properties above 1600°F have a negligible effect on the calculated residual stresses, because of the low material strengths at such high temperatures.

D.2.5 Finite Element Mesh Characteristics

The finite element models consist of ANSYS three-dimensional SOLID70 thermal and SOLID45 structural elements. All elements are eight node solids except for isolated locations where degenerate wedge shaped elements are used. A 15-degree segment of the RPV and shroud support structure were modeled as shown in Figure D-2. Refined meshes were used in the vicinities of the welds where temperature and stress gradients are high as shown in Figures D-3 and results figures. Larger elements were used for the remainder of the model.

Weld passes are modeled with two elements through the thickness of the pass and four elements across the width of the weld. Welds were generated in layers that extend across the entire 15 degrees of circumference (welds H8 and H9) or the full width of the support leg (welds H10, H11 and H12). The model of the RPV was extended sufficiently far from the points of attachment of the shroud support structure to provide realistic restraints on the structure.

All weld material elements were initially "killed" with the ANSYS "EKILL" command in both the thermal and structural analysis. For each weld, the specified weld preparation requires a small contact land between the two parts. In the FEA models, these lands were initially left connected across the joints. This serves to restrain rigid body motion of the components until they are welded. As part of the weld sequence modeling, the elements in these lands are "killed" to simulate back gouging of the first side weld root. This removes any stresses that have been generated in the lands as the result of previous welds.

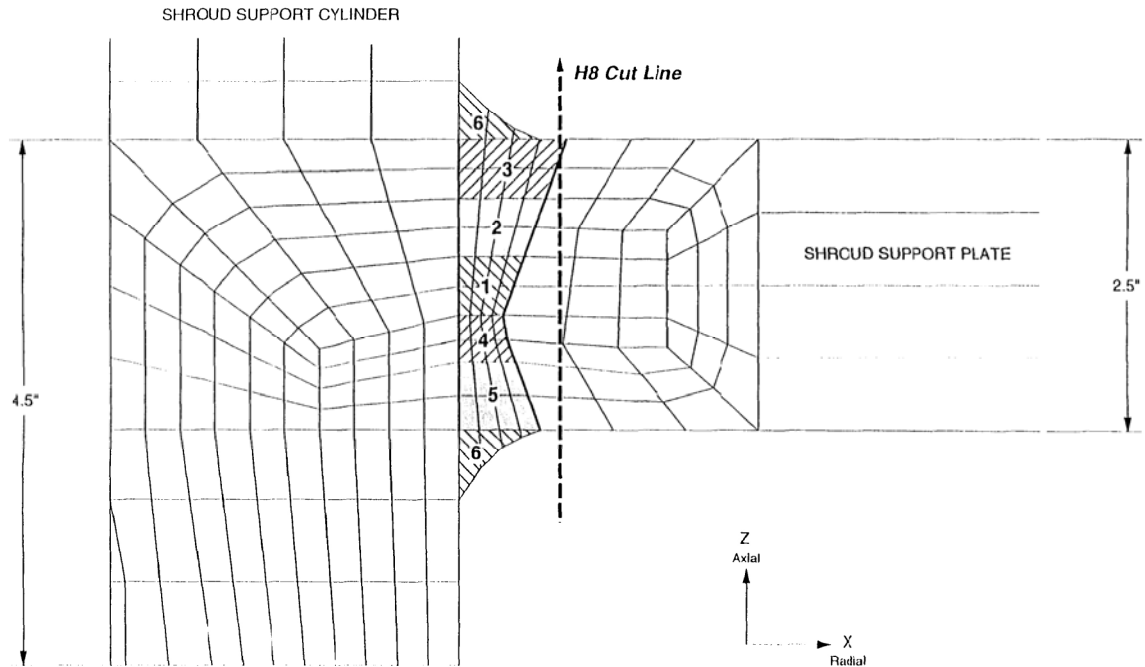


Figure D-3
Weld H8 Weld Sequence and Approximate Mesh

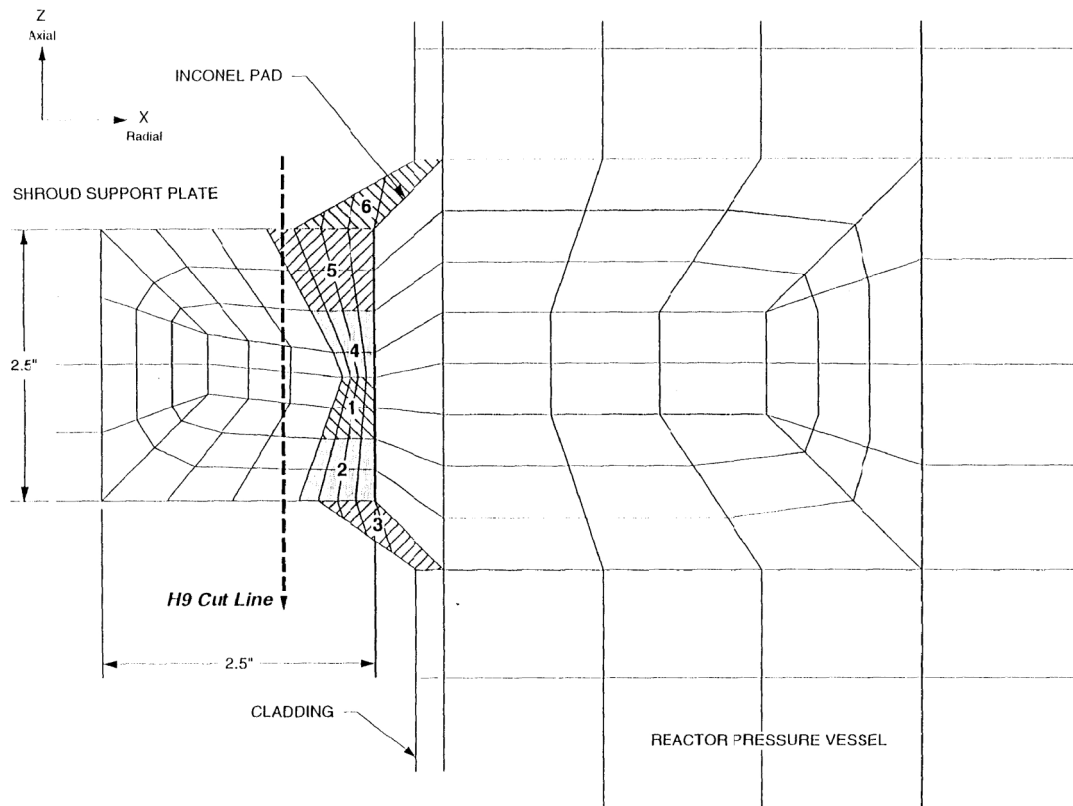


Figure D-4
Weld H9 Weld Sequence and Approximate Mesh

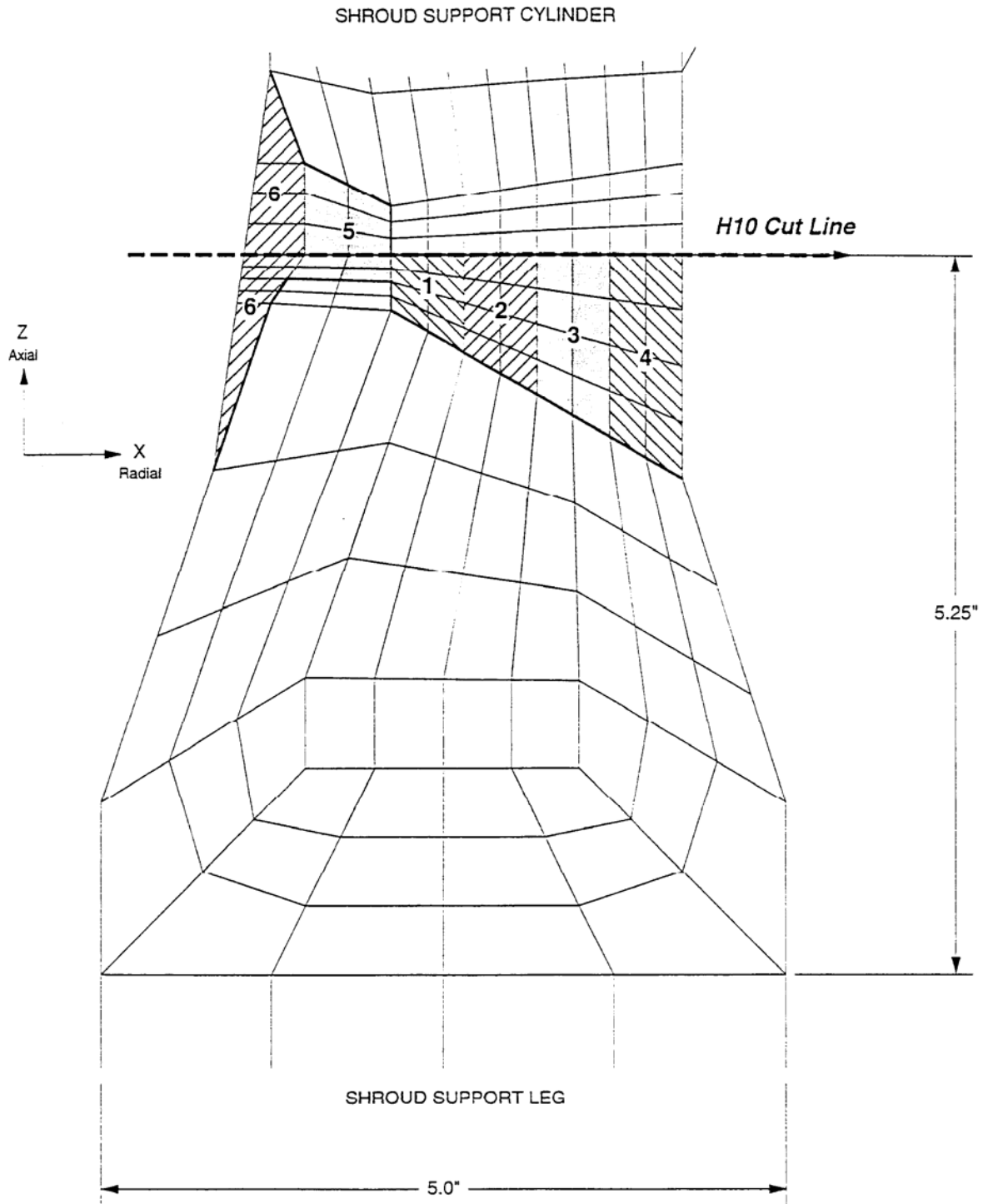


Figure D-5
Weld H10 Weld Sequence and Approximate Mesh

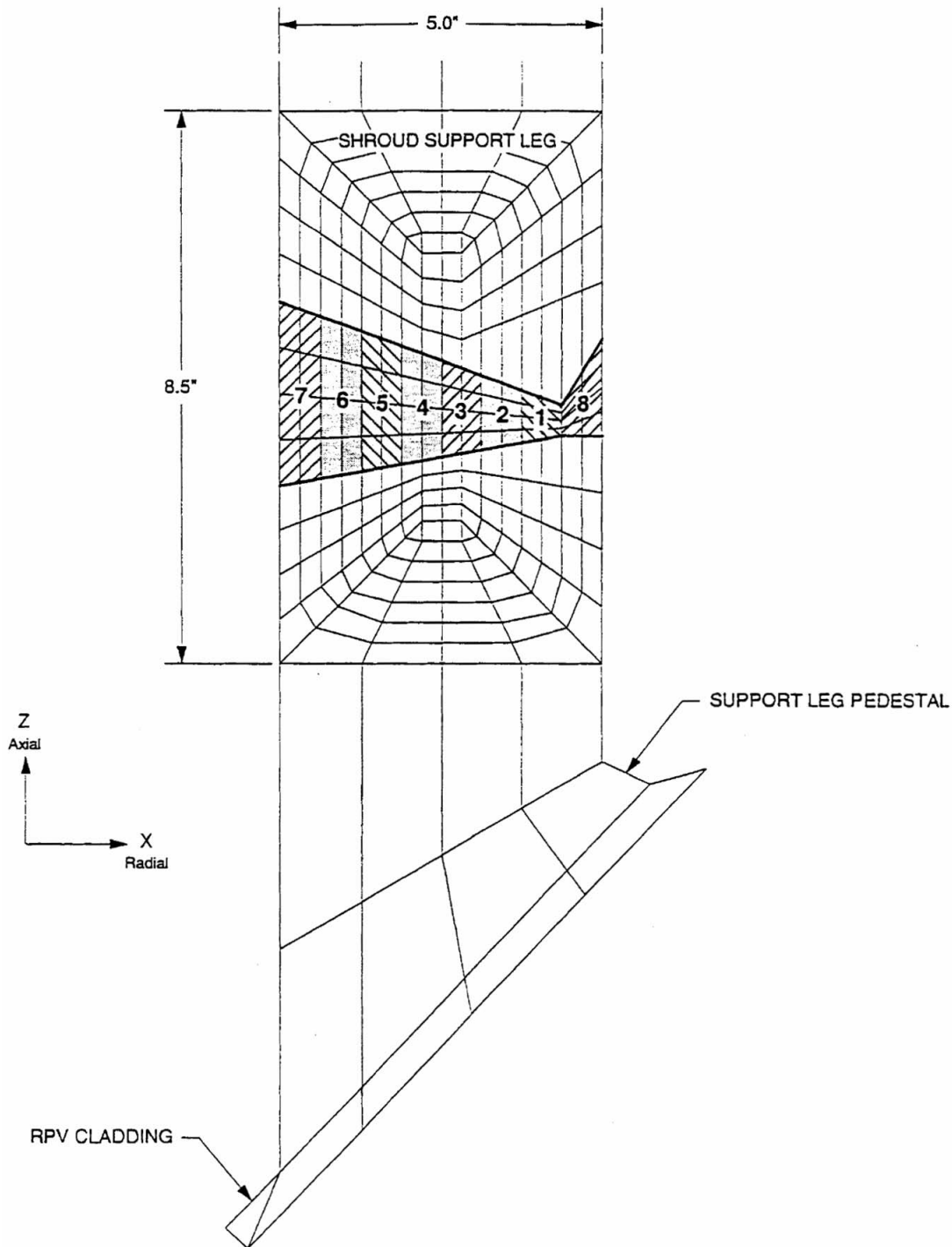


Figure D-6
Weld H11 Weld Sequence and Approximate Mesh

The H12 weld has a different geometry from the other welds (see Figure D-7). There is no formal description of the procedure used to make this weld; all welds for this location were initially believed to be H11 welds. The weld geometry and welding sequence for the H12 weld were based on the etchings of the experimental pieces.

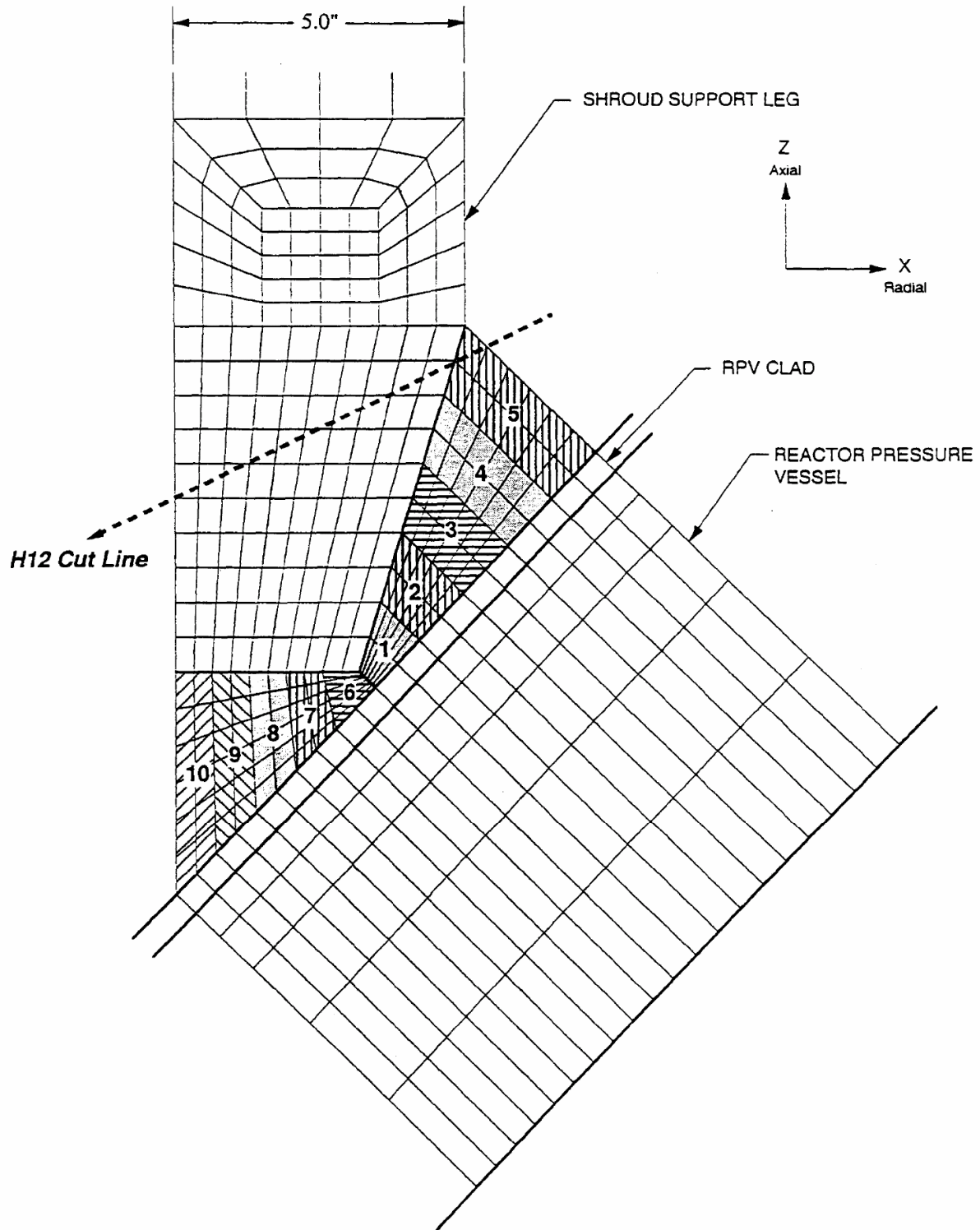


Figure D-7
Weld H12 Weld Sequence and Approximate Mesh

D.2.6 Fabrication Sequence

Four welds were initially modeled sequentially in the FEA. H11 was made first, followed by H8, H10, and H9 in that order. The purpose of analyzing the four welds in a combined model was to assure that any effects of subsequent welding on the residual stresses at welds made previously was simulated correctly. Because the final state of a weld is for some portion of it to be stressed to the yield strength, any distortion that occurs during subsequent welding may cause additional plastic deformation in the finished welds, thus redistributing the local residual stresses (i.e., mechanical stress relief). The results show that there are changes in the residual stress patterns associated with making subsequent welds. However, as is discussed in the section on results, the changes in stress from making subsequent welds is typically less than 10%, which is less than the uncertainties inherent in the model. As discussed earlier, the H12 weld analysis was performed separately from the main, four-weld model. Additionally, the H9 and H10 results presented in this appendix are also from separate weld analyses.

Welds H8, H9, and H11 are double groove full penetration welds. These welds were modeled by completing the weld on one side from the root to flush with the final surface, back gouging the root of this first side weld, and then completing the weld on the second side. The back gouging was accomplished by “killing” a layer of elements at the root of the welds with the ANSYS EKILL command and then regenerating these elements with the EALIVE command as part of the first layer of the second side weld. Figures D-3, D-4, and D-6 show the approximate weld mesh and weld sequence for welds H8, H9, and H11, respectively.

According to the CBIN drawings, the weld at the top of the leg (H10) is not a full penetration weld, with the weld being made almost entirely from one side. However, as discussed above, etchings of the experimental piece from the H10 weld showed weld geometry more like a double groove full penetration weld. Instead of an unwelded land approximately 0.5 in. wide being left at the top of the leg (as indicated in the CBIN drawing), the land was shown to be back-gouged away and the region filled with weld metal. A fairly large cap weld is made on the second side of the leg to blend in the transition from the rectangular leg to the cylindrical shroud support ring. Figure D-5 shows the approximate weld mesh and weld sequence for weld H10.

The H12 weld has a different geometry from the other welds. There is no formal description of the procedure used to make this weld; all welds for this location were initially believed to be H11 welds. The weld geometry and welding sequence for the H12 weld were based on the etchings of the experimental pieces.

D.2.7 Modeling of Welding Process

Each weld pass is analyzed by a two step process consisting of a thermal analysis to determine the temperature distributions as a function of time and a structural analysis to determine the resultant stresses. Because the thermal and structural portions of the problem are independent, the thermal analyses can be performed for all passes before starting the structural analyses. Because the welds are widely separated, the heat input at one weld has no effect on the temperatures at other weld locations, and the thermal analyses were done as independent load cases. The temperature distributions calculated in the thermal analysis were then imposed as loads for the structural analysis. Further details regarding the thermal and structural analyses are as follows:

Thermal Model. The thermal analysis involves application of thermal boundary conditions followed by simulation of each welding pass. The thermal boundary conditions used in the models are:

1. Convection on all exterior surfaces (5 BTU/hr-ft²-°F⁵)
2. Assumed heat sinks at the upper and lower boundaries of the modeled portion of the RPV. This is achieved by holding the nodal temperatures on these boundary surfaces at 70°F.
3. Zero heat flow across the boundaries on the 0 and 15 degree planes of the model. This is the result of mirror symmetry across these boundary planes requiring the temperature gradient perpendicular to the plane to be zero.

Weld passes are simulated by successively “turning on” the elements that make up each weld pass (with the ANSYS “EALIVE” command), applying a uniform heat generation rate to all of the elements in the pass, and then allowing the weld metal and structural components to cool. Temperature distributions are calculated at a number of times during each weld pass and are saved for use with the structural model. In the final load step for each thermal weld pass, the temperature of the entire model is forced to 70°F. Although the weld procedure⁶ allows a maximum interpass temperature of 400°F, it is probable that much lower interpass temperatures occurred in practice. Because the welds are large, the elapsed time between passes was probably long, and the components are very large heat sinks for the energy input during the welding. The FEA model assumes a much higher total heat input rate in the welding process than actually occurs because of the approximation of putting the weld in whole layer at a time. In the actual welding process, where the weld metal is deposited as individual beads, the heat sink of the surrounding structure is more effective in cooling the deposited weld bead to a near ambient temperature. Starting each simulated weld pass from 70°F is considered to be a reasonable approximation of what probably occurred during fabrication and allows the finite element analysis to be done with a standard temperature cycle. The heat generation rates in the weld layer are ramped up from zero to a maximum value, held constant, and ramped down to zero. The purpose of ramping the heat generation rates is to improve convergence of the thermal and structural solutions. The maximum heat generation rates and the times of heat application are adjusted to provide peak temperatures in the weld pool above the liquidus temperature (i.e., typically 3500°F), and a temperature above 1200°F in a thin layer (approximately 0.05 inch) of the base metal adjacent to the weld to simulate a HAZ. Each weld layer is allowed to cool for 600 seconds before the entire model is forced to a uniform temperature of 70°F.

Structural Model. After calculating the temperature distributions for the welding passes, the element and nodal geometry was converted to a structural model by changing the SOLID70 thermal elements to SOLID45 structural elements. The following structural boundary conditions were used:

1. Normal displacements for all nodes on the 0 and 15 degree planes were set to zero. These mirror boundary conditions also restrain all rigid body motions of the model because the cylindrical geometry of the vessel and the spherical geometry of the lower head prevent strain free translations and rotations in all directions.

⁵ “Analysis Guidelines for Backfill Modification of RPV Water Level Instrumentation,” General Electric Company Report No. GENE-637-019-893, Rev. 0, August 1993.

⁶ “Shielded Metal Arc Welding of ASME P43 Material with GTA Pick Ups,” CBI Nuclear Company, Welding Procedure, WTS 309-2, P-43, 10/7/68, Rev. 5 1/7/75.

2. No displacement restraints were placed on the upper and lower surfaces of the RPV portion of the model. Although these free surface boundary conditions are not realistic for the artificial cut surfaces, these boundaries were placed sufficiently far from any connections between the RPV and the shroud support structure to not influence the results.
3. The upper end of the support leg was restrained in the radial direction until welds H11 and H8 were completed and was similarly restrained for the separate H12 weld analysis. Since the 0-degree plane of the model passes through the center of the leg, the symmetry boundary conditions restrain circumferential motion of the leg. The radial restraint simulates bracing that must have been used to hold the leg in place until the welds at its ends were completed.
4. The model was connected across the lands of all of the weld preparations until one side of the weld was completed. These artificial connections across uncompleted welds restrain rigid body displacements of the components and simulate bracing or tack welds that were used to hold components in position while they were welded. Because the material adjacent to these lands is subsequently removed (the elements are killed) to simulate back gouging the root of the first side weld, any stresses in the lands produced by the artificial connections are eliminated.

Residual stresses were determined by sequentially imposing the temperature distributions at each time step as loads on the structural model and then solving for the resultant stresses. Note that the elements associated with each weld pass are not activated structurally (with the EALIVE command) until the time associated with the end of heat input for these passes. Activating these elements sooner generates artificial plastic strains in the weld while it is still heating.⁷ Some plastic strain accumulates in the newly deposited weld layer as it cools from its peak temperature to the alloy solidus temperature. Because of the low yield strength assumed for the weld metal at temperatures above 2300°F and the elastic perfectly plastic assumption, these calculated plastic strains in molten metal have no effect on the final results.

D.2.8 Modeling of Post Weld Heat Treatment

Some BWR pressure vessel fabricators performed a stress relief heat treatment at 1150°F on the RPV after the shroud support structure had been installed. The purpose of the heat treatment was for post weld stress relief of the pressure vessel welds, but it also had an effect on the residual stresses in the support structure. Because the FEA does not include any time dependent material deformation mechanisms (e.g., creep), the time at temperature for the post weld heat treatment (PWHT) does not affect the calculated results. Therefore, the PWHT was modeled by ramping the temperature of the entire model from 70°F to 1150°F in 300 seconds and back again to 70°F in an additional 300 seconds. Although this is much faster heating and cooling than probably occurred in practice, ramping the temperature of the entire model together prevents temperature gradient induced stresses during the PWHT. The effect of the PWHT is to reduce the residual stresses because of the reduction of the material yield strengths at the elevated temperature.

⁷ In addition, activation of the weld elements prior to the peak of heat-up would cause artificial strains and stresses to be generated in the base metal because the weld metal has significant strength and stiffness at lower temperatures. In an actual welding process, the weld metal will not cause significant forces in the base metal until it begins to gain strength during cooling.

D.3 Analysis Results

D.3.1 Residual Stresses Without Post Weld Heat Treatment

**Content Deleted -
EPRI Proprietary Information**

**Content Deleted -
EPRI Proprietary Information**

**Figure D-8
Weld H8 After Welding Radial Stress (SX)**

**Content Deleted -
EPRI Proprietary Information**

**Figure D-9
Weld H8 After Welding Circumferential Stress (SY)**

**Content Deleted -
EPRI Proprietary Information**

**Figure D-10
Weld H9 After Welding Radial Stress (SX)**

**Content Deleted -
EPRI Proprietary Information**

**Figure D-11
Weld H9 After Welding Circumferential Stress (SY)**

**Content Deleted -
EPRI Proprietary Information**

**Figure D-12
Weld H10 After Welding Vertical Stress (SZ)**

**Content Deleted -
EPRI Proprietary Information**

**Figure D-13
Weld H10 After Welding Circumferential Stress (SY)**

**Content Deleted -
EPRI Proprietary Information**

**Figure D-14
Weld H11 After Welding Vertical Stress (SZ)**

**Content Deleted -
EPRI Proprietary Information**

**Figure D-15
Weld H11 After Welding Circumferential Stress (SY)**

**Content Deleted -
EPRI Proprietary Information**

Figure D-16
Weld H12 After Welding Perpendicular Stress (SZ)

**Content Deleted -
EPRI Proprietary Information**

Figure D-17
Weld H12 After Welding Circumferential Stress (SY)

**Content Deleted -
EPRI Proprietary Information**

**Figure D-18
Weld H10 After Welding Upper HAZ (from Above) Vertical Stress (SZ)**

**Content Deleted -
EPRI Proprietary Information**

Figure D-19
Weld H10 After Welding Lower HAZ (from Below) Vertical Stress (SZ)

**Content Deleted -
EPRI Proprietary Information**

Figure D-20
Weld H11 After Welding Upper HAZ (from Above) Vertical Stress (SZ)

**Content Deleted -
EPRI Proprietary Information**

Figure D-21
Weld H11 After Welding Lower HAZ (from Below) Vertical Stress (SZ)

**Content Deleted -
EPRI Proprietary Information**

Figure D-22
Weld H12 After Welding Upper HAZ (from Above) Perpendicular Stress (SZ)

**Content Deleted -
EPRI Proprietary Information**

Figure D-23
Weld H12 After Welding Lower HAZ (from Below) Perpendicular Stress (SZ)

D.3.2 Effects of Stress Relief Post Weld Heat Treatment

**Content Deleted -
EPRI Proprietary Information**

**Content Deleted -
EPRI Proprietary Information**

**Figure D-24
Weld H8 After PWHT Radial Stress (SX)**

**Content Deleted -
EPRI Proprietary Information**

**Figure D-25
Weld H8 After PWHT Circumferential Stress (SY)**

**Content Deleted -
EPRI Proprietary Information**

**Figure D-26
Weld H9 After PWHT Radial Stress (SX)**

**Content Deleted -
EPRI Proprietary Information**

**Figure D-27
Weld H9 After PWHT Circumferential Stress (SY)**

**Content Deleted -
EPRI Proprietary Information**

**Figure D-28
Weld H10 After PWHT Vertical Stress (SZ)**

**Content Deleted -
EPRI Proprietary Information**

**Figure D-29
Weld H10 After PWHT Circumferential Stress (SY)**

**Content Deleted -
EPRI Proprietary Information**

**Figure D-30
Weld H11 After PWHT Vertical Stress (SZ)**

**Content Deleted -
EPRI Proprietary Information**

**Figure D-31
Weld H11 After PWHT Circumferential Stress (SY)**

**Content Deleted -
EPRI Proprietary Information**

**Figure D-32
Weld H12 After PWHT Perpendicular Stress (SZ)**

**Content Deleted -
EPRI Proprietary Information**

**Figure D-33
Weld H12 After PWHT Circumferential Stress (SY)**

Table D-2
Peak Residual Stresses

**Content Deleted -
EPRI Proprietary Information**

**Content Deleted -
EPRI Proprietary Information**

**Figure D-34
H8 Support Cylinder HAZ After Welding – Leg Centerline**

**Content Deleted -
EPRI Proprietary Information**

**Figure D-35
H8 Support Cylinder HAZ After Stress Relief – Leg Centerline**

**Content Deleted -
EPRI Proprietary Information**

**Figure D-36
H8 Support Plate HAZ After Welding – Leg Centerline**

**Content Deleted -
EPRI Proprietary Information**

**Figure D-37
H8 Support Plate HAZ After Stress Relief – Leg Centerline**

**Content Deleted -
EPRI Proprietary Information**

**Figure D-38
H8 Weld Centerline After Welding – Leg Centerline**

**Content Deleted -
EPRI Proprietary Information**

**Figure D-39
H8 Weld Centerline After Stress Relief – Leg Centerline**

**Content Deleted -
EPRI Proprietary Information**

**Figure D-40
H9 Reactor Vessel HAZ After Welding – Leg Centerline**

**Content Deleted -
EPRI Proprietary Information**

**Figure D-41
H9 Reactor Vessel HAZ After Stress Relief – Leg Centerline**

**Content Deleted -
EPRI Proprietary Information**

**Figure D-42
H9 Support Plate HAZ After Welding – Leg Centerline**

**Content Deleted -
EPRI Proprietary Information**

**Figure D-43
H9 Support Plate HAZ After Stress Relief – Leg Centerline**

**Content Deleted -
EPRI Proprietary Information**

**Figure D-44
H9 Weld Centerline After Welding – Leg Centerline**

**Content Deleted -
EPRI Proprietary Information**

**Figure D-45
H9 Weld Centerline After Stress Relief – Leg Centerline**

**Content Deleted -
EPRI Proprietary Information**

**Figure D-46
H10 Upper HAZ After Welding – Leg Centerline**

**Content Deleted -
EPRI Proprietary Information**

**Figure D-47
H10 Upper HAZ After Stress Relief – Leg Centerline**

**Content Deleted -
EPRI Proprietary Information**

**Figure D-48
H10 Lower HAZ After Welding – Leg Centerline**

**Content Deleted -
EPRI Proprietary Information**

**Figure D-49
H10 Upper HAZ After Stress Relief – Leg Centerline**

**Content Deleted -
EPRI Proprietary Information**

**Figure D-50
H10 Weld Centerline After Welding – Leg Centerline**

**Content Deleted -
EPRI Proprietary Information**

**Figure D-51
H10 Weld Centerline After Stress Relief – Leg Centerline**

**Content Deleted -
EPRI Proprietary Information**

**Figure D-52
H11 Upper HAZ After Welding – Leg Centerline**

**Content Deleted -
EPRI Proprietary Information**

**Figure D-53
H11 Upper HAZ After Stress Relief – Leg Centerline**

**Content Deleted -
EPRI Proprietary Information**

**Figure D-54
H11 Lower HAZ After Welding – Leg Centerline**

**Content Deleted -
EPRI Proprietary Information**

**Figure D-55
H11 Lower HAZ After Stress Relief – Leg Centerline**

**Content Deleted -
EPRI Proprietary Information**

**Figure D-56
H11 Weld Centerline After Welding – Leg Centerline**

**Content Deleted -
EPRI Proprietary Information**

**Figure D-57
H11 Weld Centerline After Stress Relief – Leg Centerline**

**Content Deleted -
EPRI Proprietary Information**

**Figure D-58
H12 Upper HAZ After Welding – Leg Centerline**

**Content Deleted -
EPRI Proprietary Information**

**Figure D-59
H12 Upper HAZ After Stress Relief – Leg Centerline**

**Content Deleted -
EPRI Proprietary Information**

**Figure D-60
H12 Lower HAZ After Welding – Leg Centerline**

**Content Deleted -
EPRI Proprietary Information**

**Figure D-61
H12 Lower HAZ After Stress Relief – Leg Centerline**

**Content Deleted -
EPRI Proprietary Information**

**Figure D-62
H12 Weld Centerline After Welding – Leg Centerline**

**Content Deleted -
EPRI Proprietary Information**

**Figure D-63
H12 Weld Centerline After Stress Relief – Leg Centerline**

D.4 Comparison of Calculated and Measured Residual Stresses

As part of a separate effort, experimental procedures were used to measure the residual stresses in the H8, H9, H10, and H12 welds, using samples of these welds cut from the duplicate River Bend shroud. No stresses could be obtained for the H11 weld geometry because this geometry did not exist for the duplicate shroud. The procedures used and the results obtained are detailed in Reference [D-8]. A brief comparison of the calculated and measured residual stresses is included in this section; a more detailed discussion is included elsewhere in the report.

Comparison of the calculated and measured residual stresses can be done using the stress path plots contained in Figures D-64 through D-67. The location and direction of the paths used in making the stress plots for the “FEA As Calculated” cases are as close as possible to the locations and directions of the cuts used to measure the residual stresses. Additionally, similar to the measured stress plots contained in Reference [D-8], the calculated stresses are plotted versus normalized distance for ease of comparison between the measured and calculated stresses. For the H12 weld, the lower (second) weld was analytically cut out (using the “EKILL” command) before the cut line data were taken, better to match the conditions of the experiment specimen (which had the bottom weld cut off). The data set labeled “Experimental” is a plot of the experimentally measured cut line stress data used for Reference [D-8].

As demonstrated in Figures D-64 through D-67, the “FEA As Calculated” and “Experimental” data sets do not agree very well. This is due, as noted on the figures, to the large residual moments and forces that are present in the analytical model but not in the specimens used for the experimental data. The residual moments and forces were relaxed when the vessel was sectioned and the specimen was removed. It is noted that when the weld specimens were cut out of the vessel, an attempt was made to measure the relaxation due to the cutting. However, the strain gauges used to record the relaxation were destroyed in the process of obtaining the specimens. In order to provide a basis for comparison between analytical and experimental data, the “FEA As Calculated” data were adjusted to have no net force or moment, yielding the “FEA Adjusted” data sets.

Comparing the “FEA Adjusted” and “Experimental” stress plots; it can be concluded that reasonable agreement exists between the measured and calculated residual stresses. While the precise details of stress versus distance do not always match, the general shape and trend (compressive in the center, tensile at the edges) of both sets of stress plots are in agreement. This result is not unexpected due to the idealized process used to determine the calculated stress values.

Residual stresses were also determined experimentally on a cut through the reactor pressure vessel (RPV) below the H9 weld. Figure D-68 shows a comparison between the experimentally determined stresses and those calculated by the FEA model. The FEA model had a very coarse mesh in the RPV because the vessel was modeled only to provide restraint to the welds. Thus the results shown in Figure D-68 for the FEA are linear interpolations between five calculated points through the vessel thickness. However, the conclusion from both the FEA and experimental measurements is that residual stresses do not extend significantly below the vessel to cladding interface. Therefore, if a crack is initiated in the H9 weld or in the vessel cladding adjacent to the weld, it will not propagate into the RPV wall.

**Content Deleted -
EPRI Proprietary Information**

**Figure D-64
H8 Cut Line Residual Stresses Perpendicular to Cut Line**

**Content Deleted -
EPRI Proprietary Information**

**Figure D-65
H9 Cut Line Residual Stresses Perpendicular to Cut Line**

**Content Deleted -
EPRI Proprietary Information**

Figure D-66
H10 Cut Line Residual Stresses Perpendicular to Cut Line – Large Weld Cap on Backgouge

**Content Deleted -
EPRI Proprietary Information**

Figure D-67
H12 Cut Line Residual Stresses Perpendicular to Cut Line – After Removal of Bottom Weld

**Content Deleted -
EPRI Proprietary Information**

Figure D-68
Residual Stress through RPV Wall Below H9 Weld

D.5 Use of FEA Results in Predicting Crack Stress Intensities

The results from the finite element analyses described in this appendix were used as inputs to models predicting crack stress intensities for the different welds. During analysis of the preliminary stress data, it was determined that, for the weld geometries considered, the progression of crack stress intensity with crack growth was heavily dependent on the overall cross section residual forces and moments. The reason for the dependence is that the overall cross section residual forces and moments do not relax as rapidly as the crack grows, as do local stress fields, which are balanced within the weld and produce no net force or moment. Therefore, it was determined that it is important to preserve the net force and moment on each weld when using correlations to estimate crack tip stress intensity.

This section describes the additional FEA work that was required to determine these cross section residual forces and moments and thereby provide the most accurate inputs possible to the crack stress intensity predictive models. As discussed in the report, two different predictive models were used: one for the H8 and H9 welds and one for the H10 and H12 welds. Further discussion of the predictive models themselves and of the results of the predictive models is contained elsewhere in this report.

D.5.1 FEA Work Supporting H8 and H9 Weld Crack Predictive Models

The crack stress intensity model used for the H8 and H9 welds does not by itself consider the relaxation of the applied force and moment as the crack propagates through thickness. Thus the crack tip stress intensity is predicted to increase rapidly as the size of the remaining uncracked ligament is reduced. In reality, the stresses on the welds are the result of displacement boundary conditions from the constraint of the rest of the structure. With displacement boundary condition loading, it is expected that the forces and moments will decrease as the section cracks through and the compliance increases. Therefore, in order to determine both the local stress field and the cross section forces and moments that do not relax, a series of analyses were run in which a line of elements through the weld centerline was “killed” one layer at a time (using the EKILL command). Analyses were performed for both the H8 and H9 welds in both the as-welded and the post-weld heat treated conditions. After each row of elements was killed, stress path data were gathered on the experimental cut line for the leg centerline circumferential position.

Uniform and linear stress distributions were added to the stress path, as appropriate, to include the effects of net forces and moments generated by making subsequent welds. This was achieved by using the ANSYS “FSUM” command to determine the forces and moments acting on the plane of the subject weld as a result of each of the other welds. Because the H8 and H12 welds are made independently of each other, only the effects of H10 and H9 were considered for the H8 weld stress data. Because the H9 weld is the last weld made, the individual analysis for the weld already considers the effects of the other welds (i.e., in the model for the H9 weld, the structure is connected at all other weld locations). Figures D-69 and D-70 plot the final result (i.e., including all effects due to other welds) stress path data for the H8 and H9 welds, respectively. The figures contain a family of curves plotting stress (ksi) versus proportional distance along the cut line for various crack depth to width (a/t) ratios.

**Content Deleted -
EPRI Proprietary Information**

Figure D-69
Weld H8 Residual Stress (Sx) – Stresses on Cut Line – Crack Propagating from Bottom to Top

**Content Deleted -
EPRI Proprietary Information**

Figure D-70

Weld H9 With PWHT Residual Stress (S_x) – Stresses on Cut Line – Crack Propagating from Top to Bottom

Once all effects had been taken into account, the stress path data for each EKILL step were then analyzed to determine the residual force and moment, thereby determining force and moment relaxation as a function of crack depth. These functions were then used as inputs for the crack stress intensity model.

D.5.2 FEA Work Supporting H10 and H12 Weld Crack Predictive Models

The method used to calculate the crack stress intensity for the H10 and H12 welds was a two dimensional model for an edge cracked plate with displacement boundary conditions at the ends. This model internally accounts force and moment relaxation as a function of crack growth. Because the predictive model for the H10 and H12 welds considers a horizontal crack in a two-dimensional leg, the stress path data provided was an average of the stresses through the width of the leg. This gives a stress distribution which has the correct total net force and moment applied to the leg.

The ANSYS "FSUM" command was used in the same way as for the H8 weld to determine the effects of the other welds on the H10 and H12 welds. Again, because the H8 weld was made independently of the H10 and H12 welds, the effect of H8 was not included for either H10 or H12. The effects from the H10 and H9 welds were added into the H12 data; the effects from the H9 weld only were added into the H10 data.

D.6 References

- D-1. ANSYS Finite Element Program, Revision 5.3, Swanson Analysis Systems, Inc.
- D-2. David W. Gandy, et al., "Reactor Pressure Vessel Internals Survey," EPRI Repair Applications Center, June 12, 1989.
- D-3. David W. Gandy, et al., "Reactor Pressure Vessel Internals Survey," EPRI Repair Applications Center, June 12, 1989.
- D-4. "Evaluation of Crack Growth in BWR Stainless Steel RPV Internals," BWR Vessel and Internals Project, Topical Report TR-105873, 2nd Draft Report, November 1995, Appendix H.
- D-5. ASME Boiler and Pressure Vessel Code, Section II, Part D, 1995 Edition, American Society of Mechanical Engineers, New York, 1995.
- D-6. "Analysis Guidelines for Backfill Modification of RPV Water Level Instrumentation," General Electric Company Report No. GENE-637-019-893, Rev. 0, August 1993.
- D-7. "Shielded Metal Arc Welding of ASME P43 Material with GTA Pick Ups," CBI Nuclear Company, Welding Procedure, WTS 309-2, P-43, 10/7/68, Rev. 5 1/7/75.
- D-8. Weili Cheng, et al., "Measurements of Residual Stresses in BWR Core Shroud Support Welds."

E

ANALYTICAL PREDICTION OF RESIDUAL STRESSES IN BWR SHROUD SUPPORT STRUCTURE WELDS (INTEGRATED MODEL RESULTS)

May 2003

Prepared by
D. J. Gross
A. P. L. Turner
E. S. Hunt

Prepared for
EPRI
3412 Hillview Avenue
Palo Alto, CA 94303

BWR Shroud Support Structure Weld Residual Stresses (Integrated Model)

The original analyses described in Appendix D of this report were performed in support of the first draft of BWRVIP-59 issued in December 1998. This work was performed over a period of time from 1997 to 1998, and was therefore subject to the practical computational limitations of the software and hardware available at that time. At the time that the work in Appendix D was developed, it was exceptionally computationally expensive to generate and solve an integrated model of the four welds that are found in the shroud support structure. Therefore, this work made use of a number of separate models of the individual welds. The effects of subsequent welding on the locked-in moments predicted in welds produced earlier in the assembly sequence were compensated for using superposition. Later review of this work raised several issues:

- Care must be taken in using linear superposition in an elastic-plastic model, where localized yielding may compromise the validity of the results.
- Subsequent to this work described in Appendix D, it was discovered that a number of reactor vessels manufactured by Chicago Bridge and Iron Nuclear (CBIN), including River Bend, had their shroud support structures assembled in a significantly different sequence.¹ (see Sections E.1 and E.2 for more discussion).

¹ E-mail correspondence from Jaishanker Brihmadessam of Entergy Operations, Inc. to Raj Pathania of EPRI, "RE: Welding sequence for BWR Vessel Shroud Support (BWRVIP-59)," dated February 10, 2000.

- The weld pass sequence assumed for each of the welds in the shroud support structure was based (in part) on data from destructive examination of the River Bend 2 shroud. However, it is reasonable to expect that other shroud support structures were assembled using a different weld pass sequence. It is unclear whether some of these alternate weld pass sequences produce higher stresses than those investigated in Appendix D.
- It is also not clear that the cut line locations used for reported results in Appendix D are the most conservative locations for use in crack growth calculations. These cut lines were selected to match the locations of experimental sections performed in support of BWRVIP-59, but no sensitivity study has been performed to show that these locations predict that shortest time for cracks to grow through the section.

It has been previously determined that the local peak residual stresses at each of these welds is largely independent of weld installation sequence. However, the degree of global constraint present when each weld is made has a more significant effect on the locked-in forces and moments in the structure. These locked-in forces and moments are an important variable in calculating the rate at which a surface crack propagates through thickness, and whether such cracks are expected to continue to propagate through the entire thickness or become self-limited at a specific depth.

It has been argued that the difference between the two possible weld installation sequences could be expected to be minor. As described in Appendix D of this report, the finite element model assumed all of the various members of the shroud support system to be connected by small lands at the center of each weld. These lands served to restrain lateral deflections of the members so that the structure maintained its gross alignment as subsequent welding was performed. As a result of this approach, even members assumed to be installed early in the assembly process were generally well constrained during welding. Therefore, additional constraint induced by making the weld later in the installation sequence was not expected to make a significant difference.

At the time of this writing, computational capabilities have improved to the point that it is practical to create integrated models that incorporate all four welds in the shroud support structure, and to further perform a number of parametric runs which vary both the weld assembly sequence (which weld is made first) and the weld pass sequence (whether the top or bottom side of the weld is made first). The purpose of this Appendix is to investigate the impact of the assembly sequence, weld sequence, and assumed crack plane location on the stresses that are used for subsequent crack growth rate prediction elsewhere in this report. The focus of this sensitivity study is on the as-found weld configuration determined for the River Bend reactor pressure vessel (RPV). Nonetheless, it is expected that the general conclusions of this sensitivity study are applicable to many similar shroud support configurations.

E.1 Weld Joints and Sequences Analyzed

A number of different weld configurations were analyzed and are discussed in Appendix D of this report. The configuration of particular interest is the as-built weld configuration found by destructive examination of the River Bend 2 RPV. The River Bend 2 RPV was found to have H8, H9, H10, and H12 welds, with shapes and weld bead sequences as given in Figures D-3, D-4, D-5, D-7 (see Appendix D). In the interest of reduced solution time, the local weld models

described in Appendix D were analyzed separately and the forces and moments were adjusted using linear superposition. The work performed in this Appendix considered these same weld configurations and bead sequences, but in a single combined model (see Figure E-2). In this Appendix, we also investigate the stresses associated with the less-massive H11 weld, which is sometimes used in place of the H12 weld (see Appendix D for more discussion of weld configurations).

The finite element model of the River Bend BWR core shroud support structure is described more fully in Appendix D. The model consists of a 15-degree segment of the RPV and shroud support structure, including a full 15-degree slice of the cylindrical members (vessel, shroud support plate, shroud support cylinder), and a half section of one of the twelve shroud support legs. Symmetry boundary conditions are employed in such a way that this 15-degree model fully represents the twelve-fold symmetric structure being modeled.

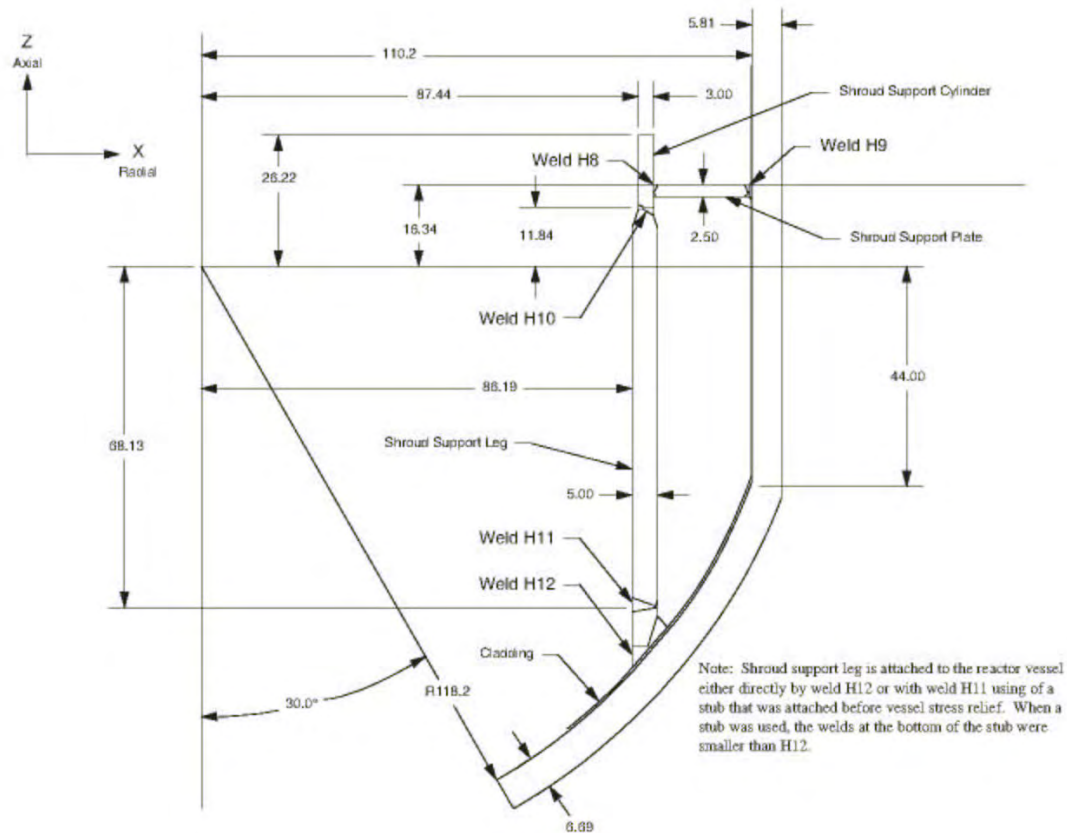


Figure E-1
Reactor Vessel and Shroud Support Model

Four weld locations are of interest in this sensitivity analysis. The weld locations are shown in Figure E-1 and are given designations as follows:

H8 Weld connecting the ID of the shroud support plate to the OD of the shroud support cylinder.

- H9 Weld connecting the OD of the shroud support plate to the ID of the RPV.
- H10 Weld between the top of a support leg and the bottom of the shroud support cylinder.
- H11/H12 Weld between the bottom of a support leg and the lower head of the RPV. When the weld is made directly to the vessel lower head, it is referred to as an H12 weld. In some cases a pedestal is built up on the lower head prior to vessel stress relief and a horizontal butt weld, referred to as an H11 weld, is made. Destructive examination shows that an H12 weld was used to attach the support leg to the lower head of the RPV at River Bend 2.

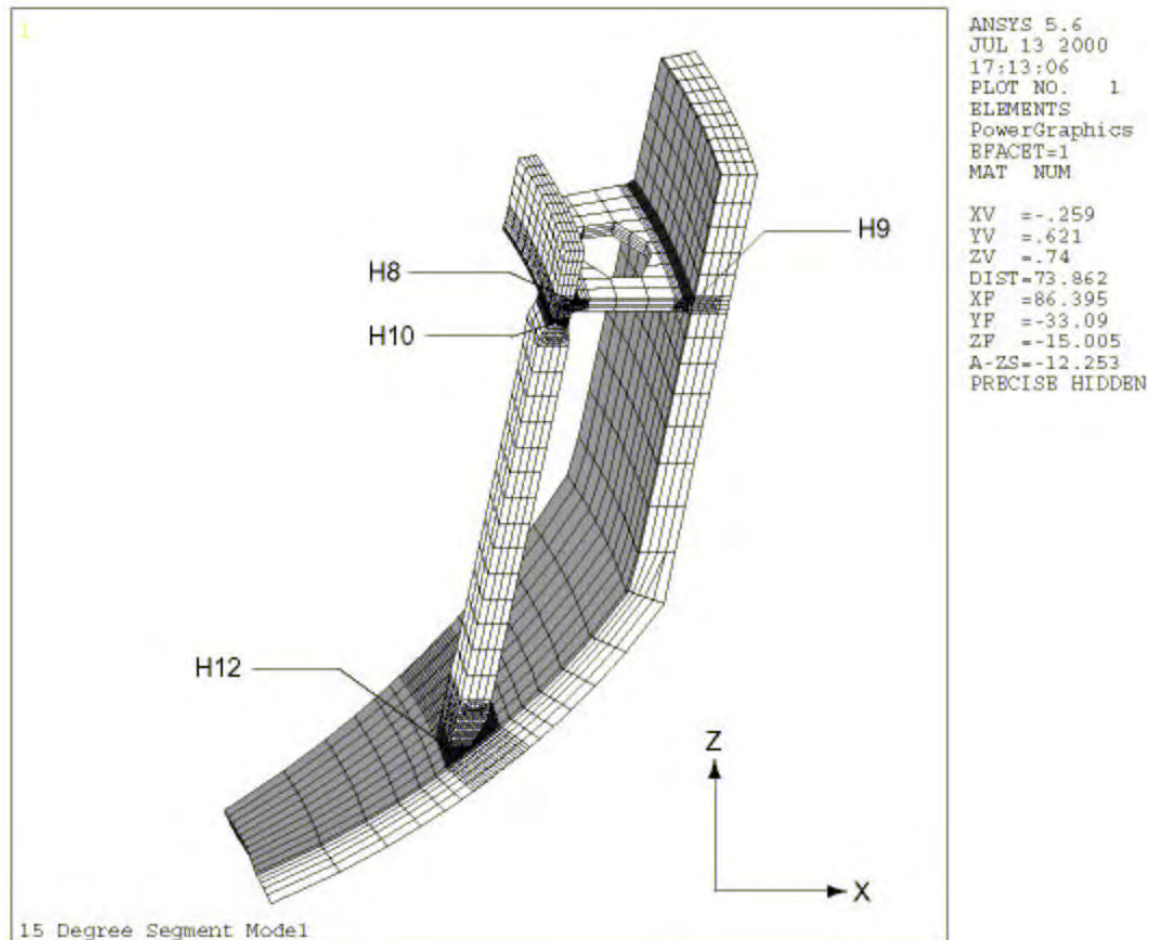


Figure E-2
Model Weld Geometry

As discussed in the introduction to this Appendix, work described in Appendix D of this report concerned the weld residual stresses with an assumed weld assembly sequence, based on the best information available at that time. The original weld sequence assumed in Appendix D of this report may be described as follows (see Figure E-1 for weld location definitions):

- The shroud support cylinder is first attached to the shroud support plate via weld H8. This weld is performed in the shop prior to any field fabrication of subsequent joints.
- The shroud support legs are then connected to the vessel lower head, either by welding directly to the reactor vessel (weld H12) or to a pedestal built up on the lower head prior to vessel stress relief (weld H11). The shroud support legs are assumed to be laterally restrained at their upper ends during welding to prevent gross misalignment caused by weld shrinkage stresses.
- The shroud support cylinder is then placed on the shroud support legs, and the legs are connected to the shroud support cylinder by weld H10.
- Finally, the shroud support plate is attached to the reactor vessel shell at weld H9.

This alternate sequence is understood to be as follows:

- The shroud support cylinder is attached to the shroud support plate via weld H8. This weld is performed in the shop prior to any field fabrication of subsequent joints.
- The shroud support cylinder is temporarily supported in position, and the shroud support plate is attached to the reactor vessel shell at weld H9.
- The shroud support legs are then fit between the shroud support cylinder and the vessel lower head, and welded into the lower head and support cylinder simultaneously. The weld at the upper end of the legs is H10, and the connection to the lower head is made using either an H11 or an H12 weld, depending on whether the optional pedestal was used.

As was indicated in the introduction, another purpose of this Appendix was to perform a sensitivity study of the effects of weld pass sequence on the stress distributions used for crack growth calculations. The weld sequence used in the base work is shown in Figures D-3 to D-7, as follows:

- H8 The original sequence idealized this joint to be welded top first in three passes, then bottom with two passes, and finally with a sixth cover pass “simultaneously” both top and bottom.
- H9 This joint was assumed to be welded bottom first in three passes, followed by a three-pass top weld.
- H10 The outside (OD) side of the joint was welded in four passes, followed by two passes on the inside.
- H11 H11 welding was performed in seven passes on the inside, followed by a single backgouge and weld pass on the outside.
- H12 H12 was assumed to be welded in five passes on the outside, followed by five passes on the inside.

There is a fairly large analysis space that could be investigated by permuting all possible weld assembly sequences (legs first vs. last), configurations (H11 or H12 geometry), and reversal of each of the four weld locations, for a total of 64 unique cases. This analysis space was limited by

considering the reversal of only welds H9 (which is similar in nature to H8) and H12 (which is the most constrained weld configuration on the legs), and only reversing these welds one at a time. This produced an eight-case matrix, designated as follows:

Run A: The base assembly case using the H12 weld for the sequence believed to have been used for River Bend 2 (H8 first, then H9, finally H10 and H12 simultaneously), and using the base case weld pass sequences as given in Figures D-3 to D-7.

Run B: Identical to Run A, but with weld H9 welded top first, then bottom.

Run C: Identical to Run A, but with weld H12 welded inside first, then outside.

Run D: The base assembly case using the H12 weld for the assembly sequence originally used in Appendix D (H8 first, then H10 and H12, and finally H9, and using the base case weld pass sequences.

Run E: Identical to Run D, but with weld H9 welded top first, then bottom.

Run F: Identical to Run D, but with weld H12 welded inside first, then outside.

Run G: Identical to Run A, but using an H11 geometry rather than H12.

Run H: Identical to Run D, but using an H11 geometry rather than H12.

Limiting to these cases allowed for a reasonable sensitivity study to be performed without generating so much data that subsequent analysis becomes overly difficult.

E.2 Analysis Approach

Welding residual stresses in the support leg and baffle plate welds were computed using the ANSYS finite element code, Revision 5.7, on an HP J6700 workstation. The analysis approach is very similar to that previously described in Appendix D of this report, and the reader is directed to Appendix D for more details of the general analysis approach.

The two key modifications to the models relate to the sequencing of welds, as described previously in this Appendix:

E.2.1 Fabrication Sequence

The global model, shown in Figure E-2, was used to simulate welding in the sequence H8, then H9, followed by H10 and H11/H12 simultaneously for Runs A, B, C, and G. For the other four runs, the sequence used was: H8, followed by H10 and H11/H12 simultaneously, and finally H9. Because a combined model was used, there was no need to perform linear superposition of the various weld models as was done in Appendix D.

E.2.2 Treatment of H10 and H11/H12 Welds

In the modeling described in this Appendix, the shroud support legs are assumed to be fit up in between the shroud support cylinder and the reactor vessel lower head, and welded at the top and bottom of each leg simultaneously. Some assumptions had to be made regarding the timing of these simultaneous welds, as the number of passes in welds H11 and H12 are greater than the number of passes in weld H10. A different number of weld passes was used for each joint so as to keep each weld pass comparable in size, rather than changing the average size of the weld passes in proportion to the thickness of the weld. As a result, weld H10 is modeled to have been fabricated using four passes on the OD side of the shroud support ring, followed by a backgouge of the temporary land and two weld passes on the ID side of the connection. Weld H12, on the other hand, is modeled to be constructed using five passes on the OD side of the joint, followed by a backgouge and another five passes on the ID side of the joint, and weld H11 is modeled to be constructed from seven passes on the inside of the joint, followed by a single backgouge pass on the outside.

Both joints were assumed to be initiated at the same time, and each of the passes in welds H10 and H11/H12 are constructed in parallel during both the thermal and structural steps of the finite element model. Accordingly, the first side of weld H10 is completed one pass sooner than the first side of welds H11 or H12. The first side of weld H12 is assumed to be completed before backgouging is initiated in weld H10. Therefore, the last welding pass on the first side of welds H11 or H12 is made while there is no activity at weld H10.

The second sides of welds H10 and H11/H12 are treated similarly to the first. The backgouge and weld-out of the root passes are modeled simultaneously, as are the subsequent passes of the second side of the welds. When H12 is present, weld H10 is completed before H12, as the second half of weld H10 consists of only two passes while H12 consists of five. Therefore, the remaining three passes of weld H12 are subsequently completed with no further activity at weld H10. On the other hand, weld H11 has only one backgouge pass, so H10 actually completes last.

Upon completion of welding, the model described in this Appendix is also used for investigation of the potential effects of post-weld heat treatment (PWHT) at 1150°F on the residual stress field. Although the impact of the PWHT on the residual stress has been calculated, the results presented in this Appendix are all given prior to PWHT, just after the last pass of welding. The stresses prior to PWHT lead to more conservative predictions of crack growth rates, and it is believed that only some of the RPV's (not including River Bend) of interest were subjected to PWHT.

E.3 Post-Processing Section Line Locations

As indicated above, one of the objectives of this Appendix is to determine the most limiting stress profile ("cut line" or "section line") location for reporting of stress for use in subsequent crack growth calculations. A set of five section lines at each weld were used in an attempt to locate the most limiting location. See Figure E-3 to E-7 for section line definitions. For welds H8, H9, H10, and H12, it is noted that one of the section lines in each case corresponds to the section used for post-processing the corresponding weld in the Appendix D work. No section results reported for weld H11 because corresponding results from destructive examination are not available for comparison.

When using the section line stress results, it should be noted that stresses are reported normal to the section line. The direction of travel from start to end on the section line are also important to be aware of. This direction of travel is indicated by the arrows on Figures E-3 to E-7. All of the section lines in the set of five run in the same direction, and for welds H9 to H12, they all run in the same direction as the corresponding cut line defined in Appendix D. Care should be taken, however, to note that the direction of the section lines for H8 in this Appendix is opposite that used in Appendix D.

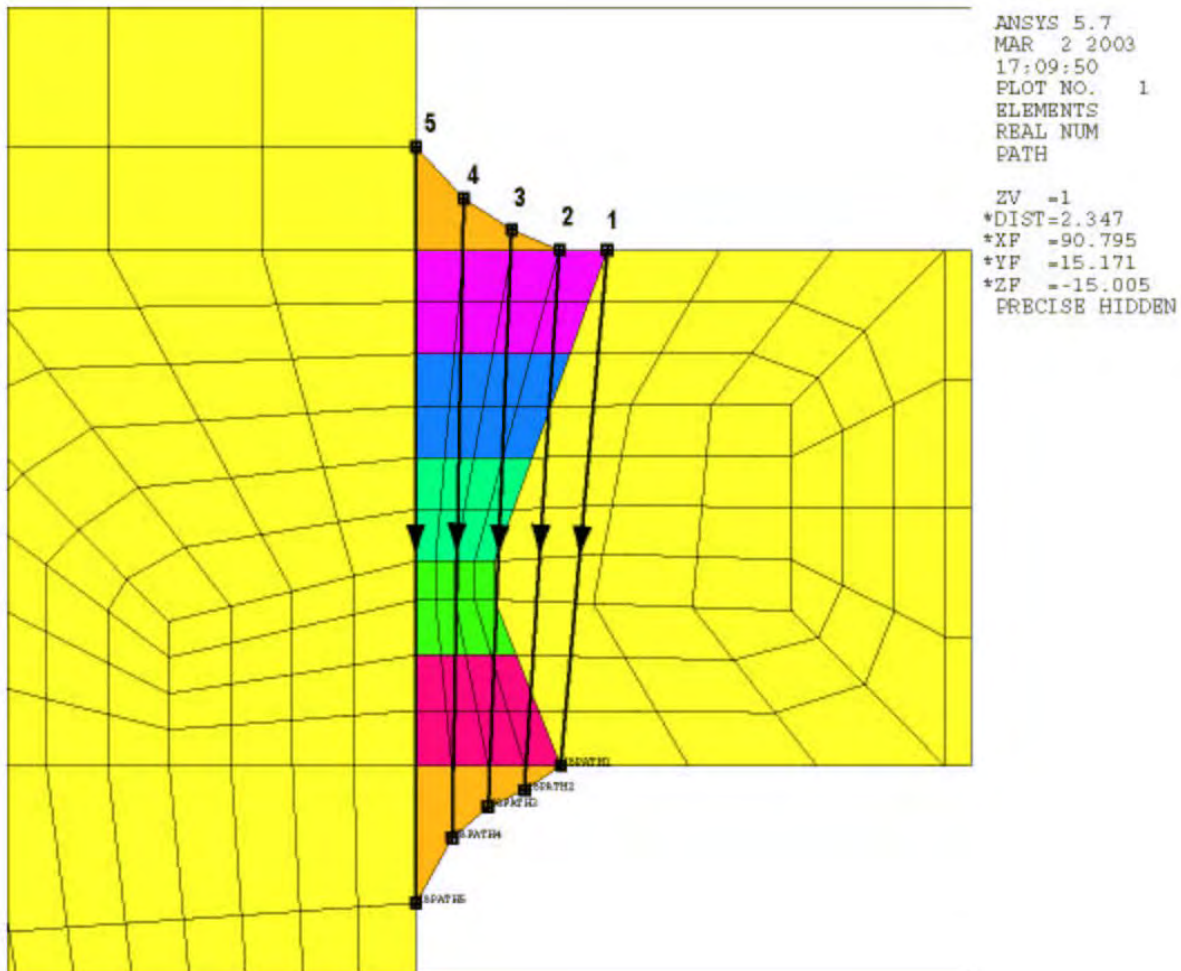


Figure E-3
Weld H8 Section Line Definitions

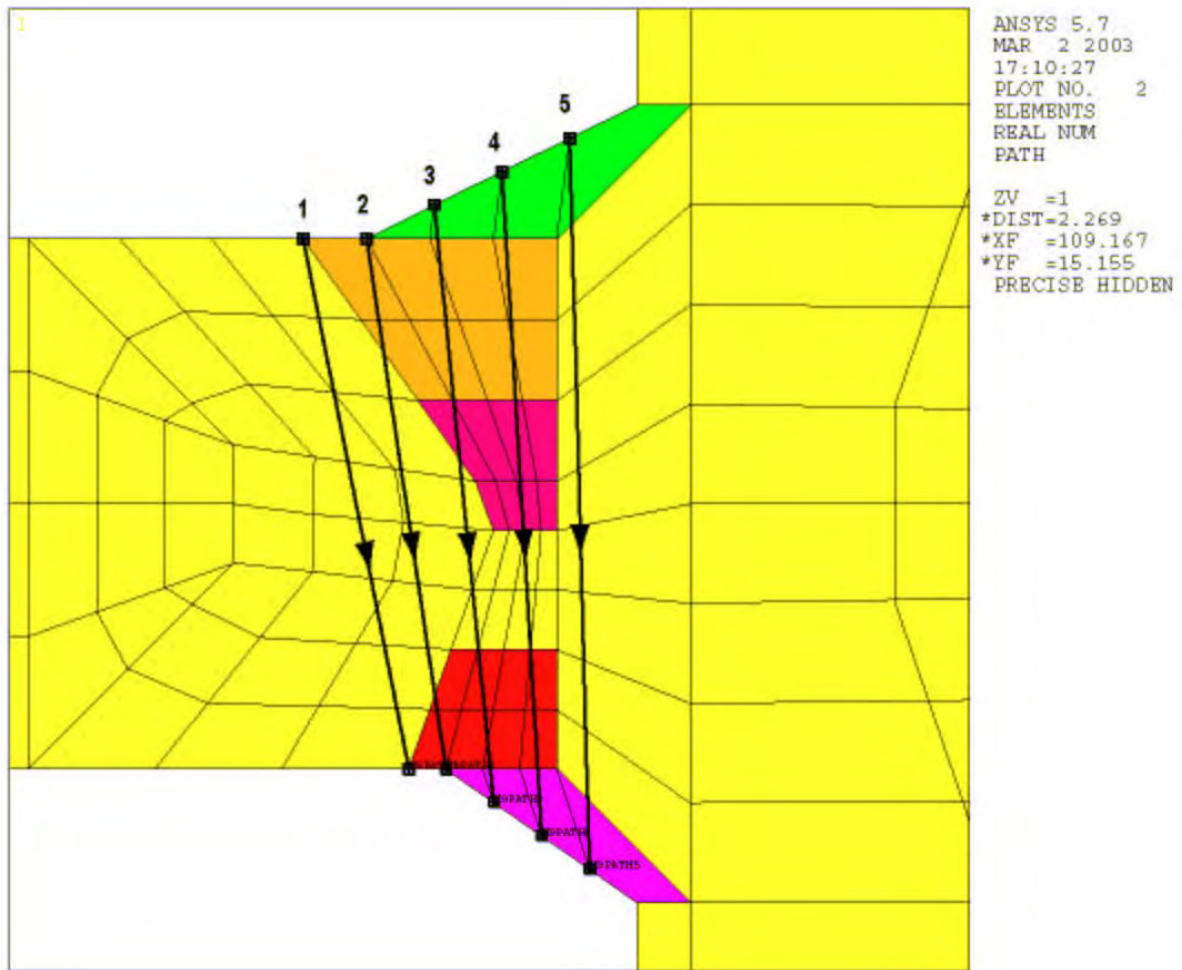


Figure E-4
Weld H9 Section Line Definitions

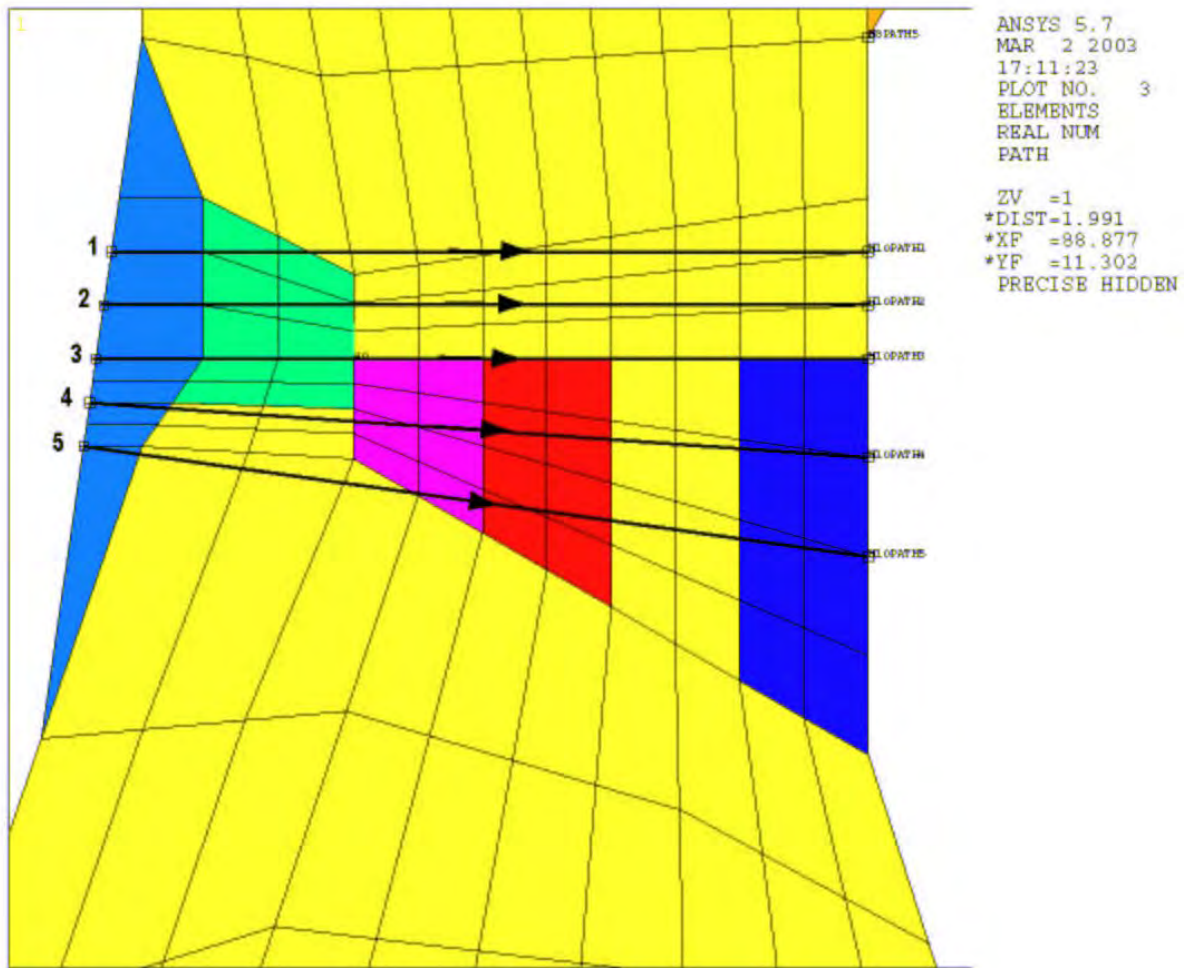


Figure E-5
Weld H10 Section Line Definitions

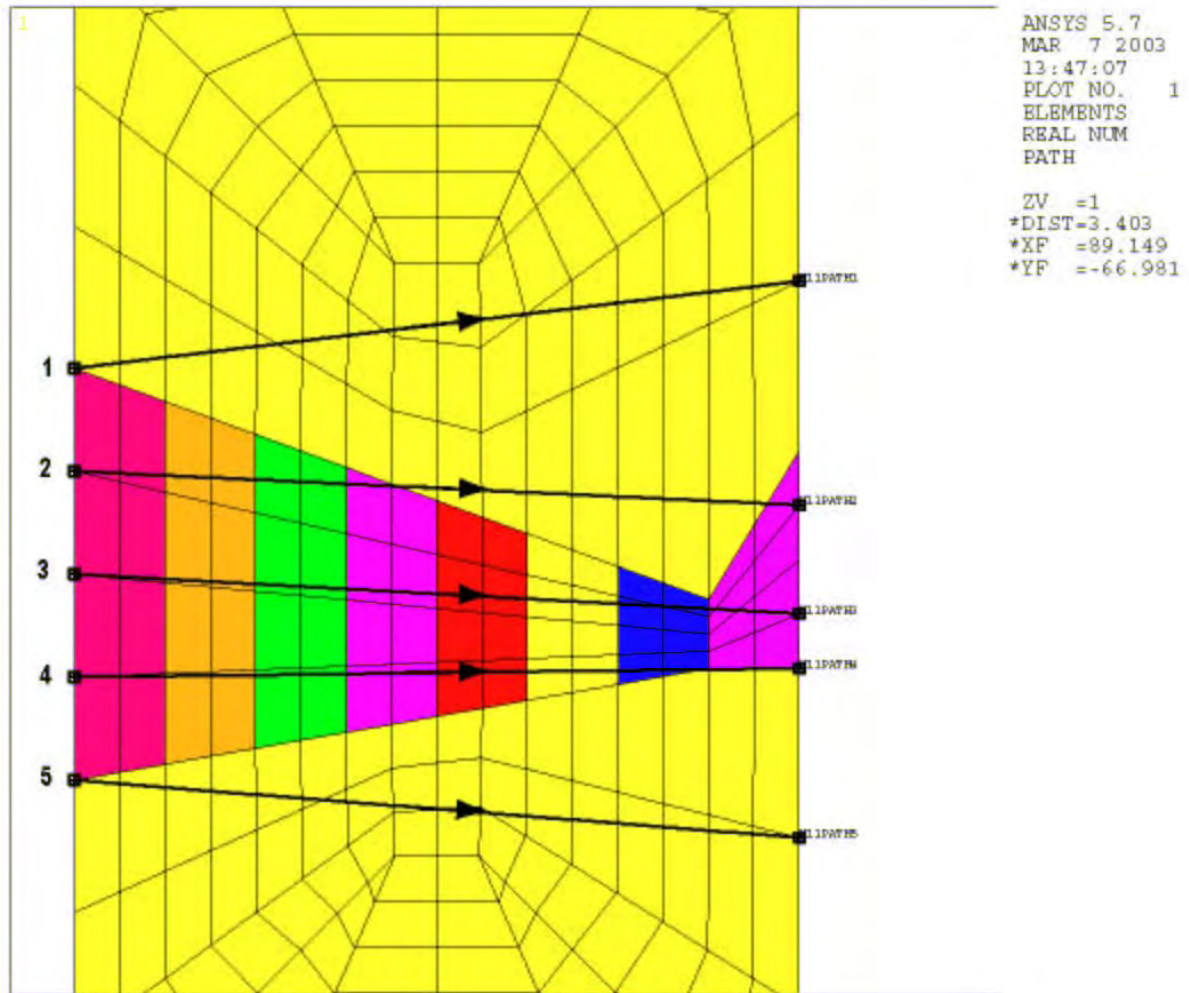


Figure E-6
Weld H11 Section Line Definitions

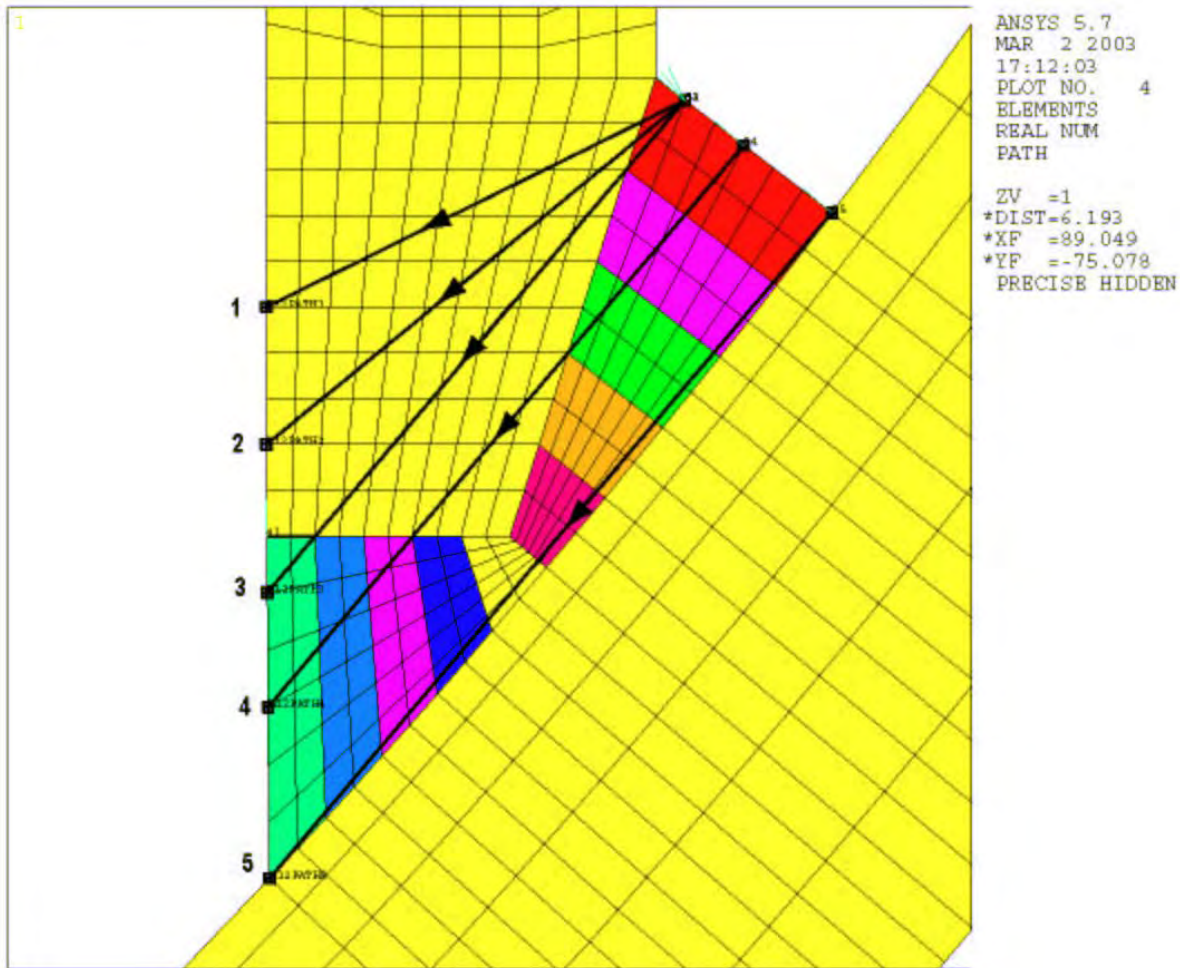


Figure E-7
Weld H12 Section Line Definitions

E.4 Analysis Results

E.4.1 Residual Stresses Without Post Weld Heat Treatment

Contour plots of the stress distributions at the completion of all welding, but before any PWHT, for the different welds are shown in Figures E-8 to E-35. Figures E-8 to E-17 give the stresses in each weld for the alternate assembly sequence, and Figures E-18 to E-27 give the stresses for the original assembly sequence. None of these figures include weld reversal. The results for welds H8, H9, H10, and H12 come from the base case runs A and D. Stresses in weld H11 come from runs G and H. The weld reversal cases are compared to their nearest base run case in Figures E-28 to E-35.

**Content Deleted -
EPRI Proprietary Information**

Figure E-8
Weld H8 After Welding Radial Stress (SX) (Run A-Alt. Sequence With H12 Geometry)

**Content Deleted -
EPRI Proprietary Information**

Figure E-9
Weld H8 After Welding Circumferential Stress (SY) (Run A-Alt. Sequence With H12 Geometry)

**Content Deleted -
EPRI Proprietary Information**

Figure E-10
Weld H9 After Welding Radial Stress (SX) (Run A-Alt. Sequence With H12 Geometry)

**Content Deleted -
EPRI Proprietary Information**

Figure E-11
Weld H9 After Welding Circumferential Stress (SY) (Run A-Alt. Sequence With H12 Geometry)

**Content Deleted -
EPRI Proprietary Information**

Figure E-12
Weld H10 After Welding Vertical Stress (SZ) (Run A-Alt. Sequence With H12 Geometry)

**Content Deleted -
EPRI Proprietary Information**

Figure E-13
Weld H10 After Welding Circumferential Stress (SY) (Run A-Alt. Sequence With H12 Geometry)

**Content Deleted -
EPRI Proprietary Information**

Figure E-14
Weld H11 After Welding Vertical Stress (SZ) (Run G-Alt. Sequence With H11 Geometry)

**Content Deleted -
EPRI Proprietary Information**

Figure E-15
Weld H11 After Welding Circumferential Stress (SY) (Run G-Alt. Sequence With H11 Geometry)

**Content Deleted -
EPRI Proprietary Information**

Figure E-16
Weld H12 After Welding Perpendicular Stress (SZ) (Run A-Alt. Sequence With H12
Geometry)

**Content Deleted -
EPRI Proprietary Information**

Figure E-17
Weld H12 After Welding Circumferential Stress (SY) (Run A-Alt. Sequence With H12
Geometry)

**Content Deleted -
EPRI Proprietary Information**

Figure E-18
Weld H8 After Welding Radial Stress (SX) (Run D-Orig. Sequence With H12 Geometry)

**Content Deleted -
EPRI Proprietary Information**

Figure E-19
Weld H8 After Welding Circumferential Stress (SY) (Run D-Orig. Sequence With H12 Geometry)

**Content Deleted -
EPRI Proprietary Information**

Figure E-20
Weld H9 After Welding Radial Stress (SX) (Run D-Orig. Sequence With H12 Geometry)

**Content Deleted -
EPRI Proprietary Information**

Figure E-21
Weld H9 After Welding Circumferential Stress (SY) (Run D-Orig. Sequence With H12 Geometry)

**Content Deleted -
EPRI Proprietary Information**

Figure E-22
Weld H10 After Welding Vertical Stress (SZ) (Run D-Orig. Sequence With H12 Geometry)

**Content Deleted -
EPRI Proprietary Information**

Figure E-23
Weld H10 After Welding Circumferential Stress (SY) (Run D-Orig. Sequence With H12 Geometry)

**Content Deleted -
EPRI Proprietary Information**

Figure E-24
Weld H11 After Welding Vertical Stress (SZ) (Run H-Orig. Sequence With H11 Geometry)

**Content Deleted -
EPRI Proprietary Information**

Figure E-25
Weld H11 After Welding Circumferential Stress (SY) (Run H-Orig. Sequence With H11 Geometry)

**Content Deleted -
EPRI Proprietary Information**

Figure E-26
Weld H12 After Welding Perpendicular Stress (SZ) (Run D-Orig. Sequence With H12
Geometry)

**Content Deleted -
EPRI Proprietary Information**

Figure E-27
Weld H12 After Welding Circumferential Stress (SY) (Run D-Orig. Sequence With H12
Geometry)

**Content Deleted -
EPRI Proprietary Information**

Figure E-28
Weld H9 After Welding Radial Stress (SX) (Run A-Alt. Sequence With H12 Geometry)

**Content Deleted -
EPRI Proprietary Information**

Figure E-29
Weld H9 After Welding Radial Stress (SX) (Run B-Alt. Sequence With H12 Geometry and Weld H9 Reversed)

**Content Deleted -
EPRI Proprietary Information**

Figure E-30
Weld H12 After Welding Perpendicular Stress (SZ) (Run A-Alt. Sequence With H12
Geometry)

**Content Deleted -
EPRI Proprietary Information**

Figure E-31
Weld H12 After Welding Perpendicular Stress (SZ) (Run C- Alt. Sequence With H12
Geometry and Weld H12 Reversed)

**Content Deleted -
EPRI Proprietary Information**

Figure E-32
Weld H9 After Welding Radial Stress (SX) (Run D- Orig. Sequence With H12 Geometry)

**Content Deleted -
EPRI Proprietary Information**

Figure E-33
Weld H9 After Welding Radial Stress (SX) (Run E- Orig. Sequence With H12 Geometry and Weld H9 Reversed)

**Content Deleted -
EPRI Proprietary Information**

Figure E-34
Weld H12 After Welding Perpendicular Stress (SZ) (Run D- Orig. Sequence With H12
Geometry)

**Content Deleted -
EPRI Proprietary Information**

Figure E-35
Weld H12 After Welding Perpendicular Stress (SZ) (Run F- Orig. Sequence With H12
Geometry and Weld H12 Reversed)

For each weld, the normal stresses perpendicular and parallel (i.e., in the circumferential direction) to the weld are shown. Normal stress parallel to the weld is designated SY in all cases. Normal stress perpendicular to the weld is SZ for welds H10, H11 and H12; and SX for welds H8 and H9. For weld H12, in order to show meaningful stress distributions for all portions of the weld, SZ refers to stresses perpendicular to an axis rotated 30° from the horizontal. Normal stresses through the thickness of the welded component are typically small and are not shown. In all figures, the contour plots represent the distribution of stress on the 0-degree plane of the model (a plane through the centerline of the leg). Welds H8 and H9 are essentially axisymmetric so the contour plots of these welds are representative of any radial plane through the weld. Welds H10, H11 and H12 are not axisymmetric, so the contours shown in the other figures are specific to the leg center plane. However, previous work has shown that the stresses in the leg welds are greater along the leg centerline (0-degree azimuth) than on other planes, so reported results are limited to the leg centerline in this Appendix.

Figures E-8 through E-27 are each arranged with the in-plane stress component (radial for welds H8/H9, vertical for the rest) are on top, and circumferential stress is on bottom. The same stress scale is used for each plot.

The effects of some of the sensitivity cases are plotted to permit comparison between the base case (top plot) and the sensitivity test case (bottom plot). Each plot makes use of the same stress contour legend. Figures E-28 and E-29 compares the stresses in H9 for Run A vs. Run B, Figures E-30 and E-31 compares the stresses in H12 for Run A vs. Run C, Figures E-32 and E-33 compares the stresses in H9 for Run D vs. Run E, and Figures E-34 and E-35 compares the stresses in H12 for Run D vs. Run F.

Examination of these figures leads to the following conclusions:

**Content Deleted -
EPRI Proprietary Information**

E.5 Section Line Data for Use in Crack Growth Calculations

A family of section line plots have been produced on the five section lines for each of four welds and each of the eight runs, and are given in Figures E-36 to E-67. These data may be used as inputs to the crack growth calculations in the main body of this report. Examination of this figures shows that the sections with the highest stresses driving crack growth as follows: Cut line 3 on weld H8, cut line 4 on weld H9, cut line 5 in weld H10, cut line 3 on weld H11, and cut line 4 on weld H12.

The stresses at the limiting cut line locations are compared in Figures E-68 to E-73. Figure E-68 compares the stresses in weld H8 and shows that Run E (original sequence with H9 reversed) produces higher stresses than many other cases. Figure E-69 shows that Run E is also a limiting case for weld H9. Runs C and D represent the extreme cases for weld H10, as shown in Figure E-70. Finally, Figures E-71 to E-73 show welds H11 and H12 to be insensitive to effects elsewhere in the model, although the original weld sequence is apparently the more conservative for weld H12.

**Content Deleted -
EPRI Proprietary Information**

**Figure E-36
H8 Cut Line Residual Stresses Perpendicular to Cut Line (Run A)**

**Content Deleted -
EPRI Proprietary Information**

Figure E-37
H9 Cut Line Residual Stresses Perpendicular to Cut Line (Run A)

**Content Deleted -
EPRI Proprietary Information**

Figure E-38
H10 Cut Line Residual Stresses Perpendicular to Cut Line (Run A)

**Content Deleted -
EPRI Proprietary Information**

Figure E-39
H12 Cut Line Residual Stresses Perpendicular to Cut Line (Run A)

**Content Deleted -
EPRI Proprietary Information**

Figure E-40
H8 Cut Line Residual Stresses Perpendicular to Cut Line (Run B)

**Content Deleted -
EPRI Proprietary Information**

Figure E-41
H9 Cut Line Residual Stresses Perpendicular to Cut Line (Run B)

**Content Deleted -
EPRI Proprietary Information**

Figure E-42
H10 Cut Line Residual Stresses Perpendicular to Cut Line (Run B)

**Content Deleted -
EPRI Proprietary Information**

Figure E-43
H12 Cut Line Residual Stresses Perpendicular to Cut Line (Run B)

**Content Deleted -
EPRI Proprietary Information**

Figure E-44
H8 Cut Line Residual Stresses Perpendicular to Cut Line (Run C)

**Content Deleted -
EPRI Proprietary Information**

Figure E-45
H9 Cut Line Residual Stresses Perpendicular to Cut Line (Run C)

**Content Deleted -
EPRI Proprietary Information**

Figure E-46
H10 Cut Line Residual Stresses Perpendicular to Cut Line (Run C)

**Content Deleted -
EPRI Proprietary Information**

Figure E-47
H12 Cut Line Residual Stresses Perpendicular to Cut Line (Run C)

**Content Deleted -
EPRI Proprietary Information**

Figure E-48
H8 Cut Line Residual Stresses Perpendicular to Cut Line (Run D)

**Content Deleted -
EPRI Proprietary Information**

Figure E-49
H9 Cut Line Residual Stresses Perpendicular to Cut Line (Run D)

**Content Deleted -
EPRI Proprietary Information**

Figure E-50
H10 Cut Line Residual Stresses Perpendicular to Cut Line (Run D)

**Content Deleted -
EPRI Proprietary Information**

Figure E-51
H12 Cut Line Residual Stresses Perpendicular to Cut Line (Run D)

**Content Deleted -
EPRI Proprietary Information**

Figure E-52
H8 Cut Line Residual Stresses Perpendicular to Cut Line (Run E)

**Content Deleted -
EPRI Proprietary Information**

Figure E-53
H9 Cut Line Residual Stresses Perpendicular to Cut Line (Run E)

**Content Deleted -
EPRI Proprietary Information**

Figure E-54
H10 Cut Line Residual Stresses Perpendicular to Cut Line (Run E)

**Content Deleted -
EPRI Proprietary Information**

Figure E-55
H12 Cut Line Residual Stresses Perpendicular to Cut Line (Run E)

**Content Deleted -
EPRI Proprietary Information**

Figure E-56
H8 Cut Line Residual Stresses Perpendicular to Cut Line (Run F)

**Content Deleted -
EPRI Proprietary Information**

Figure E-57
H9 Cut Line Residual Stresses Perpendicular to Cut Line (Run F)

**Content Deleted -
EPRI Proprietary Information**

Figure E-58
H10 Cut Line Residual Stresses Perpendicular to Cut Line (Run F)

**Content Deleted -
EPRI Proprietary Information**

Figure E-59
H12 Cut Line Residual Stresses Perpendicular to Cut Line (Run F)

**Content Deleted -
EPRI Proprietary Information**

Figure E-60
H8 Cut Line Residual Stresses Perpendicular to Cut Line (Run G)

**Content Deleted -
EPRI Proprietary Information**

Figure E-61
H9 Cut Line Residual Stresses Perpendicular to Cut Line (Run G)

**Content Deleted -
EPRI Proprietary Information**

Figure E-62
H10 Cut Line Residual Stresses Perpendicular to Cut Line (Run G)

**Content Deleted -
EPRI Proprietary Information**

Figure E-63
H11 Cut Line Residual Stresses Perpendicular to Cut Line (Run G)

**Content Deleted -
EPRI Proprietary Information**

Figure E-64
H8 Cut Line Residual Stresses Perpendicular to Cut Line (Run H)

**Content Deleted -
EPRI Proprietary Information**

Figure E-65
H9 Cut Line Residual Stresses Perpendicular to Cut Line (Run H)

**Content Deleted -
EPRI Proprietary Information**

Figure E-66
H10 Cut Line Residual Stresses Perpendicular to Cut Line (Run H)

**Content Deleted -
EPRI Proprietary Information**

Figure E-67
H11 Cut Line Residual Stresses Perpendicular to Cut Line (Run H)

**Content Deleted -
EPRI Proprietary Information**

Figure E-68
H8 Cut Line Residual Stresses Perpendicular to Cut Line 3 (Runs A to H)

**Content Deleted -
EPRI Proprietary Information**

Figure E-69
H9 Cut Line Residual Stresses Perpendicular to Cut Line 4 (Runs A to H)

**Content Deleted -
EPRI Proprietary Information**

Figure E-70
H10 Cut Line Residual Stresses Perpendicular to Cut Line 5 (Runs A to H)

**Content Deleted -
EPRI Proprietary Information**

Figure E-71
H11 Cut Line Residual Stresses Perpendicular to Cut Line 3 (Runs G and H)

**Content Deleted -
EPRI Proprietary Information**

Figure E-72
H12 Cut Line Residual Stresses Perpendicular to Cut Line 4 (Runs A to F)

**Content Deleted -
EPRI Proprietary Information**

Figure E-73
H11 and H12 Cut Line Residual Stresses Perpendicular to Cut Line 4 (No Weld Reversal)

E.6 Comparison to Previous Work

The section line data discussed above may be used to make a comparison between the original work presented in Appendix D of this report and the newer work presented here. Figures E-74 to E-77 are comparisons of the section line data from Appendix D to new corresponding data from Run D in this Appendix. Also shown in the comparison are the results obtained experimentally from sectioning portions of the River Bend 2 shroud (this work is described elsewhere in this report). It should be noted in making these comparisons that the results were taken at the same section line locations using the same path direction in each case.

Examination of these figures leads to the following conclusions:

**Content Deleted -
EPRI Proprietary Information**

**Content Deleted -
EPRI Proprietary Information**

E.7 References

- E-1. E-mail correspondence from Jaishanker Brihmadessam of Entergy Operations, Inc. to Raj Pathania of EPRI, “RE: Welding sequence for BWR Vessel Shroud Support (BWRVIP-59),” dated February 10, 2000.
- E-2. ANSYS Finite Element Program, Revision 5.7, ANSYS, Inc., Canonsburg, PA.
- E-3. David W. Gandy, et al., “Reactor Pressure Vessel Internals Survey,” EPRI Repair Applications Center, June 12, 1989.
- E-4. Weili Cheng and Iain Finnie, “Through-Thickness Residual Stress Measurement at River Bend Nuclear Station,” University of California, Berkeley Research Project B301-11, Final Report, December 1997.

**Content Deleted -
EPRI Proprietary Information**

Figure E-74
H8 Cut Line Residual Stresses Perpendicular to Cut Line 1 (Run D) vs. Appendix D Work

**Content Deleted -
EPRI Proprietary Information**

Figure E-75
H9 Cut Line Residual Stresses Perpendicular to Cut Line 2 (Run D) vs. Appendix D Work

**Content Deleted -
EPRI Proprietary Information**

Figure E-76
H10 Cut Line Residual Stresses Perpendicular to Cut Line 3 (Run D) vs. Appendix D Work

**Content Deleted -
EPRI Proprietary Information**

Figure E-77
H12 Cut Line Residual Stresses Perpendicular to Cut Line 1 (Run D) vs. Appendix D Work

F

INITIAL NRC SAFETY EVALUATION



UNITED STATES
NUCLEAR REGULATORY COMMISSION
WASHINGTON, D.C. 20555-0001

2001-247A

July 31, 2001

Carl Terry, BWRVIP Chairman
Niagara Mohawk Power Company
Post Office Box 63
Lycoming, NY 13093

SUBJECT: SAFETY EVALUATION OF BWR VESSEL AND INTERNALS PROJECT
BWRVIP-59 REPORT (TAC NO. MA4467)

Dear Mr. Terry:

By letter dated December 23, 1998, as supplemented by letters dated December 4, 2000, and February 19, 2001, the Boiling Water Reactor Vessel and Internals Project (BWRVIP) submitted for staff review and approval the Electric Power Research Institute (EPRI) Proprietary Report TR-108710, "BWR Vessel and Internals Project, Evaluation of Crack Growth in BWR Nickel Base Austenitic Alloys in RPV Internals (BWRVIP-59)," dated December 1998. The staff requested additional information in a letter dated November 29, 1999. The BWRVIP provided its response by letter dated December 4, 2000. The February 19, 2001, letter proposed an interim crack growth rate (CGR) of 2.5×10^{-5} in/hr for nickel base austenitic alloys in BWR plants under hydrogen water chemistry/noble metal chemical application conditions (HWC/NMCA).

The BWRVIP-59 report provides a methodology for assessing crack growth in BWR nickel base alloy shroud support structures and in other nickel base alloy components. This methodology, specifically developed for crack growth in the radial (through-thickness) direction, would apply to Alloy 82 and 182 weld materials and Alloy 600 types of nickel base austenitic materials. Residual and applied stresses and stress intensity factors have been developed for crack propagation in the same direction.

The staff has reviewed the BWRVIP-59 report, the BWRVIP response to the staff's request for additional information (RAI), and the proposed interim CGR. The NRC staff, with assistance from Argonne National Laboratory (ANL), finds that the use of the calculated residual stresses and stress intensity factors combined with the crack disposition curves should generally result in conservative estimates of crack growth. However, the staff has several recommendations contained in the enclosed safety evaluation (SE). The staff requests that these recommendations be reviewed and incorporated, as appropriate, in the BWRVIP-59 report as part of the methodology presented in the BWRVIP-59 report. Please inform the staff within 90-days of the date of this letter as to your proposed actions and schedule for any revisions.

The staff also finds that the proposed interim CGR for HWC/NMCA is superseded by the CGR of 5.0×10^{-6} in/hr proposed in the BWRVIP-59 report. Based on the staff's review of the BWRVIP-59 and BWRVIP-62 reports, the CGR of 5.0×10^{-6} in/hr, subject to the same conditions as those in the BWRVIP-59 report, is acceptable for use as a reference value after a plant-specific CGR has been calculated. Therefore, the request for the interim crack growth rate of 2.5×10^{-5} in/hr for HWC/NMCA is not necessary.

Carl Terry

-2-

Please contact C. E. (Gene) Carpenter, Jr., of my staff at (301) 415-2169 if you have any further questions regarding this subject.

Sincerely,

A handwritten signature in black ink that reads "William H. Bateman". The signature is written in a cursive style with a large, stylized "W" and "B".

William H. Bateman, Chief
Materials and Chemical Engineering Branch
Division of Engineering
Office of Nuclear Reactor Regulation

Enclosure: As stated

cc: BWRVIP Service List

cc:

Joe Hagan, BWRVIP Vice Chair
Exelon Corp.
200 Exelon Way (M/S KSA 3-N)
Kennett Square, PA 19348

George Vanderheyden, Executive Chair
Assessment Committee
Exelon Corp.
Suite 400
1400 Opus Place
Downers Grove, IL 60515-1198

Bill Eaton, Executive Chair,
Inspection Committee
Grand Gulf Gen. Mgr., Plant Operations
Entergy Operations, Inc.
PO Box 756, Waterloo Rd
Port Gibson, MS 39150-0756

H. Lewis Sumner, Executive Chair
BWRVIP Mitigation Task
Vice President, Hatch Project
Southern Nuclear Operating Co.
M/S BIN B051, PO BOX 1295
40 Inverness Center Parkway
Birmingham, AL 35242-4809

George T. Jones, Executive Chair
Repair Committee
Vice President, Nuclear Engrg. & Support
PP&L, Inc.
M/S GENA61
2 N 9th St
Allentown, PA 18101-1139

Robert Carter, EPRI BWRVIP
Assessment Manager
Greg Selby, EPRI BWRVIP
Inspection Manager
EPRI NDE Center
P. O. Box 217097
1300 W. T. Harris Blvd.
Charlotte, NC 28221

Richard Cierniewicz, Technical Chair
Assessment Committee
Exelon Corp.
Peach Bottom Atomic Power Station
(M/S SMB3-6)
1848 Lay Road
Delta, PA 17314-9032

Carl Larsen, Technical Chair
BWRVIP Inspection Task
Vermont Yankee Nuclear Power Corp.
P.O. Box 157
Vernon, VT 05354

John Wilson, Technical Chair
BWRVIP Mitigation Task
AmerGen Energy Co.
Clinton Power Station, M/C T-31C
P.O. Box 678
Clinton, IL 61727

Vaughn Wagoner, Technical Chair
BWRVIP Integration Task
Carolina Power & Light Company
One Hannover Square 9C1
P.O. Box 1551
Raleigh, NC 27612

Bruce McLeod, Technical Chair
BWRVIP Repair Task
Southern Nuclear Operating Co.
Post Office Box 1295
40 Inverness Center Parkway
Birmingham, AL 35201

Tom Mulford, EPRI BWRVIP
Integration Manager
Raj Pathania, EPRI BWRVIP
Mitigation Manager
Ken Wolfe, EPRI BWRVIP
Repair Manager
Electric Power Research Institute
P. O. Box 10412 3412 Hillview Ave.
Palo Alto, CA 94303

OFFICE OF NUCLEAR REACTOR REGULATION
DIVISION OF ENGINEERING
SAFETY EVALUATION OF EPRI TOPICAL REPORT TR-108710
"BWR VESSEL AND INTERNALS PROJECT, EVALUATION OF
CRACK GROWTH IN BWR NICKEL BASE AUSTENITIC ALLOYS IN RPV INTERNALS"

1.0 INTRODUCTION

By letter dated December 23, 1998, as supplemented by letters dated December 4, 2000, and February 19, 2001, the Boiling Water Reactor Vessel and Internals Project (BWRVIP) submitted for staff review and approval the Electric Power Research Institute (EPRI) Proprietary Report TR-108710, "BWR Vessel and Internals Project, Evaluation of Crack Growth in BWR Nickel Base Austenitic Alloys in RPV Internals (BWRVIP-59)," dated December 1998. The staff requested additional information regarding the BWRVIP-59 report in a letter dated November 29, 1999. The BWRVIP provided its response by letter dated December 4, 2000. The February 19, 2001 letter proposed an interim crack growth rate (CGR) of 2.5×10^{-5} in/hr for nickel base austenitic alloys in BWR plants under hydrogen water chemistry and noble metal chemical application conditions (HWC/NMCA).

The BWRVIP-59 report provides a methodology for assessing crack growth in BWR nickel base alloy shroud support structures and in other nickel base alloy components. This methodology, specifically developed for crack growth in the radial (through-thickness) direction, would apply to Alloy 82 and 182 weld materials and Alloy 600 types of nickel base austenitic materials. Residual and applied stresses and stress intensity factors have been developed for crack propagation in the same direction.

The NRC staff, with assistance from Argonne National Laboratory (ANL), has assessed the BWRVIP's submittal, as supplemented, in this safety evaluation (SE).

1.1 Background

In 1993 and 1994, intergranular stress corrosion cracking (IGSCC) of the core shroud was identified as a significant issue for austenitic materials used in BWR internals. In response to these issues, the BWR utilities formed the Boiling Water Reactor Vessel and Internals Project to address service-related degradation of BWR vessels and internals, including those composed of nickel-base alloys. Key nickel-base components include the core shroud support plate, the access hole covers, the shroud support legs and/or gussets, and the vessel attachment brackets. To adequately schedule inspection intervals of these components, the BWRVIP is proposing to use a CGR based on crack disposition curves for normal water chemistry (NWC) and HWC/NMCA.

ENCLOSURE

1.2 Purpose

The staff reviewed the BWRVIP-59 report, as supplemented, to determine whether its crack growth methodology for BWR nickel-base reactor pressure vessel (RPV) internal components would provide acceptable levels of quality for inspection and flaw evaluation (I&E) of the subject safety-related RPV internal components. The review considered the consequences of component failures, potential degradation mechanisms, past service experience, and the ability of the proposed inspections to detect degradation in a timely manner.

1.3 Organization of the Report

This SE contains a brief summary of the BWRVIP-59 report followed by the staff's evaluation and conclusions. Because the BWRVIP-59 report is proprietary, the staff wrote this SE to exclude proprietary information presented in the report. This SE gives a brief summary of the general contents of the report in Section 2.0 and the detailed evaluation in Section 3.0. Section 4.0 contains recommendations based on the staff review and the ANL technical evaluation of the BWRVIP-59 report. This SE does not discuss the proprietary portions of the BWRVIP-59 report.

2.0 SUMMARY OF BWRVIP-59 REPORT

The BWRVIP-59 report provides a methodology for assessment of CGR's in nickel base austenitic alloy shroud support materials and welds, including attachments to the RPV made from these alloys (e.g., Alloy 82, 182, and 600). This methodology has been developed specifically for crack growth in the through-thickness direction with stress intensity factors developed for crack propagation in this orientation. The methodology involves development of crack growth disposition curves which account for the variability of IGSCC parameters on the CGR assessment for these alloys.

The development of CGR's in nickel base alloys involved the determination of the through-thickness residual stress and stress intensity distributions for core support structure welds representative of BWR's in service. The BWRVIP-59 report outlines the experimental and analytical techniques used to determine the residual stress distributions. The experimental techniques involved the use of samples from spare BWR-6 RPV's at River Bend Nuclear Station and Grand Gulf Nuclear Station, both fabricated by CBI Nuclear Company (CBIN). The analytical technique included a finite element analysis of the residual stress distribution. The residual stress distributions were used in a fracture mechanics analysis to determine the through-wall stress intensity distributions for welds H8, H9, H10, H11, and H12.

The BWRVIP submitted the analysis of two weld sequences. The first weld sequence was submitted with the December 28, 1998, BWRVIP-59 report, and the second sequence was described in Attachment 2 to the December 4, 2000, BWRVIP response to the NRC RAI dated November 29, 1999. The BWRVIP-59 report maintains that, in general, the results of the experimental measurements and the analytical techniques are comparable.

In addition, Structural Integrity Associates (SIA) used the stress intensity distributions derived from these results to determine crack growth distribution curves for three environments: (1) NWC at or below EPRI Water Chemistry Action Level 1 conditions (BWRVIP-29), (2) high purity normal water chemistry with conductivity at or below 0.15 $\mu\text{S}/\text{cm}$, and (3) HWC/NMCA

within EPRI guidelines. The crack growth distribution curves were compared to a database of Alloy 182 and Alloy 600 crack growth rates. This database was developed from a combination of General Electric Nuclear Energy (GENE) data, BWRVIP peer data such as ABB and Studsvik, and BWRVIP data generated from the in-plant crack arrest verification system (CAVS).

The crack growth disposition curves consist of a stress intensity dependent (K-dependent) portion for $K < 25 \text{ ksi } \sqrt{\text{in}}$ and a constant K-independent portion for $25 < K \leq 45 \text{ ksi } \sqrt{\text{in}}$. The K-dependent CGR's are significantly smaller (10^{-10} to 10^{-8} in/hr) than the K-independent CGR's. Therefore, the BWRVIP used the more conservative CGR's in the evaluation. The BWRVIP report recommends the crack growth rates shown in Table 1.

Environment	CGR (in/hr) ($25 < K \leq 45 \text{ ksi } \sqrt{\text{in}}$)
NWC (EPRI Guidelines)	5×10^{-5}
NWC ($\leq 0.15 \text{ } \mu\text{S/cm}$)	2.5×10^{-5}
HWC/NMCA	5×10^{-6}

Table 1: Proposed BWRVIP-59 CGR's associated with specified water environment.

3.0 STAFF EVALUATION

The staff has reviewed the BWRVIP-59 report and ANL's technical evaluation. The staff finds that the recommendations listed in Section 4.0 should be incorporated into a revised BWRVIP-59 report in order for the methodology presented in the subject report to be acceptable. Once the BWRVIP-59 report has been revised, the staff finds that the use of the calculated residual stresses and stress intensity factors combined with the crack disposition curves should generally be acceptable and result in conservative crack growth rate estimates.

4.0 RECOMMENDATIONS

The following recommendations are based on staff review and the evaluation performed by ANL.

4.1 Proposed CGR for High Purity Water Chemistry

The proposed CGR for NWC within the EPRI guidelines (5×10^{-5} in/hr) appears to bound the data that remained after the SIA screening process. However, the proposed CGR for high purity water chemistry (conductivity $\leq 0.15 \text{ } \mu\text{S/cm}$) does not bound the applicable data as rigorously as the CGR for NWC within the EPRI guidelines. To assure that the applicable data is bounded for both NWC conditions (EPRI guidelines and high purity water chemistry), the staff recommends the use of the more conservative crack disposition curve when evaluating crack growth. For example, the BWRVIP-59 proposed CGR of 5×10^{-5} in/hr for NWC conditions would be more appropriate for both NWC conditions since it is more conservative than the high purity water CGR of 2.5×10^{-5} in/hr.

4.2 Crack Growth Disposition Curves

The use of calculated residual stresses and stress intensity factors combined with crack growth disposition curves should generally result in conservative estimates of crack growth. However, the uncertainty in the residual stress/stress intensity calculations and its effect on crack growth has not been determined. To compensate for this deficiency, the staff recommends that the CGR's of 5×10^{-5} in/hr for NWC and 5×10^{-6} in/hr for HWC/NMCA be used as references after the fracture mechanics methodology presented in the BWRVIP-59 has been adjusted for plant-specific variables and applied. The staff will determine the acceptability of the plant-specific CGR's based on the accuracy of the calculations, their underlying assumptions, and the potential consequences of the predicted crack growth.

4.3 Alternate Weld Sequence

In the December 4, 2000 response to the staff's RAI's, the BWRVIP included an additional analysis of an alternate weld sequence used in the fabrication of the BWR shroud support structure. This alternate weld sequence was analyzed using the same methodology as the weld sequence presented in the original BWRVIP-59 report. The resulting crack growth rates from this alternate weld sequence are bounded by the original BWRVIP-59 sequence. However, the staff recommendations from sections 4.1 and 4.2 of this SE also apply to this alternate sequence. For plants that use the alternate weld sequence or any sequence different than the one presented in the BWRVIP-59 report, the crack disposition curves should be plant-specific and the final CGR's should appropriately bound the applicable data.

5.0 CONCLUSIONS

The staff concludes that, although the use of the calculated residual stresses and stress intensity factors combined with the crack disposition curves should generally be acceptable and result in conservative estimates of crack growth, in order to accept the methodology presented in the BWRVIP-59 report, the above recommendations in the SER should be incorporated. The staff will determine the acceptability of the plant-specific CGR's based on the accuracy of the calculations, their underlying assumptions, and the potential consequences of the predicted crack growth.

The staff also finds that the proposed interim CGR, as requested by letter dated February 19, 2001, and limited in scope to HWC/NMCA, is superseded by the CGR of 5.0×10^{-6} in/hr presented in the BWRVIP-59 report. Based on the staff's review of the BWRVIP-59 and BWRVIP-62 reports, the CGR of 5.0×10^{-6} in/hr, is acceptable for use as a reference value after a plant-specific CGR has been calculated. Therefore, the request for the interim crack rate of 2.5×10^{-5} in/hr is not necessary.

G

FINAL NRC SAFETY EVALUATION

**Entire Appendix Deleted
EPRI Proprietary Information**

H

RECORD OF REVISIONS

BWRVIP-59-A	<p>Information from the following documents was used in preparing the changes included in this revision of the report. These documents are also listed as References [23] through 30 in Section 8.0.</p> <ol style="list-style-type: none">1. BWR Vessel and Internals Project, "Evaluation of Crack Growth in BWR Nickel-Base RPV Internals (BWRVIP-59)," EPRI Report TR-108710, December, 1998.2. Letter from C. E. Carpenter (NRC) to C. Terry. (BWRVIP Chairman), "Proprietary Request for Additional Information – On EPRI TR-108710," "Evaluation of Crack Growth in BWR Nickel Base Austenitic Alloys in RPV Internals (BWRVIP-59)," (TAC NO. MA4467), November 29, 1999, Correspondence File Number 99-491).3. Letter from C. Terry (BWRVIP) to C. E. Carpenter (NRC), "BWRVIP Response to NRC Request for Additional Information on BWRVIP-59," December 4, 2000. (BWRVIP Correspondence File Number 2000-335).4. Letter from C. Terry (BWRVIP) to C. E. Carpenter (NRC), "BWRVIP Request for NRC Approval of an Interim Crack Growth Rate of 2.5×10^{-5} in/hr for Nickel Base Austenitic Alloys in BWR Plants Under Hydrogen Water Chemistry (HWC) and Noble Metal Chemical Application (NMCA) Conditions," February 19, 2001. (BWRVIP Correspondence File Number 2001-040).5. Letter from W. H. Bateman (NRC) to C. Terry (BWRVIP Chairman), "Safety Evaluation of the BWR Vessel and Internals Project BWRVIP-59 Report (TAC No. M94975)" and enclosure, July 31, 2001. (BWRVIP Correspondence File Number 2001-247A).6. Letter from W. H. Bateman (NRC) to C. Terry (BWRVIP Chairman), "Clarification to NRC Letter Regarding BWRVIP Response to BWRVIP-59 Safety Evaluation (TAC No. MA4467)," January 29, 2002. (BWRVIP Correspondence File Number 2002-037).7. Letter from W. A. Eaton (BWRVIP) to M. Khanna (NRC), "BWRVIP Response to NRC Safety Evaluation of BWRVIP-59," Including CD with Revised BWRVIP-59 Report, December 20, 2004. (BWRVIP Correspondence File Number 2004-535).8. Letter from M. A. Mitchell (NRC) to W. A. Eaton (BWRVIP Chairman), "Safety Evaluation of EPRI Report," "BWR Vessel and Internals Project, Evaluation of Crack Growth in BWR Nickel Base Austenitic Alloys in Reactor Pressure Vessel Internals (BWRVIP-59)" and enclosure, July 14, 2006. (BWRVIP Correspondence File Number 2006-386). <p>Details of the revisions can be found in Table H-1.</p>
-------------	--

Table H-1
Revision Details

Required Revision	Source of Requirement for Revision	Description of Revision Implementation
Insert Section 2.6 to explain the two fabrication sequences for the fabrication of the shroud support structure welds.	BWRVIP Response to NRC RAI (99-491) BWRVIP Response to Initial SE (2004-535)	Section 2.6 inserted to describe the two fabrication sequences used to determine the residual stresses for the shroud support structure welds.
Revise text in Section 3.1 to indicate that two welding sequences were considered in the report.	BWRVIP Response to Initial SE (2004-535)	Section 3.1 revised to describe the two welding sequences that were used in the residual evaluation of the shroud support structure welds and present results of the analysis.
Revise text in Section 3.2 to indicate that two different analytical approaches were used at different times to determine the residual stresses for the shroud support structure welds.	BWRVIP Response to Initial SE (2004-535)	Section 3.2 revised to discuss the two different analytical approaches (initial analysis with discrete models and updated analysis with integrated model) used in the determination of the weld residual stresses and present results of the analysis.
Revise Section 3.2.4 to explain the discrepancy between Figure 3-15 and Figure E-35 of report.	Final SE (2006-386)	Section 3.2.4 was revised to provide explanation that Figure 3-15 is the mirror image of Figure E-35, Run E, Section 4 of Appendix E of the report since the crack initiation can occur from either the top or bottom surface of Weld H9 depending on where the K distribution is higher.
Update Figures 3-14 and 3-15 to show third order polynomial fits to the stress distributions.	Final SE (2006-386)	Third order polynomial stress fits and associated equations were provided in Figures 3-14 and 3-15 for the residual stress distributions for Welds H8 and H9 respectively which are used in subsequent fracture mechanics evaluations.
Revise text in Section 4.0 to indicate which residual stress results will be used in the fracture mechanics evaluation.	BWRVIP Response to Initial SE (2004-535)	Text in Section 4.0 revised to indicate that the most critical residual stress distributions from the updated analysis results will be used in the fracture mechanics evaluations for all welds.

Table H-1
Revision Details (Continued)

Required Revision	Source of Requirement for Revision	Description of Revision Implementation
Revise text in Section 4.1 to indicate that the results from the updated analysis were used for subsequent evaluations of Weld H8 and H9.	BWRVIP Response to Initial SE (2004-535)	Section 4.1 revised to explain that the results of the integrated model were used to determine the bounding residual stress distribution for subsequent fracture mechanics evaluations for Welds H8 and H9.
Revise text in Section 4.1 to indicate that the polynomial stress fits in Figure 3-14 and 3-15 were used in the fracture mechanics evaluation.	Final SE (2006-386)	Section 4.1 revised to indicate that for Welds H8 and H9, the polynomial stress fits for the entire residual stress distribution was used with the ASME Section XI methodology to determine the through-wall K distribution.
Revise text in Section 4.1 to place limitation on the aspect ratio applicability of the K solutions for Weld H8 and H9.	Final SE (2006-386)	Section 4.1 revised to indicate that the K solutions for Welds H8 and H9 are limited to aspect ratios greater than or equal to 0.1. Furthermore, it is indicated that for aspects ratios less than 0.1, a plant specific analysis is required to calculate K or that the bounding K independent CGR discussed in Sections 5 and 6 be used.
Revise text in Section 4.2 to indicate that the results from the updated analysis were used for subsequent evaluations of Weld H10, H11 and H12.	BWRVIP Response to Initial SE (2004-535)	Section 4.2 revised to explain that the results of the integrated model were used to determine the bounding residual stress distribution for subsequent fracture mechanics evaluations for Welds H10, H11 and H12.
Add Section 5.7 to address the effect of fluence on crack growth.	Final SE (2006-386)	Revise Section 5.7 to indicate that the fluence level at the shroud support plates are reasonably low and should not affect crack growth.

Table H-1
Revision Details (Continued)

Required Revision	Source of Requirement for Revision	Description of Revision Implementation
Revise text in Section 6.0 to indicate that only the normal water chemistry (NWC) and hydrogen water chemistry cases were used in crack growth evaluation.	BWRVIP Response to Initial SE (2004-535)	Section 6.0 revised to remove reference to the high purity water case and reinforce the use of only the NWC and HWC cases as presented in Section 5 for crack growth evaluation.
Revise text in Section 6.0 to provide updated results.	Not Applicable	Section 6 revised to provide updated crack growth results based on updated analyses in Sections 3 through 5.
Revise Section 7.0 to be consistent with all changes made in revised document.	Not Applicable	Section 7 revised (Summary and Conclusions) consistent with all changes made in revised document.
Revise Section 8.0 to be consistent with new References added to the report.	Not Applicable	Section 8.0 revised (References consistent with new References added to the report).
Revise Appendix C with new results	Not Applicable	Appendix C replaced in its entirety with results of revised analyses.
Revise Appendix D to clarify welding sequence.	BWRVIP Response to Initial SE (2004-535)	Appendix D revised to clarify the welding sequence used by CB&I in the fabrication of the shroud support structure.
Revise Appendices to include new Appendix E.	BWRVIP Response to Initial SE (2004-535)	New Appendices E, providing results of updated analysis included in the report.
Revise Executive Summary to reflect changes made to the report.	Not Applicable	Revised Executive Summary to reflect changes made to report.
Add NEI 03-08 Implementation Requirements.	Not Applicable	Section 1.5 added ("Implementation Requirements").
End of Revisions.		



WARNING: This Document contains information classified under U.S. Export Control regulations as restricted from export outside the United States. You are under an obligation to ensure that you have a legal right to obtain access to this information and to ensure that you obtain an export license prior to any re-export of this information. Special restrictions apply to access by anyone that is not a United States citizen or a permanent United States resident. For further information regarding your obligations, please see the information contained below in the section titled "Export Control Restrictions."

Export Control Restrictions

Access to and use of EPRI Intellectual Property is granted with the specific understanding and requirement that responsibility for ensuring full compliance with all applicable U.S. and foreign export laws and regulations is being undertaken by you and your company. This includes an obligation to ensure that any individual receiving access hereunder who is not a U.S. citizen or permanent U.S. resident is permitted access under applicable U.S. and foreign export laws and regulations. In the event you are uncertain whether you or your company may lawfully obtain access to this EPRI Intellectual Property, you acknowledge that it is your obligation to consult with your company's legal counsel to determine whether this access is lawful. Although EPRI may make available on a case-by-case basis an informal assessment of the applicable U.S. export classification for specific EPRI Intellectual Property, you and your company acknowledge that this assessment is solely for informational purposes and not for reliance purposes. You and your company acknowledge that it is still the obligation of you and your company to make your own assessment of the applicable U.S. export classification and ensure compliance accordingly. You and your company understand and acknowledge your obligations to make a prompt report to EPRI and the appropriate authorities regarding any access to or use of EPRI Intellectual Property hereunder that may be in violation of applicable U.S. or foreign export laws or regulations.

The Electric Power Research Institute (EPRI), with major locations in Palo Alto, California; Charlotte, North Carolina; and Knoxville, Tennessee, was established in 1973 as an independent, nonprofit center for public interest energy and environmental research. EPRI brings together members, participants, the Institute's scientists and engineers, and other leading experts to work collaboratively on solutions to the challenges of electric power. These solutions span nearly every area of electricity generation, delivery, and use, including health, safety, and environment. EPRI's members represent over 90% of the electricity generated in the United States. International participation represents nearly 15% of EPRI's total research, development, and demonstration program.

Together...Shaping the Future of Electricity

Program:

Nuclear Power

© 2007 Electric Power Research Institute (EPRI), Inc. All rights reserved. Electric Power Research Institute, EPRI, and TOGETHER...SHAPING THE FUTURE OF ELECTRICITY are registered service marks of the Electric Power Research Institute, Inc.

Printed on recycled paper in the United States of America

1014874NP

Electric Power Research Institute

3420 Hillview Avenue, Palo Alto, California 94304-1338 • PO Box 10412, Palo Alto, California 94303-0813 USA
800.313.3774 • 650.855.2121 • askepri@epri.com • www.epri.com